UNIVERSITÁ DEGLI STUDI DI MILANO
FACOLTÁ DI MEDICINA E CHIRURGIA

DOTTORATO DI RICERCA IN FISIOLOGIA
SETTORE SCIENTIFICO DISCIPLINARE BIO-09
CICLO XXVI

Tesi di Dottorato di Ricerca

BREAKDOWN OF CAUSALITY AND CORTICAL DOWNSTATE WITHIN THE SLEEPING BRAIN

Dottorando: Dott. Andrea Pigorini
Matricola: R09110

Tutor: Dott. Marcello Massimini

Coordinatore: Prof. Michele Mazzanti

Anno Accademico 2012-2013

SUMMARY

ABSTRACT

Theoretically, consciousness depends on the brain's ability to engage in complex activity patterns that are, at once, distributed among interacting cortical areas (integrated) and differentiated in space and time (information-rich). In a recent series of experiments the electroencephalographic response to a direct cortical stimulation in humans was recorded during wakefulness and non-rapid eyes movement sleep (NREM) by means of a combination of transcranial magnetic stimulation (TMS) and high-density electroencephalogram (hd-EEG). TMS/hd-EEG measurements showed that, while during wakefulness the brain is able to sustain long-range specific patterns of activation, during NREM sleep, when consciousness fades, this ability is lost: the thalamocortical system, despite being active and reactive, either breaks down in causally independent modules (producing a local slow wave), or it bursts into an explosive and non-specific response (producing a global EEG slow wave). We hypothesize that, like spontaneous sleep slow waves, the slow waves triggered by TMS during deep sleep are due to bistability between periods of hyperpolarized down-state in cortical neurons, and periods of activation (up-state). In this condition, the inescapable occurrence of a silent, down-state after an initial activation could impair the ability of thalamocortical circuits to sustain long-range, differentiated patterns of activation, a theoretical requisite for consciousness. According to animal experiments the extracellular signature of the downstate is a transient suppression of high frequency (<20Hz) power in the local field potential (LFP). However, detecting this feature in human EEG recording is challenging because of the resistive properties of the skull, muscular artifacts and the high distance of scalp electrodes from deeper cortical sources making difficult to observe a modulation of gamma activity. These drawbacks can nevertheless be overcome by using a perturbational approach similar to TMS and simultaneous intracranial recordings. To this aim, in the present thesis we employ intracerebral electrical stimulation (ICS) and simultaneous stereotactic electroencephalographic (stereo-EEG) recordings. Specifically, we recorded cortico-cortical evoked potentials (CCEPs) during wakefulness and NREM sleep and analyzed them by means of time-frequency analysis and phase locking measures both within (phase-locking factor, PLF) and across (phase-locking value, PLV) recording sites. We observed that, while during wakefulness ICS triggers a widespread pattern of sustained causal effects (phase-locked activity), during NREM sleep the same initial activation induces a cortical downstate in its cortical targets – as reflected by a clear-cut suppression of high frequency (>20Hz) oscillations – that is followed by a loss of both PLF and PLV, in spite of restored levels of neuronal activity. These results point to bistability as the underlying critical mechanism that prevents the emergence of complex interactions in human thalamocortical networks when consciousness is lost during NREM sleep. This finding is particularly relevant because a similar mechanism may play a role in other conditions where loss of consciousness is paralleled by the appearance of spontaneous (or TMS evoked) slow waves such as some kind of anesthesia and in brain injured subjects.

OUTLINE and MY CONTRIBUTION

CHAPTER 1: this section provides a general definition of consciousness illustrating an established theoretical framework in consciousness research: the Information Integration Theory (IIT) by Giulio Tononi (2004). According to this theory, consciousness is thought to require the joint presence of functional integration and functional differentiation in thalamo-cortical networks, otherwise defined as brain complexity.

CHAPTER 2: in this chapter I move from theory towards an empirical approach to evaluate qualitatively the level of complexity of human brain. In particular, I report a summary of a series of recent studies published by our group in which TMS combined with EEG has been employed to qualitatively evaluate brain complexity in wakefulness and during physiological (sleep), pharmacological (anesthesia) and pathological (brain injury) loss of consciousness (LOC). These studies invariably show that the complexity of the cortical response to TMS is high during wakefulness, during dreaming, and in patients that recover consciousness after brain injury while it collapses when consciousness is lost during deep sleep, anesthesia and vegetative state following severe brain injury. In this chapter I focus specifically on two studies I have contributed to:

- **Pigorini, A.,** Casali, A. G., Casarotto, S., Ferrarelli, F., Baselli, G., Mariotti, M., Massimini, M. and Rosanova, M., "Time-frequency spectral analysis of TMS-evoked EEG oscillations by means of Hilbert-Huang transform", J. Neurosci. Methods 198:236-45, 2011.
- Casarotto, S., Romero Lauro, L. J., Bellina, V., Casali, A. G., Rosanova, M., **Pigorini, A.,** Defendi, S., Mariotti, M. and Massimini, M., "EEG Responses to TMS Are Sensitive to Changes in the Perturbation Parameters and Repeatable over Time". Plos ONE, 5:e10281, 2010.

CHAPTER 3: following the observations derived from CHAPTER 2, in this section I propose a possible neurophysiological mechanism responsible for the collapse of brain complexity during LOC. Specifically I describe a study, the main project of this thesis, where intracranial electrical stimulation and recordings has been employed to demonstrate that during NREM sleep (a physiological model of LOC), a perturbation of thalamo-cortical system induces local (and/or global) downstates, possibly impairing the ability of diffuse thalamocortical modules to engage in causal interactions, a theoretical requirement for consciousness as described in the first section.

This chapter is entirely focused on a recently submitted study:

- **Pigorini, A.,** Sarasso, S., Proserpio, P., Szymansky, C., Arnulfo, G., Casarotto, S., Rosanova, M., Fecchio, M., Mariotti, M., Palva, J.M., Nobili, L. and Massimini, M., "Breakdown of causality and cortical downstate within the sleeping brain", *submitted.*

CHAPTER 4: in this section I deepen the investigation over the neurophysiological mechanisms described in CHAPTER 3 by reporting some preliminary results from an ongoing *in vitro* study. Here we employ electrical stimulation and simultaneous electrical recording of LFP activity derived from ferret cortical slices treated with different kind of drugs.

CHAPTER 5: in this final chapter I merge empirical evidences and theoretical predictions by summarizing a recent methodological study by our group. Here, we showed that it is possible to quantitatively measure causal interactions within the human brain, assessing Φ, a theory-driven measure of consciousness derived from IIT. This chapter consist in a summary of the study:

- Chang, J.Y., **Pigorini, A.**, Massimini, M., Tononi, G., Nobili, L. and Van Veen, B.D., "Multivariate autoregressive models with exogenous inputs for intracerebral responses to direct electrical stimulation of the human brain", Front Hum Neurosci. 2012 Nov 30;6:317.

LIST OF PUBLICATIONS

- Sarasso S, Proserpio P, **Pigorini A**, Moroni F, Ferrara M, De Gennaro L, De Carli F, Lo Russo G, Massimini M, Nobili L.: Hippocampal sleep spindles preceding neocortical sleep onset in humans. Neuroimage. 2013 Oct 28. pii: S1053-8119(13)01054-9. doi: 10.1016/j.neuroimage.2013.10.031

- Silvia Casarotto, Paola Canali, Mario Rosanova, **Andrea Pigorini**, Matteo Fecchio, Maurizio Mariotti, Adelio Lucca, Cristina Colombo, Francesco Benedetti, Marcello Massimini (2013). Assessing the Effects of Electroconvulsive Therapy on Cortical Excitability by Means of Transcranial Magnetic Stimulation and Electroencephalography. Brain topography. Apr;26(2):326-37. doi: 10.1007/s10548-012-0256-8.

- Chang JY, **Pigorini A**, Massimini M, Tononi G, Nobili L, Van Veen BD (2012). Multivariate autoregressive models with exogenous inputs for intracerebral responses to direct electrical stimulation of the human brain. Front Hum Neurosci. 2012;6:317. doi: 10.3389/fnhum.2012.00317

- Nobili L, De Gennaro L, Proserpio P, Moroni F, Sarasso S, **Pigorini A**, De Carli F, Ferrara M (2012). Local aspects of sleep: Observations from intracerebral recordings in humans. Prog in Brain Res. 199:219-32. doi: 10.1016/B978-0-444-59427-3.00013-7

- Casarotto S, Määttä S, Herukka S-K, **Pigorini A**, Napolitani M, Gosseries O, Niskanen E, Könönen M, Mervaala E, Rosanova M, Soininen H, Massimini M (2011): Transcranial magnetic stimulation-evoked EEG/cortical potentials in physiological and pathological aging. Neuroreport, 22: 592-597. doi: 10.1097/WNR.0b013e328349433a.

- **Pigorini A**, Casali AG, Casarotto S, Ferrarelli F, Baselli G, Mariotti M, Massimini M, Rosanova M (2011): Time-frequency spectral analysis of TMS-evoked EEG oscillations by means of Hilbert-Huang transform. Journal of Neuroscience Methods, 198: 236-245. doi:10.1016/j.jneumeth.2011.04.013

- Casarotto S, Romero Lauro JL, Bellina V, Casali AG, Rosanova M, **Pigorini A**, Defendi S, Mariotti M, Massimini M (2010): EEG responses to TMS are sensitive to changes in the perturbation parameters and repeatable over time. PLoS One, 5(4): e10281. doi:10.1371/journal.pone.0010281

- Rosanova M, Casarotto S, **Pigorini A**, Canali P, Casali AG, Massimini M (2012): Combining Transcranial Magnetic Stimulation with Electroencephalography to study human cortical excitability and effective connectivity, Neuromethods, Springer Science+Business Media PP. 435-457

- Casarotto S, **Pigorini A**, Casali AG, Canali P, Rosanova M, Massimini M. (2011): Approccio elettrofisiologico allo studio dell'eccitabilità e connettività corticale nell'uomo: metodi ed applicazioni cliniche. In: Neuroinformatica, MM Fato, MC Gilardi, A Schenone Ed. Bologna: Pàtron Editore. pp. 71-85.

- **Pigorini A**, Szymanski C, Casali AG, Casarotto S, Rosanova M, Lo Russo G, Mariotti M, Proserpio P, Nobili L, Massimini M (2010): Cortical effective connectivity across sleep-wake cycle: an intracerebral study in humans. Proceedings of the 16th Annual Meeting of the Organization for Human Brain Mapping, 6-10 Jun 2010, Barcelona, Spain (Selected as Top Ranked abstract, E-Poster, and Trainee Abstract Travel Award).

LIST OF ABBREVIATIONS

AEP : Auditory Evoked Potential
BA : Brodmann's Area
bPL : Broad-band Phase-locking
CCEP: Cortico-Cortical Evoked Potential
CRS-R : Coma Recovery Scale-Revised
CT : Computerized Tomography
DI : Divergence Index
DOC : Disorders of Consciousness
EEG : Electroencephalography
EMCS : Emergence from Minimally Conscious State
EMD: Empirical Mode Decomposition
EOG : Electrooculogram
ERP: Event-related Potential
ERSP : Event-related Spectral Perturbation
fMRI : Functional Magnetic Resonance Imaging
gERSP : Global Event-related Spectral Perturbation
GMFP : Global Mean Field Power
hd-EEG : high-density Electroencephalography
ICS: Intracerebral Electrical Stimulation
LIS : Locked-in Syndrome
LOC : Loss of Consciousness
MCS : Minimally Conscious State
MEG : Magnetoencephalography
MNI : Montreal Neurological Institute
MRI : Magnetig Resonance Imaging
NBS : Navigated Brain Stimulation
NCC : Neural Correlates of Consciousness
NREM: Non-rapid Eye Movement
OAA/S : Observer's Assessment of Alertness/Sedation
PET : Positron Emission Tomography
PLF: Phase Locking Factor
PLV: Phase Locking Value
REM : Rapid Eye Movement
ROC : Receiver Operating Characteristic
SCD : Significant Current Density
SCS : Significant Current Scattering
SEP : Somatosensory Evoked Potential
SS : Statistically Significant Sources
TMS : Transcranial Magnetic Stimulation
VS : Vegetative State
WMN : Weighted Minimum Norm

LIST OF FIGURES

CHAPTER 1 - INTRODUCTION

1.1 – Defining consciousness

Everyone knows what consciousness is: it is what vanishes when we fall into dreamless sleep and reappears when we wake up or when we dream (Tononi, 2008) – in other words, it is synonymous with experience. Assessing consciousness is often straightforward: if we see purposeful, intelligent behavior in a person, we assume he/she is conscious. If in doubt, as when someone is resting with eyes closed, we can ask: if she/he answers that she/he was thinking or daydreaming, we infer she/he was conscious. But at times matters are less clear: someone fast asleep shows no purposeful activity and will not respond to questions, yet she/he may be dreaming. Similarly, some patients with brain damage may be behaviorally unresponsive and thus judged clinically unconscious, yet they may be able to generate brain signals indicating they understood a question or a command (Cruse et al., 2011; Owen et al., 2006). In general, the problem is that while we assess the level of consciousness based on an individual's ability to connect and respond to the external environment, these features are not necessary for consciousness. Yet, to this day, we do not have a scientifically well-grounded measure of the level of consciousness that is independent of processing sensory inputs and producing appropriate motor outputs.

Neuroscience is certainly making progress in identifying the neural correlates of consciousness. While many of the proposed neural substrates of consciousness undoubtedly have heuristic value, empirical evidence still does not provide criteria for necessity and sufficiency. For example, measurements performed during seizures (Blumenfeld and Taylor, 2003) where subjects are unconscious and unresponsive despite increased brain metabolism suggested that the overall levels of brain activity may not be a reliable marker of the presence of consciousness. Along the same lines, positron emission tomography (PET) measurements showed that brain-injured patients can recover consciousness from vegetative state, without necessarily increasing their brain metabolic rates (Laureys et al.,

2004). On the other hand, the hypothesis that the level of consciousness could be critically determined by the power/synchronization of spontaneous, fast frequency oscillations in the thalamocortical system has been questioned by recent measurements. Indeed, this hypothesis fails to explain the loss of consciousness (LOC) observed during NREM sleep, propofol anesthesia and generalized tonic-clonic seizures, where hyper-synchronous broad-band oscillations can be observed (Arthuis et al., 2009). As a consequence, even apparently simple questions like "why does consciousness fades during early NREM sleep?" and "why does it restores during dreaming?" have been (and still are) unanswered, thus pointing to the need of robust empirical studies complemented by a self-consistent, general and parsimonious theoretical approach.

To this aim, it is necessary (i) to start from a theory that suggests which properties are fundamental for a physical system to give rise to conscious experience and (ii) implementing a practical measuring method to weigh up, at least at a general level, these properties in a real brain. Once these issues were solved, the further steps should consist in (iii) identifying possible neurophysiologic mechanisms responsible for variation of those properties across different states of consciousness and (iv) developing short indices to quantitatively weight the brain's capacity for conscious experience, possibly in line with theoretical prediction.

In the present work, we start in this chapter by reporting the IITC (Tononi, 2008, 2005, 2004), a theory that argues that consciousness is integrated information and that a physical system should be able to generate consciousness to the extent that it can enter any of a large number of available states (information), yet it cannot be decomposed into a collection of causally independent subsystems (integration). Then, in the second chapter, we devise a practical method to gauge the brain capacity to integrate information. To do this we employ a combination of transcranial magnetic stimulation and electroencephalography (TMS/EEG), a technique that allows stimulating directly different subsets of cortical neurons and recording the immediate reaction of the rest of the brain. Based on measurements performed in sleeping subjects (Massimini et al., 2007, 2005), anaesthesia (Ferrarelli et al., 2010) and patients affected by disorder of consciousness (Rosanova et al., 2012) we argue that this

method represents an effective way to appreciate, at a general level, to what extent different regions of the thalamocortical system can interact globally (integration) to produce specific responses (information). Starting from the results showed in chapter 2, in the third and fourth chapters we propose a possible neurophysiological mechanism responsible for reducing interactions between different thalamocortical regions during deep sleep. Finally, in the fifth chapter we report a recent work from our group developing a short index to measure the balance between information and integration and, possibly, the brain's capacity for conscious experience.

1.2 – Theoretical guidelines: the Integrated Information Theory of Consciousness

The IITC takes its start from phenomenology and, by making a critical use of thought experiments, argues that subjective experience is integrated information. Therefore, according to the IITC, any physical system will have subjective experience to the extent that it is capable of integrating information. In this view, experience, i.e. information integration, is a fundamental quantity that is in principle measurable, just as mass or energy are. Information and integration are, on the other hand, the very essence of subjective experience. Classically, information is the reduction of uncertainty among alternatives: when a coin falls on one of its two sides, it provides 1 bit of information, whereas a die falling on one of six faces provides 2.6 bits. But then having any conscious experience, even one of pure darkness, must be extraordinarily informative, because it rules out countless other experiences instead (think of all the frames of every possible movie). In other words, having any experience is like throwing a die with a trillion faces and identifying which number came up. On the other hand, every experience is an integrated whole that cannot be subdivided into independent components. For example, with an intact brain you cannot experience the left half of the visual field independently of the right half, or visual shapes independently of

their color. In other words, the die of experience is a single one; throwing multiple dice and combining the numbers will not do.

If the capacity for consciousness corresponds to the capacity to integrate information, then a physical system should be able to generate consciousness to the extent that it can discriminate among a large number of available states (information), yet it cannot be decomposed into a collection of causally independent subsystems (integration). How can one identify such an integrated system, and how can one measure its repertoire of available states? To measure the repertoire of different states that are available to a system, one can use the entropy function, but this way of measuring information is completely insensitive to whether the information is integrated. Thus, measuring entropy would not allow us to distinguish between one million photodiodes with a repertoire of two states each, and a single integrated system with a repertoire of 21,000,000 states. To measure information integration, it is essential to know whether a set of elements constitute a causally integrated system, or they can be broken down into a number of independent or quasi-independent subsets among which no information can be integrated.

Indeed, the theory claims that the level of consciousness of a physical system is related to the repertoire of different states (information) that can be discriminated by the system as a whole (integration). Thus, a measure of integrated information, called phi (Φ), has been proposed in order to quantify the information generated when a system discriminates one particular state of its repertoire, above and beyond the information generated independently by its parts (Balduzzi and Tononi, 2008; Tononi, 2004).

As demonstrated through computer simulations, information integration is optimized (Φ is highest) if the elements of a complex are connected in such a way that they are both functionally specialized (connection patterns are different for different elements) and functionally integrated (all elements can be reached from all other elements of the network). If functional specialization is lost by replacing the heterogeneous connectivity with a homogeneous one, or if functional integration is lost by rearranging the connections to form small modules, the value of Φ decreases considerably (Tononi and Sporns, 2003).

According to the IITC, this is exactly why, among many structures of the brain, the thalamocortical system is so special for consciousness: it is naturally organized in a way that appears to emphasize at once both functional specialization and functional integration. Thus, it comprises a large number of elements that are functionally specialized, becoming activated in different circumstances (Bartels and Zeki, 2005). This is true at multiple spatial scales, from different cortical systems dealing with vision, audition, etc., to different cortical areas dealing with shape, colour, motion, etc., to different groups of neurons responding to different directions of motion. On the other hand, the specialized elements of the thalamocortical system are integrated through an extended network of intra- and inter-areal connections that permit rapid and effective interactions within and between areas (Engel et al., 2001).

But then, the theory also explicitly predicts that the fading of consciousness should be associated with either a reduction of integration within thalamocortical circuits (e.g., they could break down into causally independent modules) or a reduction in information (the repertoire of available states might shrink), or both. This specific prediction is however difficult to test in humans, since, in practice, can only be measured rigorously for small, simulated systems. In the next chapter, we try to identify an empirical method to approximate a measure of the capacity for integrated information in a human brain.

CHAPTER 2 - EMPLOYING TMS/EEG TO EVALUATE THALAMO-CORTICAL INTEGRATION AND INFORMATION CAPACITY

Different methods have been proposed in order to infer on a subject's level of consciousness solely based on brain activity. Some of these methods, such as spectral analysis (Berthomier et al., 2007) and the proprietary 'bispectral index' (Myles et al., 2004) seem to correlate empirically with consciousness but have no clear theoretical foundation. Other measures, such as neural complexity (Tononi et al., 1994) and causal density (Seth, 2005), are theoretically motivated (Seth et al., 2008) but have not yet been tested empirically. More or less explicitly, all these measures attempt to capture the coexistence of functional integration and functional differentiation in spontaneous (mainly EEG) brain signals. Yet, to dependably appreciate the brain's capacity for consciousness (defined as integrated information) one should go beyond spontaneous activity levels or patterns of temporal correlation among distant neuronal groups (functional connectivity). First, this is because the repertoire of available states is, by definition, potential and, thus, not necessarily observable. Second, because it is difficult to say whether a system is actually integrated or not by just observing the spontaneous activity it generates (Massimini et al., 2009). Indeed, the ability to integrate information can only be demonstrated from a causal perspective; one must employ a perturbational approach (effective connectivity) and examine to what extent subsets of neurons can interact causally as a whole (integration) to produce responses that are specific for that particular perturbation (information) (Massimini et al., 2009). Moreover, one should probe causal interactions by directly stimulating the cerebral cortex in order to avoid possible subcortical filtering or gating. Finally, since causal interactions among thalamocortical neurons develop on a sub-second time scale (just as phenomenal consciousness does), it is very important to record the neural effects of the perturbation with the appropriate temporal resolution.

Thus, in practice, one should find a way to stimulate different subsets of cortical neurons and measure, with good spatial-temporal resolution, the effects produced by these perturbations in the rest of the thalamocortical system. Today, this measurement can be performed non invasively in humans thanks to the development of a novel electrophysiological technique, based on the combination of TMS and hd-EEG (Ilmoniemi et al., 1997) (Figure 2.1).

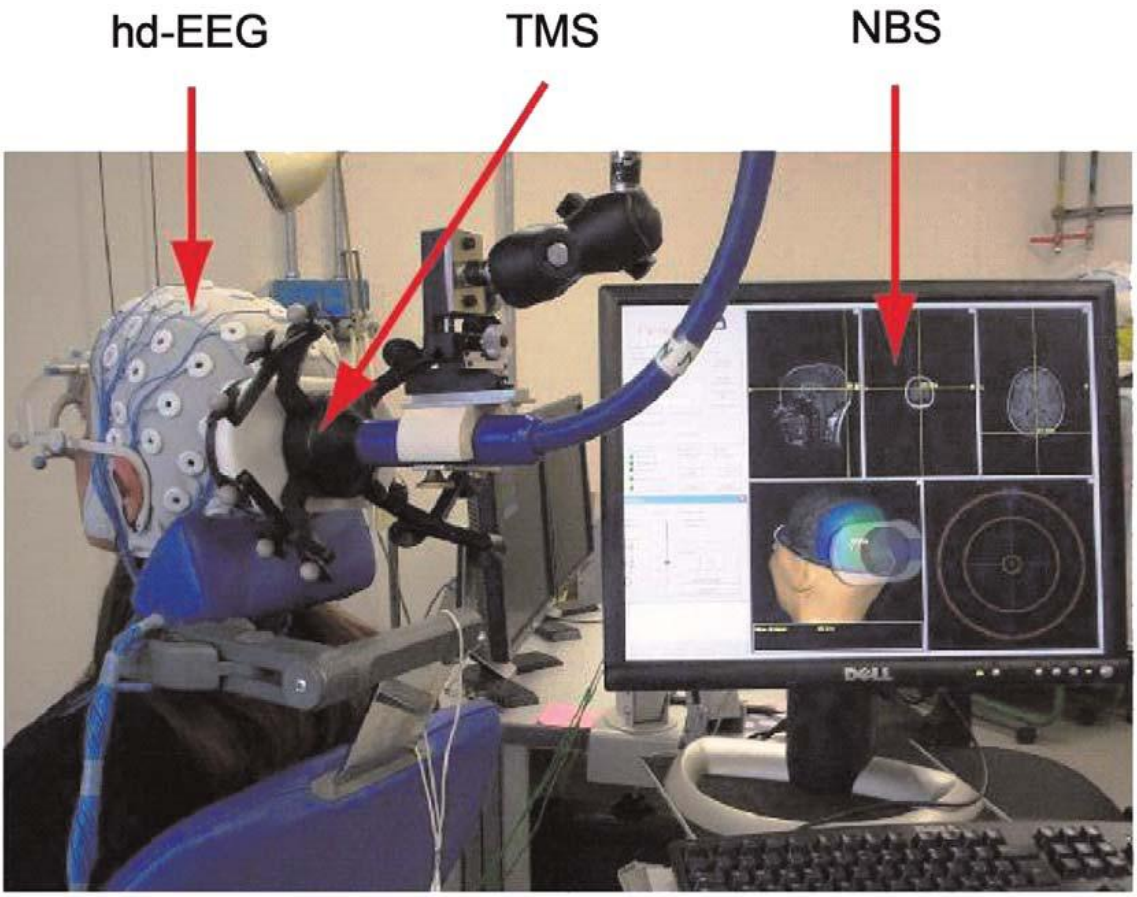

Figure 2.1: TMS/EEG setup.
In this example, a subject is sitting on an ergonomic chair while TMS is targeted to the occipital cortex. The red arrows indicate, from left to right, the three fundamental elements that compose the set-up: (1) a cap for high-density (60 channels) EEG recordings (hd-EEG) that is connected to a TMS-compatible amplifier; (2) a focal figure-of-eight stimulating coil (TMS), held in place by a mechanical arm; (3) the display of the navigated brain stimulation system (NBS). This system employs an infrared camera (not visible in this picture) to navigate TMS on a 3D reconstruction of the subject's MRI. The location and the intensity of the electric field induced by TMS are estimated and displayed in real time. To prevent the subject from perceiving the click associated with the coil's discharge, noise masking is played through inserted earplugs.

With TMS, the cerebral cortex is stimulated directly by generating a brief but strong magnetic pulse (<1 ms, 2 Tesla) through a coil applied to the surface of the scalp. The rapid change in magnetic field strength induces a current flow in the tissue, which results in the activation of underlying neuronal populations. The synchronous volley of action potentials thus initiated

propagates along the available connection pathways and can produce activations in target cortical regions. By integrating TMS with MR-guided infrared navigation systems, it is also possible to render the perturbation controllable and reproducible, in most cortical regions. Finally, using multi-channel EEG amplifiers that are compatible with TMS (Virtanen et al., 1999) one can record, starting just a few milliseconds after the pulse, the impact of the perturbation on the stimulated target and in distant cortical areas. Indeed, the integrated use of neuro-navigation systems, TMS and multichannel TMS-compatible EEG amplifiers together constitute a new brain scanning method in which stimulation is navigated into any desired brain target and the concurrently recorded scalp potentials are processed into source images of the TMS-evoked neuronal activation (Komssi and Kähkönen, 2006).

It is worth highlighting some of the specific advantages that TMS/EEG may offer as a tool to probe the brain:

1) TMS-evoked activations are intrinsically causal (Paus, 2005). Thus, unlike methods based on temporal correlations, TMS/EEG immediately captures the fundamental mechanism that underlies integration, that is the ability of different elements of a system to affect each other.
2) TMS/EEG by-passes sensory pathways and subcortical structures to probe directly the thalamocortical system. Therefore, unlike peripherally evoked potentials and evoked motor activations, TMS/EEG does not depend on the integrity of sensory and motor systems and can access any patient (deafferentated or paralyzed). Moreover, with TMS one can stimulate most cortical areas (including associative cortices) employing several different parameters (intensity, angle, current direction), thus probing a vast repertoire of possible responses, above and beyond observable ongoing brain states.
3) TMS-evoked potentials can be recorded with millisecond resolution, a time scale that is adequate to capture effective synaptic interactions among neurons.

4) TMS/EEG does not require the subject to be involved in a task and the observed activations are not affected by the willingness of the subject to participate nor by his effort and performance. Hence, this approach is well suited to assess the objective capacity of thalamo-cortical circuits independently on behaviour.

5) TMS/hd-EEG can be made portable in order to overcome the logistical and economic hurdles that may separate severely brain-injured patients from advanced imaging facilities.

Thus, at least in principle, TMS/EEG may represent an appropriate tool to approximate a theoretical measure of consciousness not only in healthy subjects, but above all at the patient's bedside. However, the question whether this technique may actually detect changes in the brain's capacity to integrate information can only be answered experimentally. For example, one should demonstrate that TMS-evoked activations are widespread (integration) and specific (information) in a conscious brain but that they become either local (revealing a loss of integration) or stereotypical (revealing a loss of information) when the same brain becomes unconscious. In this chapter we first describe methodological aspects of TMS/EEG data analysis and then we describe the results of experiments where TMS/EEG was used to understand what changes in human thalamocortical circuits when consciousness fades upon falling asleep, during anesthesia and in pathological conditions (disorder of consiousness).

2.1 – TMS/hd-EEG Recording

2.1.1 – TMS Targeting

A Focal Bipulse 8-Coil (mean/outer winding diameter ca. 50/70 mm, biphasic pulse shape, pulse length ca. 280 μs, focal area of the stimulation hot spot 0.68 cm^2) driven by a Mobile Stimulator Unit (Eximia TMS Stimulator, Nexstim Ltd., Helsinki, Finland) was targeted to specific cortical locations using a Navigated Brain Stimulation (NBS) system (Nexstim Ltd., Helsinki, Finland). Structural MRI images at 1 mm^3 spatial resolution were acquired with a

1T Philips scanner from all subjects enrolled in the studies. The NBS system employs a 3D infrared Tracking Position Sensor Unit to map the positions of TMS coil and subject's head within the reference space of individual structural MRI in order to precisely identify the TMS stimulation target. Optimal alignment between MRI fiducials and digitized scalp landmarks (nasion, left and right tragus) was verified prior to all experiments. NBS also calculates on-line the distribution and intensity of the intracranial electric field induced by TMS, using a best-fitting spherical model of subjects' head and brain and taking into account the exact shape, 3D position and orientation of the coil. TMS hot spot (i.e. 98% of the maximum stimulating electric field calculated at individually-determined depth) was kept fixed to the stimulation target with the current perpendicular to its main axis. The reproducibility of the stimulation coordinates across sessions was guaranteed by an aiming device that indicated in real-time any deviation from the desired target greater than 3 mm.

2.1.2 – hd-EEG Recording

TMS-evoked potentials were recorded by a TMS-compatible 60-channel EEG amplifier (Nexstim Ltd., Helsinki, Finland). Impedance at all electrodes was kept below 5 kΩ. The EEG signals, referenced to an additional electrode on the forehead, were filtered (0.1-500 Hz) and sampled at 1,450 Hz with 16 bit resolution. At the end of each experiment, a pen visible to the infrared camera was used to digitise the EEG electrode positions on the subject's head. Two extra electrodes were used to record the vertical EOG.

During EEG recording, subject's perception of the clicks produced by TMS coil's discharge was eliminated by means of inserted earplugs continuously playing a masking noise (always below 90 dB). A thin layer of foam was placed between coil and scalp (resulting in less than 1 mm thickness when coil was pressed against the head) in order to attenuate bone conduction. As previously demonstrated, this procedure effectively prevented any contamination of EEG signals by auditory potentials elicited by TMS-associated clicks (Massimini et al., 2007, 2005).

2.1.3 – EEG Pre-processing

Trials containing activity from other sources than neural were automatically rejected if EOG exceeded 70 μV (ocular activity) and/ or absolute power of EEG channel F8 in the fast beta range (N25 Hz) exceeded 0.9 μV^2/Hz (van de Velde et al., 1998) (indicating activity of fronto-temporal muscles). After averaging, channels with bad signal quality or large residual artifacts were excluded from further analysis. In all TMS sessions we retained at least 50 good channels, with an inter-session variation of at most 4 channels in each subject, thus ensuring an estimation of cortical generators that was reliable and comparable across sessions (Laarne et al., 2000). Before source modeling, signals were low pass filtered (80 Hz), down-sampled to 362.5 Hz and re-referenced to the common average reference. Figure 2.1.1A exhibits an example of pre-processed single-subject TMS-evoked potentials after stimulation of BA19.

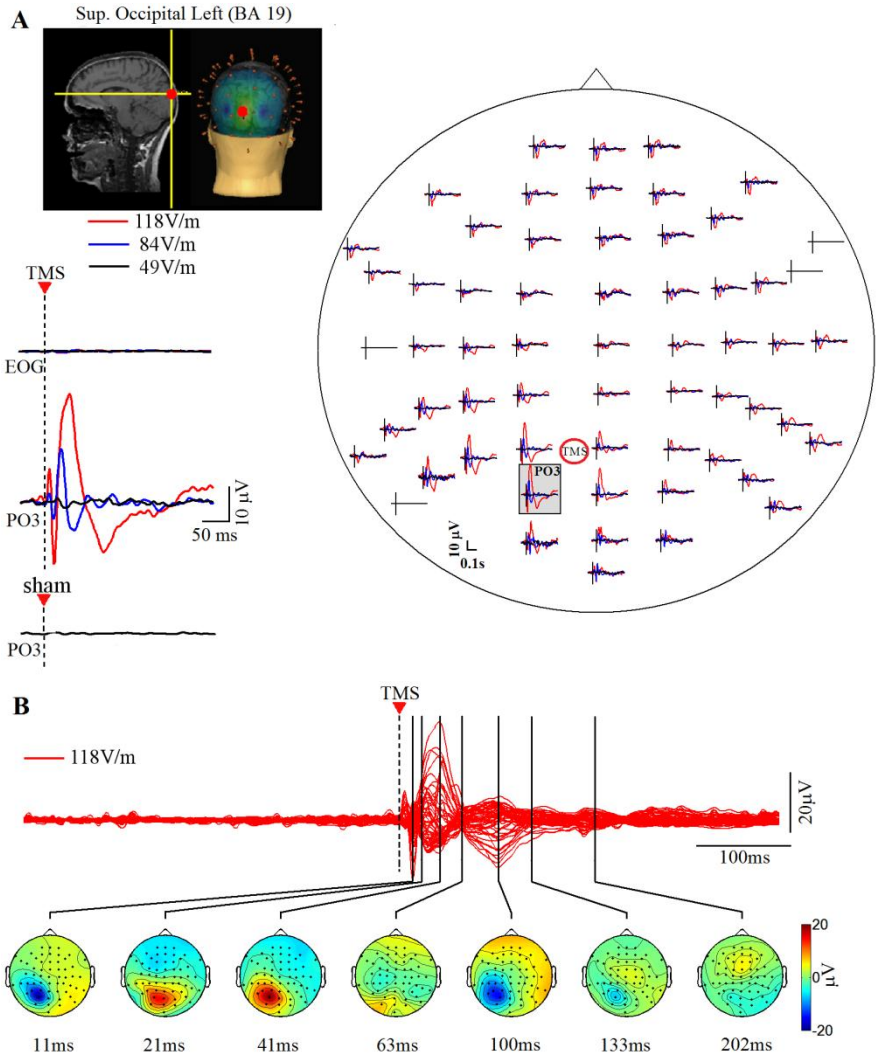

Figure 2.1.1: Single-subject TMS-evoked potentials.
A) Top Left: Location of the TMS stimulation target (left superior occipital lobule, BA 19) is shown on individual MRI, together with the approximate distribution of the electric field induced by TMS pulses in the cortex. The orange spots represent the digitized positions of EEG electrodes on the scalp. Right: Averaged TMS-evoked potentials recorded from 60 electrodes on the scalp at three different intensities of stimulation (red 118V/m, blue 84V/m, black 49V/m). Approximate location of the TMS target is reported with a red circle. Bottom left: zoom on averaged EOG activity, TMS-evoked potentials recorded on PO3 lead, and also during a sham TMS session, when the TMS coil was discharged while separated from the scalp by a 4 cm Plexiglas cube. **B)** Superimposition of the averaged TMS-evoked potentials recorded from all channels (Butterfly plot) at a stimulation intensity of 118V/m. Color-coded instantaneous topographic distribution of the potential on the scalp is displayed for 7 relevant time samples after TMS pulse delivery.

2.2 – EEG responses to TMS are sensitive to changes in the perturbation parameters and repeatable over time

A first step to correctly interpret the nature of TMS-evoked potentials is to establish to what extent responses to TMS are non-random or specific when stimulation parameters and other environmental factors are kept constant, and to what extent they are non-stereotypical or sensitive to variations of stimulation parameters. Unlike sensory stimulation, TMS activates simultaneously a rather large cortical volume containing both inhibitory and excitatory fibers, possibly belonging to different functional subsystems. Thus, it is possible that different TMS perturbations may result in EEG responses that engage many different circuits and that are largely overlapping. In addition, TMS not only perturbs cortical neurons directly but may also activate the brain indirectly, due to the stimulation of scalp nerves and to the click sound associated with the coil's discharge, when unmasked, over the subject's head. For this reason, it is also conceivable that differences in the brain's reaction to different cortical perturbation may be partially obliterated by an invariant event-related potential triggered by an unwanted somatosensory or/and acoustic stimulation. Altogether, these factors may significantly hamper the sensitivity of TMS-evoked potentials. On the other hand, due to the complexity of the technique, TMS-evoked potentials may also lack specificity, by showing accidental changes related to stimulation/recordings errors. In fact, stimulating directly the cortical surface involves the control of several factors, since a large number of cortical locations can be arbitrarily selected and perturbed, each one with several stimulation parameters (e.g. intensity, time-course, and orientation of the magnetic field). Thus, a lack of precise control of these parameters across subsequent TMS/hd-EEG sessions may result in large measurement errors and in an apparent modulation of cortical responsiveness. Similarly, other factors, such as EEG sensors positioning, coil temperature, calibration of amplifiers, etc., may, if not adequately controlled, affect the specificity of TMS-evoked potentials.

Separate experimental evidences have suggested that TMS-evoked potentials have a certain degree of sensitivity to changes in stimulation parameters, such as location (Seppo Kähkönen et al., 2005; Komssi et al., 2002), intensity (S Kähkönen et al., 2005; Komssi et al., 2004) and direction of the induced current with respect to the cortical surface (Bonato et al., 2006). Moreover, a few works have demonstrated that TMS-evoked potentials can also detect changes in the state of cortical circuits, such as the ones induced by alcohol intake (Kähkönen, 2005), by falling asleep (Massimini et al., 2007, 2005) and by induction of cortical potentiation with repetitive TMS (Esser et al., 2006). Specificity has been evaluated at the group level and the amplitude and latency of selected components of TMS-evoked potentials tend to be stable over time when stimulation parameters are constant (Lioumis et al., 2009).

But in actual fact, deciding whether a change in the EEG response to TMS is biologically relevant, or not, requires a systematic quantification of the trade-off between sensitivity and specificity. In Casarotto et al (Youden, 1950) we addressed this question by performing a statistical joint evaluation of the sensitivity and specificity of TMS/hd-EEG measures. In order to test for sensitivity, subjects were submitted to different, randomly ordered, TMS sessions in the same day (day1), varying only one stimulation parameter at a time (either stimulation site, or stimulation intensity, or angle of the TMS-induced current). TMS-evoked potentials were considered sensitive to the extent that they changed when stimulation parameters were changed. In order to evaluate specificity, a subset of TMS sessions was repeated later in the same day (day1) as well as one week later (day8), without changing any stimulation parameter. TMS-evoked potentials were considered specific to the extent that they did not change over time when stimulation parameters were kept constant.

2.2.1 – Quantifying sensitivity and specificity: the Divergence Index (DI)

By performing single-subject pairwise comparisons of the TMS-evoked potentials we could evaluate sensitivity when the sessions compared have different simulation parameters - “change comparisons” (C) - and specificity when they have identical stimulation parameters - “no change comparisons” (NC). In order to quantify the diversity of TMS-evoked responses in

C and NC comparisons, we applied non-parametric statistics and computed the percentage of spatial-temporal samples that differed significantly between two sessions of TMS-evoked potentials (Divergence Index – DI). At first, a Wilcoxon rank-sum test was applied to check that the baselines (250 ms pre-stimulus) of the single trials, contributing to the two TMS-evoked potentials to be compared, had the same distribution. In case of a negative result, the most deviated trials were removed and the test was repeated until the baseline distributions of the two groups of trials were statistically equivalent (p>0.05). At this point, we could test the null hypothesis that two sets of TMS-evoked potentials are equivalent. If this is the case, "mixing" together, in any random combination, the single trials collected during the two TMS/hd-EEG sessions should always result in the same TMS-evoked potential. Otherwise, the null hypothesis can be rejected. Thus, for each comparison, 1000 "mixed" TMS-evoked potentials were obtained by randomly mixing and averaging 1000 times the single trials collected in two different sessions (Figure 2.2.1 A, B). The set of 1000 values at each post-stimulus time sample represented the instantaneous empirical null probabilistic distribution of the voltage of the TMS-evoked potentials. In order to correct for multiple comparisons in time, we computed a single distribution for the whole time interval as follows: i) all instantaneous distributions were centralized around zero, by shifting them by an amount δ(t) (Figure 2.2.1 C); ii) for each centralized distribution, we computed the maximum absolute value (Figure 2.2.1 D); iii) the one-tail (1-α)100th percentile of the distribution of the maximum absolute values was used to estimate a significance threshold G for the whole time window of interest (Figure 2.2.1 D); iv) two boundaries were computed as (+G+δ(t)) and (–G+δ(t)). The temporal profile of these boundaries is modulated by δ(t), since G is a fixed threshold. The null hypothesis of equivalence between two TMS-evoked responses at each time sample t was rejected with probability of false positives α corrected for multiple comparisons when at least one of the two original potentials at that time sample lay beyond the significance threshold (Figure 2.2.1 E). Finally, for each comparison the DI was defined as the percentage of significantly different time samples in the first 250 ms post-stimulus in

all 60 EEG channels out of the total number of spatial-temporal samples. In this way, the DI was systematically calculated at the sensor level for all pair-wise comparisons (n= 92).

2.2.2 – TMS-evoked potentials are sensitive and specific for changes in perturbation parameters

We performed a total of 62 comparisons with data obtained from ten right handed healthy volunteers enrolled into the study: 22 comparisons for stimulation site varying between BA6, BA7, and BA19; 20 comparison changing stimulation intensity from I% and I%+10% (I%, expressed as a percentage of maximum stimulator's output of the stimulator, was kept between 40-75% for all subjects, corresponding to an electric field between 110-120 V/m on the cortical surface); and 20 comparisons varying stimulation angle (10 comparisons 0° vs. 45° and 10 comparisons 0° vs. 90°). We also performed 3 NC comparisons for each subject with identical sessions repeated in the same day (10 comparisons) and one week apart (20 comparisons).

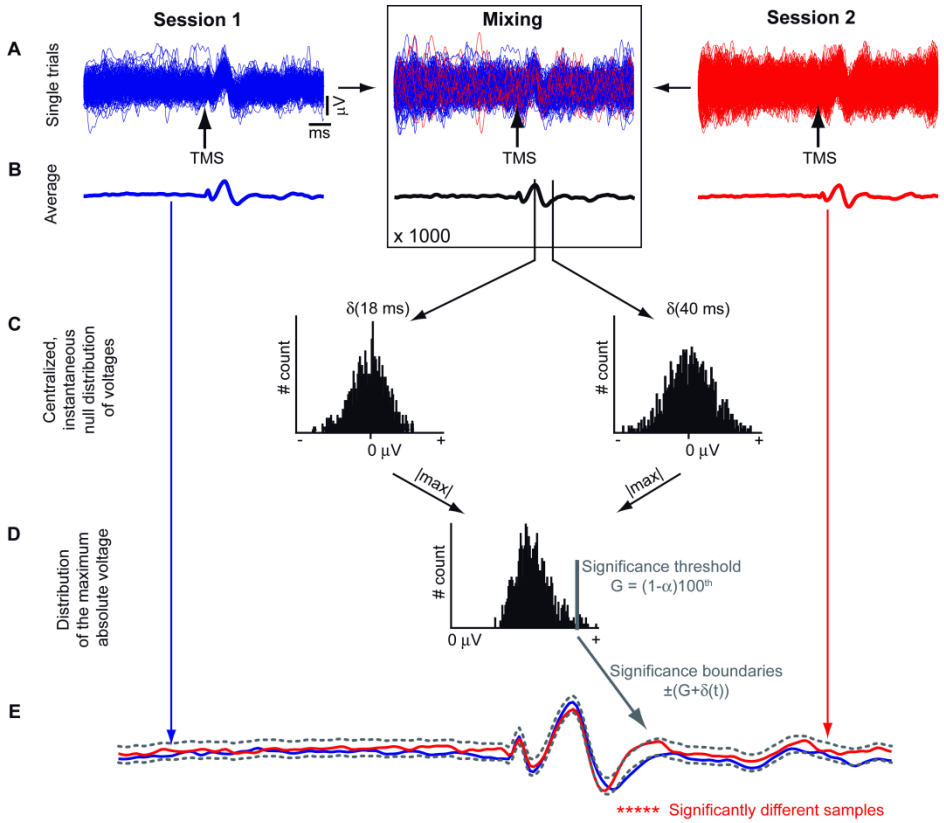

Figure 2.2.1: Non-parametric statistical procedure to perform single-subject pairwise comparisons between TMS-evoked potentials.
Single-trial recordings from two different conditions (blue and red lines) were randomly mixed 1000 times (**A**) and averaged (**B**). Instantaneous distributions of averaged voltages were computed and centralized around zero by keeping record of the displacement δ(t) (**C**). The distribution of maximum absolute values of each centralized distribution was computed and used to define a significance threshold G as the $(1-\alpha)100^{th}$ percentile (**D**). Significance boundaries (gray dotted lines) were computed as (±G + δ(t)) and used to define the significantly different time samples (red stars) between conditions at a specific channel (**E**) (adapted from Casarotto et al., 2010).

Results of a representative subject are reported in Figure 2.2.2. While TMS-evoked scalp potentials and cortical currents tended to overlap in the NC comparison, they were clearly characterized by divergent spatiotemporal patterns in all the C comparisons, suggesting that the spatiotemporal characteristics of the brain response to a direct perturbation markedly depended on each and every stimulation parameter, e.g. site, intensity and angle.

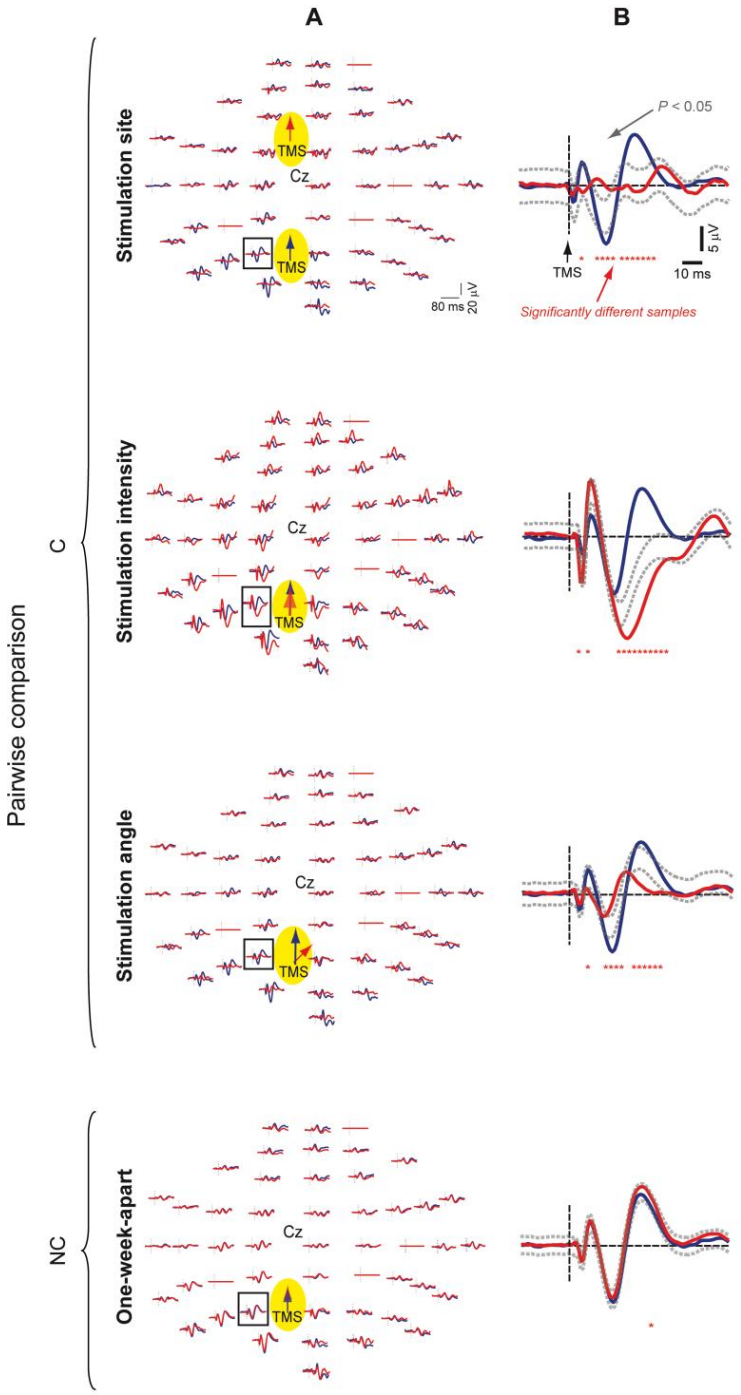

Figure 2.2.2: Results of pairwise comparisons between TMS-evoked potentials of a representative subject.

Here, one particular TMS/hd-EEG session (stimulation of BA19 at I% intensity and 0° angle on day1) is taken as a reference (blue) and compared with four other sessions (red), where stimulation parameters are varied one at a time. Specifically, the site (BA19 vs. BA6), the intensity (I% vs. I%+10%), the angle (0 vs. 45°) and the day (day1 vs. day8) of stimulation were varied, resulting in three C comparisons and one NC comparison. For each comparison, superimposition of pairs of TMS-evoked potentials in all sensors is displayed in the panel **A**, while enlarged view of P1 channel is shown in the panel **B**, together with significance boundaries (dotted gray traces) and significantly different samples (red stars) (adapted from Casarotto et al., 2010).

Figure 2.2.3 A summarizes the general results obtained from all subjects: each colored dot represents the DI computed for a specific pairwise comparison.

Generally, comparing the brain responses evoked by TMS pulses delivered over different cortical sites revealed obvious differences in the space distribution and time course of voltages and currents, and the average DI of all 22 C comparisons between different stimulation sites was 11.45 ± 5.7% (range 3-19.7%).

Varying stimulation intensity resulted in amplitude and latency changes of the main TMS-evoked components, while the general topographical distribution of voltages and currents tended to be preserved. The average DI across the 20 C comparisons between different intensities of stimulation (Figure 2.2.2 A, black dots) was 10.88 ± 6% (range: 2.31-22.2%).

When changing the angle of the TMS-induced current, the morphology of cortical responses varied in a rather unpredictable way. The average DI value was 3.92 ± 3% (range: 0.7-13.8%), with no systematic difference between 0° vs. 45° and 0° vs. 90° pairwise comparisons.

Finally, when TMS was applied with identical stimulation parameters at different times, the morphology and the spatial-temporal dynamics of TMS-evoked potentials were largely preserved. The average DI was 0.28±0.4% (range 0-1.2%) when comparing same-day recordings and 0.43±0.4% (range: 0-1.67%) for pairwise comparisons between one-week-apart sessions.

Figure 2.2.3B shows that the relative difference in DI values is preserved across latencies. For each type of pairwise comparison, the average DI computed at early latencies (0-60 ms) was significantly higher ($p < 0.05$) as compared to the one computed for late latencies (120-250 ms), although the relative differences among types of comparison were preserved across all time intervals ($p < 0.01$).

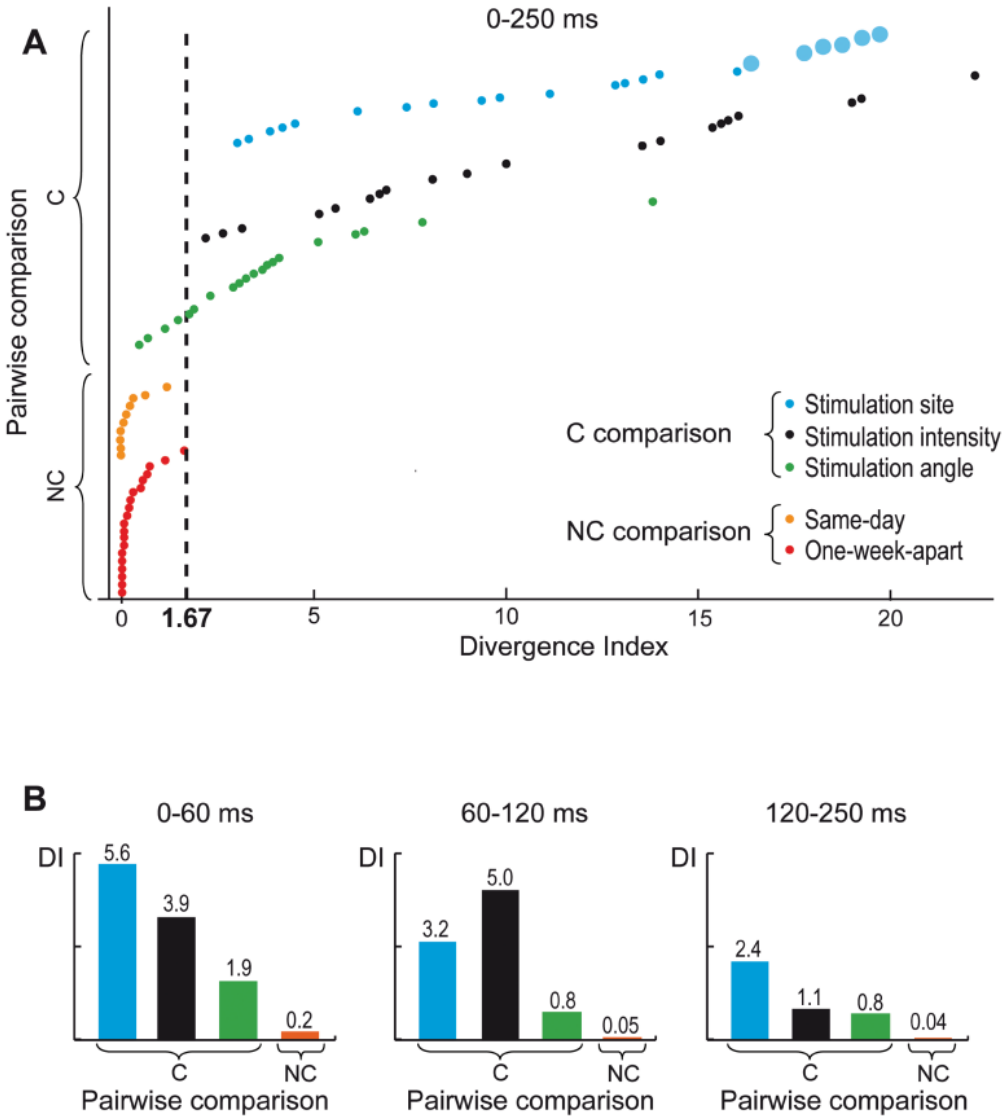

Figure 2.2.3: Divergence Index of all pairwise comparisons between TMS-evoked potentials.
Single DI values computed over the entire post-stimulus period (250 ms) are shown (**A**) with the following color-coding: DIs of the C comparisons for changes in the stimulation site, intensity and angle are represented by cyan, black and green dots, respectively, while DIs of NC comparisons are depicted in yellow for same-day sessions and in red for one-week-apart sessions. DI values computed over different temporal windows of interest (0–60 ms, 60–120 ms, 120–250 ms) are reported in the panel **B** with the same color-coding, except for NC comparisons that are summed together and plotted in orange (adapted from Casarotto et al., 2010).

At this point, considering each DI as a threshold, we performed receiver operating characteristic (ROC) analysis and we computed the true positive rate or sensitivity rate (the number of C comparisons with DI > threshold) and the true negative rate or specificity rate (the number of NC comparisons with a DI < threshold). Plotting the ROC curve as sensitivity vs specificity, the optimal DI threshold was set in correspondence to the maximum of the Younden index (Youden, 1950), computed as [sensitivity + specificity - 1]. The optimal DI threshold according to Younden index was 1.67% and yielded a 95.1% sensitivity and 100%

specificity, corresponding to an overall accuracy of 96.7%. The efficacy of DI in reliably quantifying the pairwise differences between TMS-evoked potentials was 99.1%.

These results confirm that TMS-evoked potentials, rather than being stereotypical or noisy responses, reflect, to a large extent, deterministic properties of the stimulated cortical circuits. Changing stimulation parameters almost invariably resulted in higher DIs compared to the no-change conditions. Importantly, this finding was not limited to the early latencies, and indeed DI values for the C conditions were significantly larger until 250 ms post-stimulus. This evidence demonstrates that the EEG response to TMS is primarily due to direct cortical stimulation and to the ensuing reverberation of activity in a specific network of connected elements. Indeed, changing the site of stimulation resulted in very different responses and in high DI values that were even higher when the responses triggered in areas located far away (area 19 vs. area 6) where compared. This variability in the cortical response reflects specific properties of the stimulated circuits and may be ascribed to local differences in cortical excitability (Kähkönen et al., 2005), to differences in the frequency tuning of corticothalamic modules (Kähkönen et al., 2005b) and to differences in the pattern of cortico-cortical connectivity (Ilmoniemi et al., 1997; Komssi et al., 2002).

Moreover, TMS-evoked potentials, besides being sensitive to changes, are also very stable over time. Repeating after one week a given perturbation and observing a DI >1.67% would strongly indicate that, in the meantime, some change occurred in the brain circuits. In principle, identifying a cut-off level above which one can decide whether a change in brain responsiveness occurred, or not, is crucial if one wants to use TMS/hd-EEG to track over time pathological alterations, plastic changes and therapy-induced modifications in cortical circuits.

2.3 - Time-frequency spectral analysis of TMS-evoked EEG oscillations by means of Hilbert–Huang transform

Single pulse Transcranial Magnetic Stimulation (TMS) triggers EEG oscillations that reflect local properties of the stimulated corticothalamic circuits. For instance, it has been reported that each cortical region tends to generate EEG oscillations at a characteristic frequency either when directly (Paus et al., 2001; Rosanova et al., 2009; Van Der Werf and Paus, 2006) or indirectly (Rosanova et al., 2009) activated by a TMS pulse. Moreover, the surgical lesion of motor thalamic nuclei have been shown to significantly reduce the EEG oscillations in the beta band (15-30 Hz) that are typically evoked by the stimulation of the primary motor cortex (Van Der Werf et al., 2006). On the other hand, TMS-evoked oscillations appeared to be linked to information transmission within the corticothalamic system. Thus, during deep sleep (Massimini et al., 2005) and deep sedation induced with midazolam (Ferrarelli et al., 2010), the sustained TMS-evoked oscillations recorded in wakefulness are reduced together with effective intracortical interactions. Similarly, a decrease in TMS-evoked potentials in the γ-band (30-50 Hz) and a reduced spreading of activation have been observed in schizophrenic patients as compared to healthy controls (Ferrarelli et al., 2008). These measurements suggest a tight link between TMS-evoked oscillations and corticocortical connectivity. Thus, novel analytical tools designed to study the origin, the time onset and the time-course of TMS-evoked EEG oscillations in different frequency bands may contribute to reveal the mechanisms of information transfer among cortical oscillators.

Several methods are available to decompose event-related EEG oscillations in the time-frequency domain and the most used ones are based on the Wavelet Transform (WT) (Delorme and Makeig, 2004; Pfurtscheller and Aranibar, 1979). Although WT-based algorithms have been useful to study the frequency content of TMS-evoked EEG oscillations (Ferrarelli et al., 2008; Rosanova et al., 2009), they present some limitations (Huang et al., 1998). In particular, it is difficult to exactly localize a single oscillatory event contemporarily in time and frequency. Indeed, every individual wavelet (the basis function of WT-based

algorithms) that is well-defined in frequency cannot be localized in a well-defined time window and vice versa.

To overcome this issue, in this work we developed a novel algorithm based on the Hilbert-Huang Transform (HHT) (Huang et al., 1998) to decompose TMS-evoked EEG oscillations with high resolution simultaneously in time and frequency domains.

2.3.1 – Theoretical background: the Hilbert-Huang transform (HHT)

This paragraph summarizes the analytical features of HHT (for a more detailed description refer to Huang *et al*. (2003)). HHT was implemented with MATLAB (The MathWorks, Natick, MA) by customizing a script freely available (http://perso.ens-lyon.fr/patrick.flandrin/emd.html). HHT is based on EMD and Hilbert transform. We applied EMD on single-trial and at a single-channel level in order to decompose each trial into a set of oscillatory components (IMFs). Then, Hilbert Spectra (HS) were computed for every IMF of each TMS/EEG trial and summated. Finally, HS for a set of trials (a single TMS/EEG session) was obtained by averaging individual HS across trials.

Empirical Mode Decomposition. EMD is the first step of HHT and consists in decomposing a time-series into a finite number of components, labelled Intrinsic Mode Functions (IMFs). This name indicates the oscillation mode embedded in the data (Huang et al., 1998). Each component can be defined as IMF satisfying the following two constraints: (1) the number of extrema and the number of zero-crossings must either be equal or differ at most by one; (2) at any data sample, the mean value of the two envelopes defined respectively by local maxima and local minima must be zero (Huang et al., 1998). IMFs are extracted from the original signal by means of *sifting,* which is the core of EMD. For an arbitrary time series *x(t)*, the sifting process starts with the identification of all extrema and then connects all the local maxima using a cubic spline (upper envelope) and similarly all the local minima (lower envelope). The first proto-IMF can be computed from the mean of the upper and lower envelope m_1 as follows:

$$h_1(t) = x(t) - m_1(t).$$

h_1 is labeled proto-IMF because it does not necessarily satisfy the rigorous constraints that define an IMF. Therefore, the sifting process is applied again on h_1:

$$h_1(t) - m_{11}(t) = h_{11}(t),$$

where m_{11} is the mean of the upper and lower envelopes of h_1. This process is generally reiterated k times until eventually h_{1k} obtained as:

$$h_{1(k-1)}(t) - m_{1k}(t) = h_{1k}(t)$$

is an IMF ($c_1(t) = h_{1k}(t)$). k is the number of iterations that allows h_{1k} to satisfy the stoppage criterion of the sifting process. In this work we used the criterion proposed by Huang *et al.* (2003), i.e. we stopped sifting when the number of extrema was equal to the number of zero crossing for K successive sifting steps. K was chosen to minimize the orthogonal index (for details please refer to Huang *et al.*(2003)). Once the first IMF $c_1(t)$is extracted from the original time series $x(t)$, the residual part $r(t)$ of the signal:

$$x(t) - c_1(t) = r_1(t)$$

can be treated as the new time series to be sifted as described above, in order to obtain a slower IMF.

The whole process has to be reiterated n times until the residue r_n is a monotonic function or a function with only one extremum. At the end of EMD analysis, the original signal $x(t)$ can be represented as the sum of n IMFs plus a residue:

$$x(t) = \sum_{i=1}^{n} c_i(t) + r_n(t).$$

Hilbert Transform. HT is the second step of HHT. It allows to express the non-stationarity of a signal through the computation of the instantaneous frequency and the instantaneous amplitude, i.e. the time-frequency-energy Hilbert Spectrum (HS). HT of a given time series *x(t)* can be computed as:

$$y(t) = \frac{1}{\pi} \rho \int_{-\infty}^{\infty} \frac{x(t')}{(t - t')} dt',$$

where *ρ* is the Cauchy principal value. *y(t)* exists for any function of L^{ρ}class. *x(t)* and *y(t)* together can be represented as a complex number *z(t)*:

$$z(t) = x(t) + iy(t) = a(t)e^{i\theta(t)},$$

where *i* is the imaginary unit and

$$a(t) = [x^2(t) + y^2(t)]^{1/2} \quad \text{and} \quad \theta(t) = \arctan\{ y(t)/x(t) \}.$$

a(t) is the instantaneous amplitude, while *θ(t)* is the instantaneous phase. Instantaneous frequency *f(t)* can be obtained as:

$$f(t) = d\theta(t)/dt .$$

A large theoretical discussion on this definition of frequency is given by Huang et al. (1998). Here we report that using EMD together with HT, it is possible to calculate time by time the periodicity (i.e. the instantaneous frequency, the frequency in a sense) of a non-stationary

signal (e.g. TMS-EEG evoked potentials) generated by a non-linear system (e.g.the cerebral cortex).

Having both frequency and amplitude as function of time, the Hilbert Spectrum *S(f,t)* can be obtained by plotting the amplitude (or the energy, i.e. amplitude square) in the time-frequency plane.

2.3.2 – HHT analysis protocol of TMS-EEG data

HHT was applied to sets of single-trial TMS-evoked responses recorded from single EEG channels. Figure 2.3.1 displays an example of the whole procedure applied to a sample trial (black trace, panel A), that was recorded from a parieto-occipital electrode (PO3) during TMS of left BA19 in a healthy volunteer. The time-frequency HS of this trial (panel B) was obtained by cumulating the HS of all the 6 IMFs obtained by the application of EMD (blue traces – Figure2.6A).

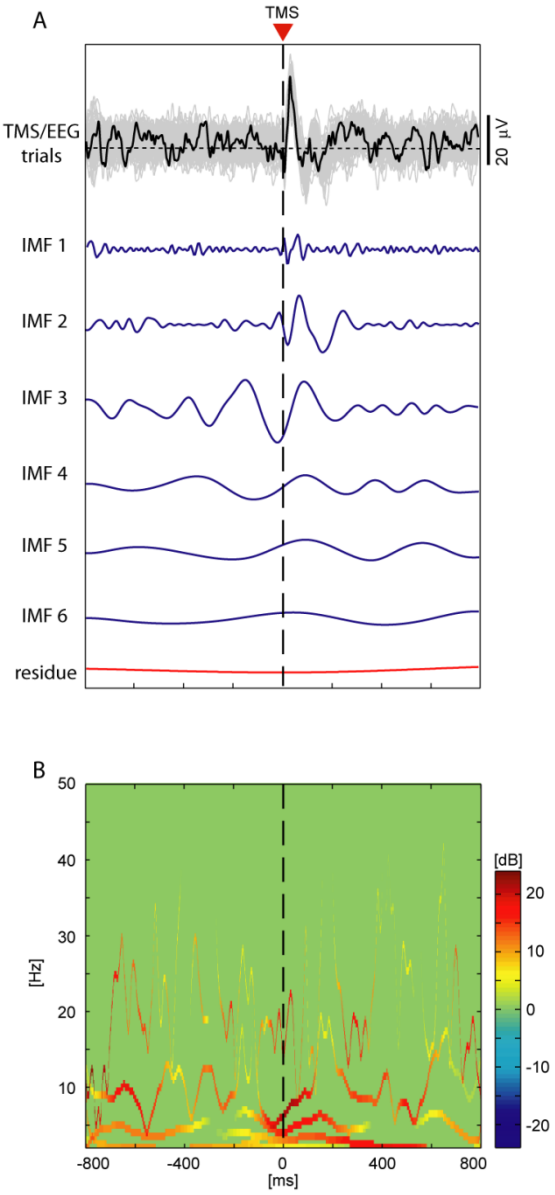

Figure 2.3.1. Hilbert-Huang transform applied to one TMS/EEG trial.
A. The grey traces represent the TMS/EEG trials (800 ms before and after the stimulus) recorded at the electrode under the stimulator (PO3) while TMS (120 V/m) is applied to the occipital cortex (left BA19) stimulated at of a healthy subject. Each blue trace represents a single IMF (in this case IMFs are six and are labelled with numbers from 1 to 6) computed by applying the Empirical Mode Decomposition (EMD) to a single TMS/EEG trial (black trace). The bottom red trace is the residue of the EMD sifting process of the IMFs. The vertical dashed line marks the time of stimulation. **B.** For each IMF the Hilbert Spectrum (HS) is calculated. The power for each time-frequency bin is cumulated over the six Hilbert Spectra (one for each IMF), plotted on the time-frequency plain and colour coded depending on the intensity (dB). The vertical dashed line marks the time of stimulation.

It should be noted that the number of IMFs changes across trials and is usually between 4-12. By averaging the HS of all single trials of the same session (grey traces, Figure 2.3.1A), it is possible to obtain the HS shown in Figure 2.3.2A. Additionally, Figure 2.3.2B displays the same averaged HS after statistical analysis, i.e. with all non-significant elements set to zero. Significance of deviations from baseline power is assessed using the bootstrap method

implemented in EEGLab (Delorme and Makeig, 2004). In particular, a surrogate data distribution is constructed by selecting spectral estimates for each trial from randomly selected latency windows of the baseline and then averaging these. This process was applied 200 times producing a surrogate baseline. The amplitude distribution of this surrogate baseline was computed and the specified percentiles (α) have been taken as significance thresholds. Here α is set to 0.05. Finally, Figure 2.3.2C illustrate the percentage of trials that contribute to form the statistically significant HS shown in Figure 2.3.2B.

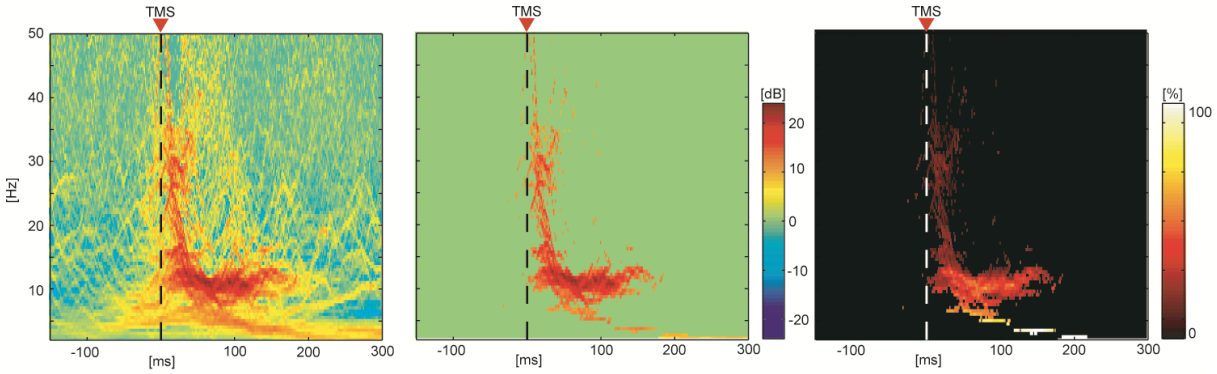

Figure 2.3.2. Time-frequency decomposition of EEG responses to TMS computed by means of the Hilbert-Huang transform.
The plot on the left side shows the time-frequency decomposition computed for all the trials collected during one TMS/EEG session (same session shown in Figure 1A) by means of the procedure shown in Figure 1 (EMD followed by Hilbert Spectrum). Hilbert Spectrum computed by averaging the HS of all single trials plotted in Figure 1A (grey traces). Application of bootstrap-based statistics to the HS shown in the left panel (α=0.05 and P=1000). Spectral energy not significantly evoked by TMS pulses is set to zero.

Setting time-frequency resolution. The time-frequency resolution of HS can be selected according to specific analysis needs and can be set independently for time and frequency. In the present work, we optimally exploited the time resolution of HS because we were specifically interested in the temporally precise identification of frequency changes of EEG oscillations. In particular, the number of time bins was set to 1161, corresponding to the number of time samples of the original signal (trials lasted 1600 ms and were sampled at 725 Hz): therefore, time resolution was 1.378 ms. Regarding the frequency, on the other hand, since we compute the Hilbert Spectrum of TMS-evoked potentials by cumulating single-trial HS, forcing the frequency resolution would produce an unwanted fragmentation of the spectral energy distribution in the time-frequency plane due to the high inter-trial variability of

the time-frequency localization of energy. Hence, we have chosen a resolution in frequency that guaranteed the best visualization of the spectral activations evoked by the TMS pulse. In particular, we set the number of frequency bins to 152, thus obtaining a frequency resolution of 0.5 Hz (given 78 Hz range of band-pass filtering 2-80 Hz, see Data processing paragraph).

2.3.3 - Time-frequency decomposition of simulated signals

TMS is known to trigger EEG oscillations with amplitudes and in frequency bands that mostly depend on the cortical site and the intensity of stimulation (Kahkonen et al., 2005a, b; Rosanova et al., 2009; Van Der Werf and Paus, 2006). However, even under controlled conditions, TMS-evoked oscillations present several unknowns, such as the onset, the amplitude and the duration of oscillations triggered in different frequency bands. Moreover, EEG signals triggered by TMS, although oscillating preferentially around one dominant frequency, are a mixture of oscillations in different frequency bands (Rosanova et al., 2009). Thus, TMS-evoked potentials are not appropriate to quantify the performance of a novel method of time-frequency spectral analysis. For this reason, we have tested the accuracy and the precision of the HHT-based algorithm and of the WWT-based one by applying both on simulated oscillatory signals.

Simulated signals were organized in three datasets called Alpha, Beta and Gamma and containing simulated signals respectively in the EEG α-band (8-13 Hz), in the EEG β-band (13-30 Hz) and in the EEG γ- band (30-50 Hz). Each trial has a duration of 1600 ms (-800/+800 ms; sampling rate: 750 Hz) and was generated by summating a colored noise signal (white noise processed using a bank of filters randomly varying between 8 and 50 Hz) and a sinusoidal signal starting at 800 ms (timepoint=0) and lasting for 350 ms with a frequency ranging from 8 to 13 Hz for dataset Alpha, from 13 to 30 for dataset Beta and from 30 to 50 Hz for dataset Gamma. The amplitude of the sinusoids (from 0 to 350 ms) was systematically increased in order to obtain a SNR varying from 1 to 10. Trials with the same SNR were grouped within the same subset. Overall, 30 subsets of 150 simulated trials were generated (3 frequency bands X 10 SNRs).

HHT and WT-based spectra were calculated for all subsets of trials and statistical significance ($p<0.05$) of spectral activations was assessed by performing a bootstrap statistical test (EEGlab).

Figure 2.3.3 shows the simulated trials, the HHT-based spectra and the WT-based spectra for respectively the dataset Alpha (panel A), the dataset Beta (panel A') and the dataset Gamma (panel A'') at three different SNR (SNR=2; SNR=5; SNR=7). From the examples shown in Figure 3.3, it is evident that significant activations in the HHT spectra are confined within the Region of Interest (dashed lines) defined by the parameters used to generate the simulated signals, such as a duration of 350 ms starting from the time 0 and a frequency span limited to the γ band for the Dataset Gamma, to the β band for the Dataset Beta and to the α band for the Dataset Alpha. On the contrary, WT-based spectra in all cases detected significant activations above and beyond the borders of the ROIs. From Panels A, A' and A'' of the Figure 2.3.3 it is also clear that while WT-based spectra start before time 0, HHT-based spectra detect significant activations right after, and never before, the start of the simulated oscillations.

In order to quantify the differences between the performances of the HHT and the WT spectra we computed for all the 30 simulated subsets the Youden Index (YI)(Youden, 1950) and the Positive Predictive Value (PPV)(Altman and Bland, 1994) that are typically used to measure respectively the statistical accuracy (ratio between the true positive values and all the positive values) and the statistical precision (sum of sensitivity and specificity minus 1) of a diagnostic test. To do so the spectral activations were first transformed into binary values (significant activation=1; non-significant activation=0). Second, for every dataset we defined three time-frequency rectangular Regions Of Interest (ROI) with different dimensions and spectral localization depending on the dataset. ROIs for α band the area between 8 and 13 Hz in frequency, and between 0 and 350 ms in time). Ideally, the points inside the ROI had to be positive (value=1) and the points falling outside the ROI had to be negative (value=0). On this basis we defined:

- true positive (TP): points inside the ROI correctly positive,
- true negative (TN): points outside the ROI correctly negative,
- false positive (FP): points outside the ROI incorrectly positive,
- false negative (FN): points inside the ROI incorrectly negative.

Using these values we calculated the Youden Index (YI) as:

$$YI = Sensitivity + Specificity - 1 = \frac{TP}{P} + \frac{TN}{N} - 1$$

and the Positive Predictive Value (PPV) as:

$$PPV = \frac{TP}{(TP + FP)}.$$

Resulting YI and PPV are shown in Figure 2.3.3B. The plots were achieved by calculating YI and PPV for SNR from 1 to 10 (real numbers). Red lines refer to γ band, green lines refer to β band, blue lines refer to α band. These data allowed to assert that HHT is less robust than WT and their performances depend severely to SNR and to the frequency band considered. On the other hand, HS are more precise than WT-based spectra for SNR higher than 3. Moreover, since the SNR of TMS-EEG single-trial data considered in this manuscript is always between 5 and 7 (see for example the signals in Figure1), we can assert that, for this kind of data, that HHT is more informative than WT. Provided that SNR is above 3, the HHT-based algorithm showed accuracy values (YI) higher than the ones scored by the WT-based one except for oscillations in the gamma band.

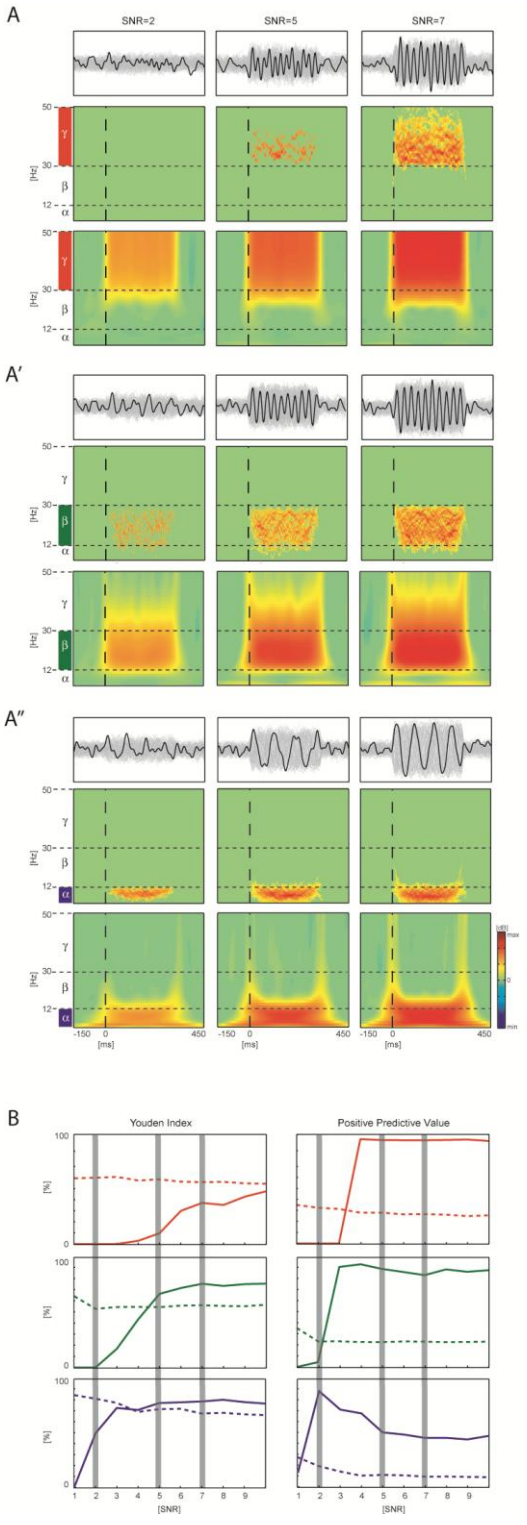

Figure 2.3.3. Simulated signals are used to compare the performance of HHT-based and WT-based time-frequency decomposition procedures.

From left to right are shown simulated EEG oscillations (grey traces and black traces) in the gamma band (30-50 Hz) (panel A'), in the beta band (13-30 Hz) (panel A'') and in the alpha band (8-13 Hz) (panel A''') computed with three different Signal to Noise ratios (SNR=2 on the left column; SNR=5 on the middle column; SNR=7 on the right column). Color plots show the time-frequency decomposition calculated by means of a HHT-based algorithm (upper plots in each panel) and WT-based algorithm (lower plots in each panel). Graphs of Panel B represent the Youden index (performance of the algorithm) and the Positive predictive value (precision of the algorithm) calculated for SNR ranging from 1 to 10. Dashed and continuous lines represent the values of the two indices calculated respectively for the HHT-based algorithm and for the WT-based algorithm (red for gamma oscillations, green for beta oscillations and blue for alpha oscillations).

2.3.4 - HHT detects the time onset of TMS-evoked EEG oscillations in α, β and γ frequency bands

Figure 2.3.4 shows TMS-evoked potentials (blue traces of panels A and B) recorded at the electrode under the stimulator and at distant electrodes when the occipital cortex (panels A and A') and the frontal cortex (panels B and B') are targeted. For the two experimental conditions and the two recording sites we have computed the HHT-based and the WT-based time-frequency spectra. Both the methods revealed a different distribution of power across frequency bands depending on the site of stimulation and recording: TMS of the occipital area (BA19) triggered immediate, short lasting oscillations, in the γ-band (30-50 Hz) and, at the same time, slower oscillations, mostly confined in the *α*-band (8-13 Hz) and lasting about 200 ms. On the other hand, TMS of the frontal cortex triggered early oscillations in the γ-band (30-50 Hz) followed by oscillations in the *α*-band (8-13 Hz). However, while the WT-based algorithm detects significant activations already before the TMS pulse, the HHT-based algorithm detects significant activations only after the TMS pulse. This effect can be attributed to the low time resolution of WT, particularly evident for slow oscillations, and represents an aberration of this approach. Indeed, the Heisenberg–Gabor inequality (Auger and Flandrin, 1995; Peng et al., 2005) imposes that time-frequency resolution of WT-based spectra depends directly on two factors that vary with stretching and shifting the mother wavelet. In particular, time resolution of spectral energy gets worse when WT is applied to lower frequency bands.

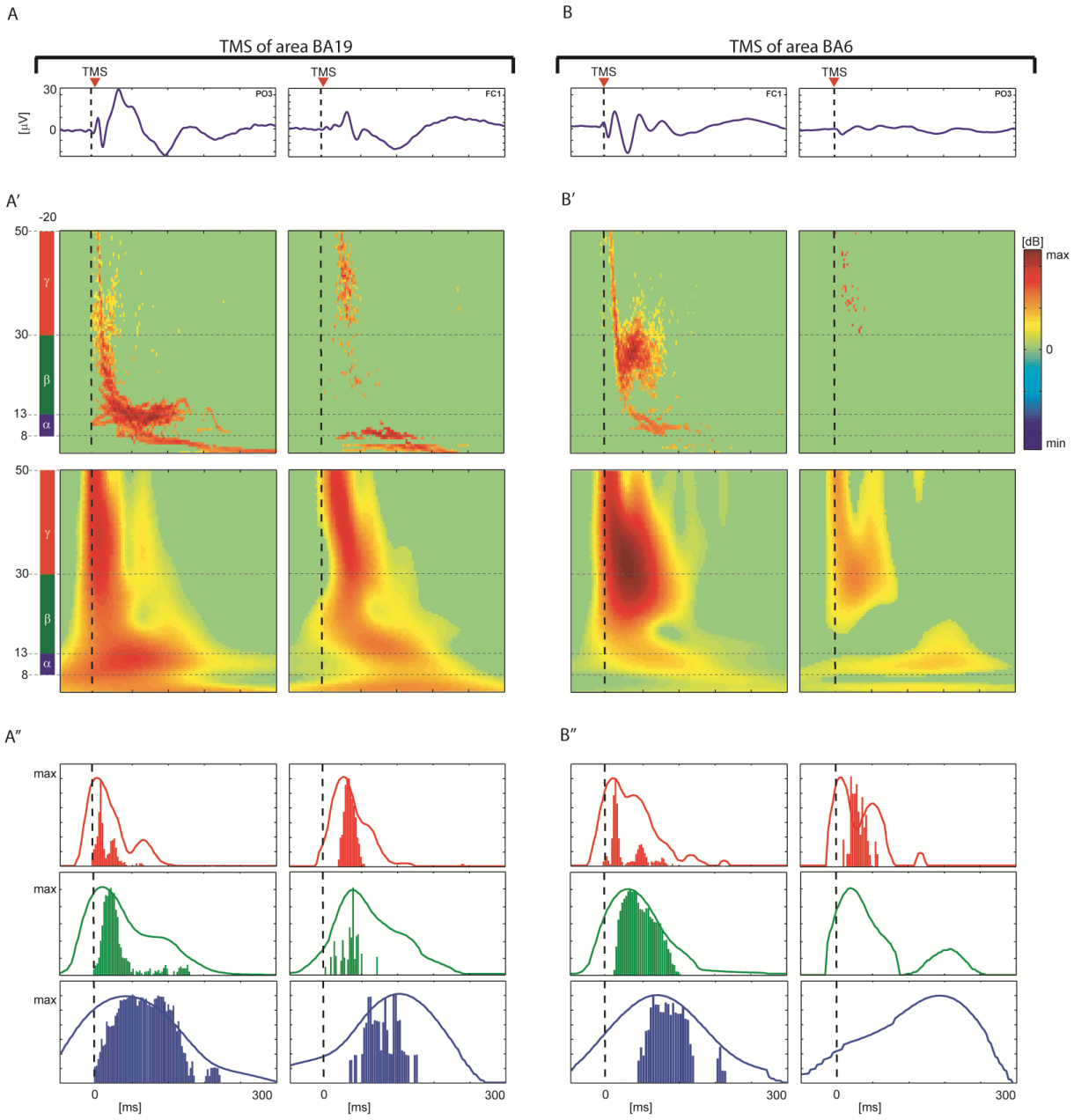

Figure 2.3.4. Time-frequency decomposition based on the Hilbert-Huang transform allows to detect the onset of TMS-evoked EEG rhythms.
Upper panels show TMS-evoked potentials (blue traces) recorded at the electrode under the stimulator (left side) and at a distant one (right side) when the occipital area BA19 (Panel A) and the frontal area BA6 (Panel B) are respectively stimulated. Panels A' and B' show the corresponding time-frequency decompositions computed by means of the Hilbert-Huang transform (upper plots) and on the Wavelet transform (lower plots). Panels A'' and B'' show the time course of the spectral energy for the electrode under the stimulator and for the distant one cumulated across three classical EEG frequency bands (α in blue, β in green, γ in red) and normalized by the total energy of each band in the time interval 0-200 ms. Histograms refer to the energy spectra computed by means of HHT and have a temporal resolution of 1.378 ms. Superimposed traces have been obtained by applying WT. Note that only the spectral profiles calculated based on the Hilbert-Huang transform time-frequency decompostion allow to detect the onset of TMS-evoked oscillations in the α, β and γ bands.

In order to better quantify the different performance between WT and HHT algorithms (Figure 2.3.4, panels A'' and B'') we wanted to extract the time courses of TMS-evoked oscillations in the α, β and γ EEG frequency bands. To do so, we cumulated the spectral power across the

frequency bins corresponding to these EEG frequency bands and we plotted the obtained values on the graph as solid lines for WT and bar histograms for HHT (red for α-band:, green for the β-band and blue for γ-band). Both algorithms reliably detected the latency of the energy peak in each EEG band, yet only the HHT was able to capture the time onset of each EEG rhythm. This, in turn, makes clear that when the occipital cortex is stimulated, oscillations in the α, β and γ EEG frequency bands arise simultaneously under the coil after the TMS pulse and with no time lag. Moreover, at a distant site from the stimulated one (frontal electrode), HHT spectra show clearly that oscillations in the γ band arise first and are followed by oscillations in the β and α bands. A similar pattern can be observed when the frontal cortex is stimulated for the oscillations evoked under the coil, while at distant sites significant activations can be detected only in the γ band. These results are highly reproducible across subjects (Figure 2.3.5).

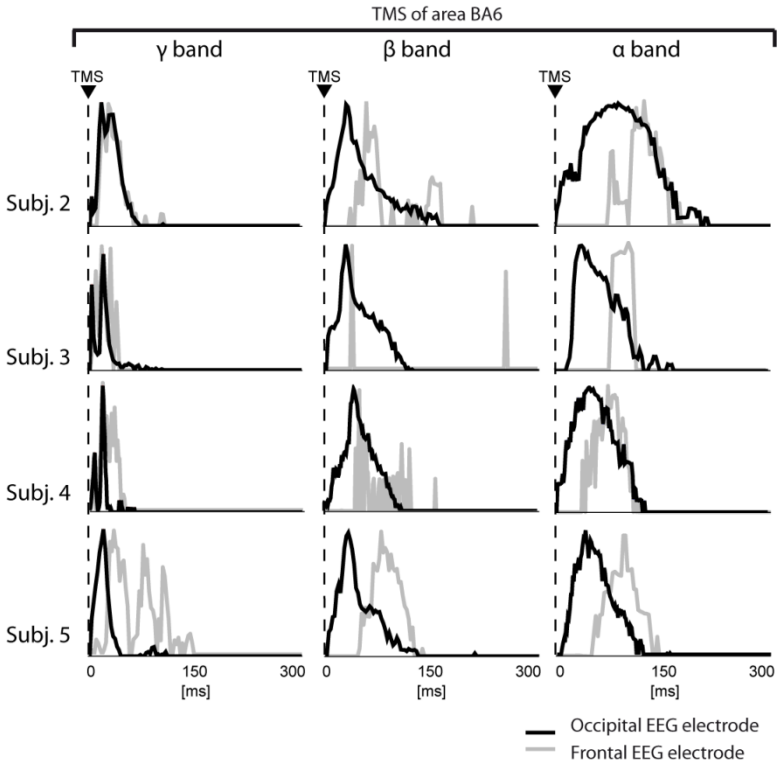

Figure 2.3.5. Inter-individual reproducibility of the time course of spectral energy of the α, β, and γ bands, computed by HHT from scalp potentials evoked by TMS of BA19.
Each trace represents the temporal profile of the HS, integrated over the γ, β and α bands, computed on the potentials evoked by stimulation of BA19 at 120V/m. Black traces refer to the results obtained from electrode PO3, while grey traces refer to electrode FC1. Results are displayed for the remaining 4 healthy subjects (results for subject 1 were already displayed in Figure 2.3.4).

Despite its limitations, WT remain the elective tool to study temporal evolution of oscillations evoked by TMS. For instance in a previous study we have shown, by means of this method of time-frequency decomposition, that that the main frequency of TMS-evoked EEG oscillations depends on the site of stimulation and that this frequency, the "natural frequency", reflects local properties of cortico-thalamic circuits (Rosanova et al., 2009). Thanks to the higher time resolution of HHT-based algorithm in a wide range of frequencies, we can confirm and extend these findings. Indeed, HHT allows to precisely detect the time lag between the rhythms forming the TMS-evoked potential. For instance, for the occipital stimulation the onset of every EEG rhythm is delayed at the frontal electrode as compared to the occipital one. Moreover, both for the occipital and frontal stimulation, the first oscillations to be evoked by the TMS are in the γ band followed by the slower ones. This difference, according to Von Stein *et al.* (2000), can be explained with different time of recruitment.

2.3.5 - Application of the Hilbert-Huang Transform to TMS/EEG data affected by large magnetic artifacts

TMS often induces electromagnetic artefacts that can make difficult the interpretation of TMS-evoked EEG oscillations. This is especially true for the analysis of TMS-evoked EEG oscillations in the time-frequency domain. Figure 2.3.6 shows a TMS-evoked response (Panel A) recorded after the stimulation of the motor cortex in a healthy subject and corrupted by a large electromagnetic artefact (50 μV), yet early and fast (0-20 ms). The time-frequency spectrum calculated by means of WT-based algorithm is affected by the short-lasting artefact for up to 250 ms that started even before the stimulation. On the contrary, the time-frequency spectrum computed by means of the HHT-based algorithm shows significant activations due to the artefact only in the first 20 ms.

Recently, it has been proven that the frontal cortical area of schizophrenic patients responds to TMS with EEG oscillations in the γ band significantly smaller than the ones recorded in healthy subjects (Ferrarelli et al., 2008). However, TMS-evoked potentials recorded from the

frontal cortex are often corrupted by electromagnetic or muscle artefacts that can make difficult the interpretation of time-frequency spectra. Thus, we have further compared the performances of WT-based and HHT-based algorithms by applying them to the following data: TMS-evoked potentials recorded after stimulation of a frontal area in a schizophrenic subject (Figure 2.3.6, Panel B) and affected by an early (0-20 ms) and large (20 μV) electromagnetic artefact; and to TMS-evoked artefact-free potentials recorded after stimulation of a frontal cortical area in a healthy subject (Figure 11, Panel C). In the first case, despite the virtual absence of TMS-evoked γ-band oscillations, the WT-based spectrum shows significant activations in this frequency range, yet that are mostly due to the artefact component. On the contrary, both WT and HHT-based time-frequency spectra reliably detect prominent oscillations in the EEG γ-band when the frontal cortex of an healthy subject is stimulated.

Overall, HHT allows to detect the time onset of TMS-evoked oscillations in all frequency bands and on a millisecond timescale suggesting that it can be used to study the temporal dynamics of different TMS-evoked EEG rhythms where they are generated and at distant sites. This can contribute, in turn, to elucidate the mechanisms of intracortical information processing and transfer in healthy and pathological conditions. Finally, the time-frequency decomposition method presented here could also complement the available offline tools to minimize the impact of short lasting (magnetic or biological) artifacts often affecting TMS-evoked cortical responses.

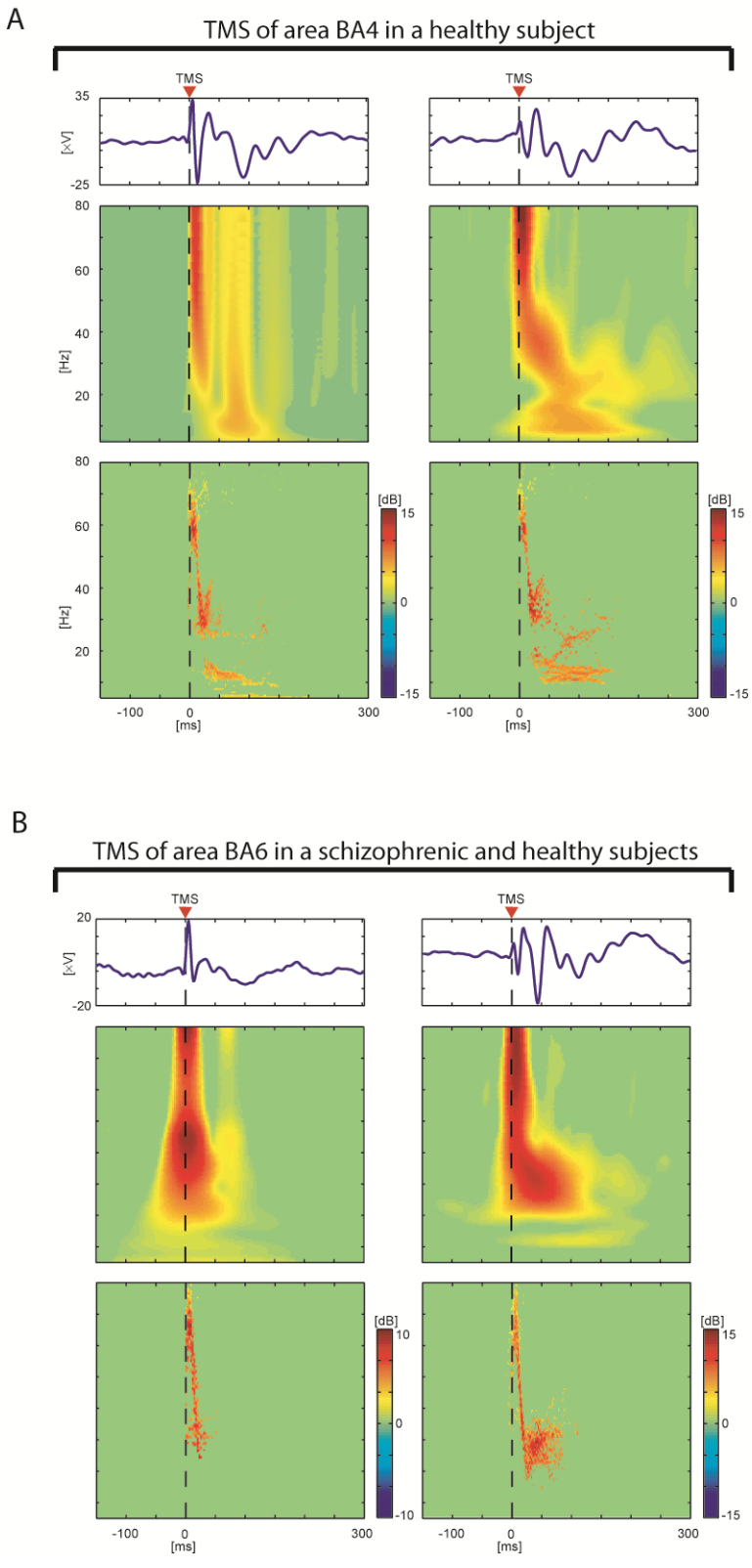

Figure 2.3.6. HHT applied to TMS-evoked responses affected by early artefact and recorded in a schizophrenic patient.

Panel A shows a TMS-evoked potential (blue trace) affected by a large (about 60 μV), early-latency (0-20 ms) artefact, recorded at the electrode FC1 during stimulation of BA6 in a healthy subject. Middle and lower plots show the time-frequency decomposition computed respectively by means of the HHT-based algorithm and the WT-based algorithm. **Panel B** shows TMS-evoked potentials recorded from electrode FC1 during stimulation of BA6 in a schizophrenic subject. Note that that the early-latency artefact is better isolated by HHT than by WT both in the time and frequency domains and that both HHT-based and WT-based time-frequency plots show a strong reduction of γ-band evoked activity in the schizophrenic patient as compared to a healthy subject (Figure 2.8).

2.4 – General indices to characterize the electrical response of the cerebral cortex to TMS

In a recent paper, Casali and colleagues (2010), has developed an automatic TMS/EEG data analysis package able to output three synthetic indices: significant current density (SCD), phase-locking (PL) and significant current scattering (SCS) (Figure 2.4.1). SCD sums up the amplitude of all significant currents induced by TMS, PL reflects the ability of TMS to reset the phase of ongoing cortical oscillations, while SCS measures the average distance of significantly activated sources from the site of stimulation. These indices are aimed at capturing different aspects of brain responsiveness, ranging from global cortical excitability towards global cortical connectivity. Casali et al. tested the three indices by analyzing the EEG responses to TMS of Brodmann's area 19 at increasing intensities in five healthy subjects. The spatial distribution and time course of SCD, PL and SCS revealed a reproducible profile of excitability and connectivity, characterized by a local activation threshold around a TMS-induced electric field of 50 V/m and by a selective propagation of TMS-evoked activation from occipital to ipsilateral frontal areas that reached a maximum at 70–100 ms. In principle, SCD, bPL and SCS may be used to characterize the effects of TMS on any cortical area and to quantitatively evaluate cortical excitability and connectivity in physiological and pathological conditions. Similar indices that enable data reduction and straightforward comparisons of TMS-evoked activations across subjects and conditions should be developed.

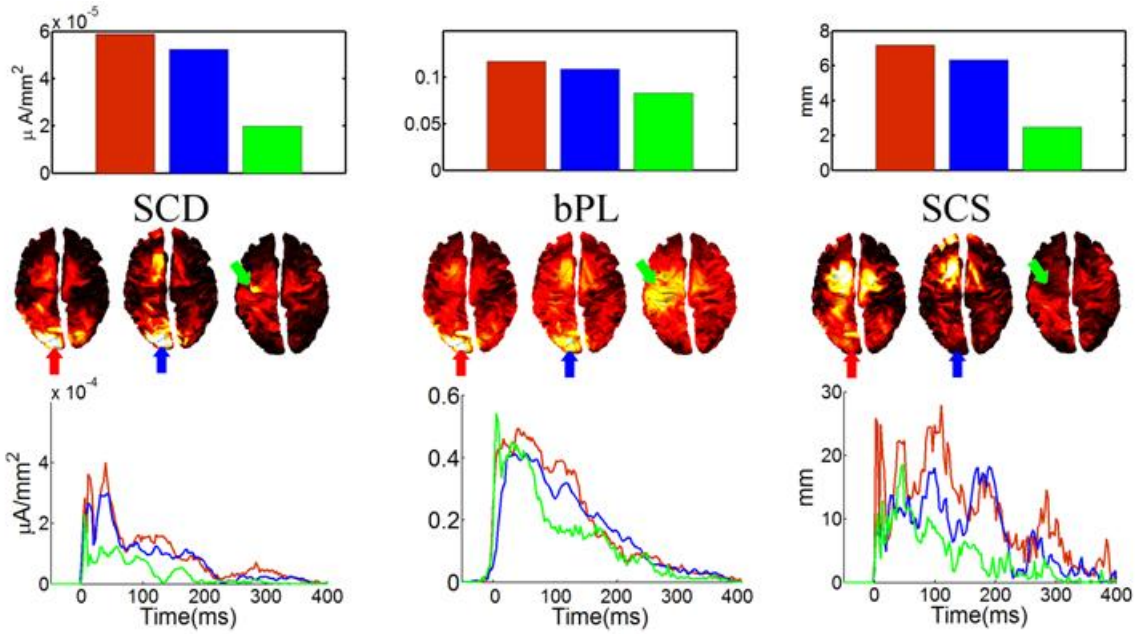

Figure 2.4.1. Indices of cortical excitability and effective connectivity.
Computation of synthetic indices of cortical responsiveness to TMS in a single subject at a stimulation 140 V/m delivered to the left occipital cortex in two different days (red and blue colors, respectively) and to the left hand motor area (green color). Source Current Density (**SCD**), Broadband Phase-Locking (bPL) and Source Current Scattering (SCS) values are cumulated either over the whole brain (time courses) or over the full post-stimulus period (spatial maps) or over both the whole brain and the post-stimulus period (bars), (adapted from Casali et al. 2010)

2.5 – TMS/hd-EEG as a tool to measure changes in the level of consciousness

The previous paragraphs described how to employ the combination of TMS and hd-EEG to perturb directly, in a controlled and reproducible way, specific cortical areas and measure the corresponding neural responses that reflect causal patterns of interaction between different groups of neurons in the thalamocortical system. What then can be said about such responses evoked by TMS in conditions such as alert wakefulness, in which consciousness is unambiguously present, or when it is clearly reduced, such as during deep sleep, anesthesia and vegetative state? In this paragraph we will show that the causal interaction of different connected neuronal modules with specific oscillatory frequencies produces qualitatively complex patterns of cortical response to TMS during alert wakefulness. We will also show that this ability of the thalamocortical system to sustain complexity is consistently impaired among unconscious healthy subjects and brain-injured patients.

2.5.1 – Alert Wakefulness

The Natural Frequencies of Corticothalamic Circuits. A system of causally interacting neurons can be generally thought as a set of coupled electrical oscillators. It is well known that the perturbation of coupled oscillators may reveal the tuning frequency, or "natural frequency" of the system, which, in turn, indicates structural properties of the state of the system under study. In Rosanova et al. (2009) we employed TMS/hd-EEG to measure the natural frequencies of different corticothalamic modules in awake healthy subjects. We targeted TMS to three different cortical areas (BAs 19, 7 and 6) of 6 subjects, stimulating each cortical area at 8 different intensities (range: 20-160 V/m). During the experiment, subjects were lying on an ergonomic chair, relaxed and with eyes open looking at a fixation point on a screen. For each intensity we delivered between 100 and 200 stimuli at a frequency jittering between 0.4-0.5 Hz (period: 2000 plus a jitter ≤ 300 ms).

Figure 2.5.1 displays the EEG responses recorded in one subject from all sensors after stimulation of area 19, area 7 and area 6 at 120V/m on the cortical surface. The butterfly plots reveal that the brain electrical response to TMS varied markedly depending on the site of stimulation: following an early (0-20 ms) stereotypical sharp component, TMS of area 19 resulted, during the first 200 ms, in a low frequency, large response; stimulation of area 7 elicited faster and smaller components; and stimulation of area 6 evoked the fastest EEG oscillations.

In order to detect the frequency of the oscillations induced by TMS at different cortical sites, we calculated the Event Related Spectral Perturbation (ERSP) based on Morlet wavelets. The procedure was implemented using the public license toolbox EEGLAB (Delorme and Makeig, 2004). ERSP decomposes the EEG response recorded from each sensor in the time-frequency space and allows tracking the significant spectral modulations induced by TMS during the post-stimulus time. We averaged, for each condition, the ERSPs matrices across all channels in order to obtain a global-ERSP (gERSP). The bottom panels of Figure 2.5.1 display the resulting plots for the three stimulation sites. In all cases, TMS resulted in a significant early (8-20 ms) activation in the β_2/γ bands (21-50 Hz). After this short-lasting

stereotypical event, the frequency content of the global brain response to TMS varied markedly depending on the stimulated area: dominant oscillations in the α range (8-12 Hz) were detected when area 19 was stimulated, in the β_1 range (13-20 Hz) when area 7 was stimulated and in the β_2/γ range (21-50 Hz) when area 6 was stimulated.

In order to extract the natural frequency associated to the TMS-evoked potentials in each condition, we averaged the gERSP in a time window between 20 and 200 ms post-stimulus, minimizing the effect of possible artifacts occurring at the time of stimulation. We detected, on the resulting spectral profiles (black trace on the right of each panel), the frequency with maximum power (indicated by a dotted line). Across all subject, at the intensity of 120 V/m, the natural frequency of the global scalp response to stimulation of area 19, area 7 and area 6 was 11 ± 1.5 Hz, 18.3 ± 2.0 Hz and 29 ± 2.0, respectively.

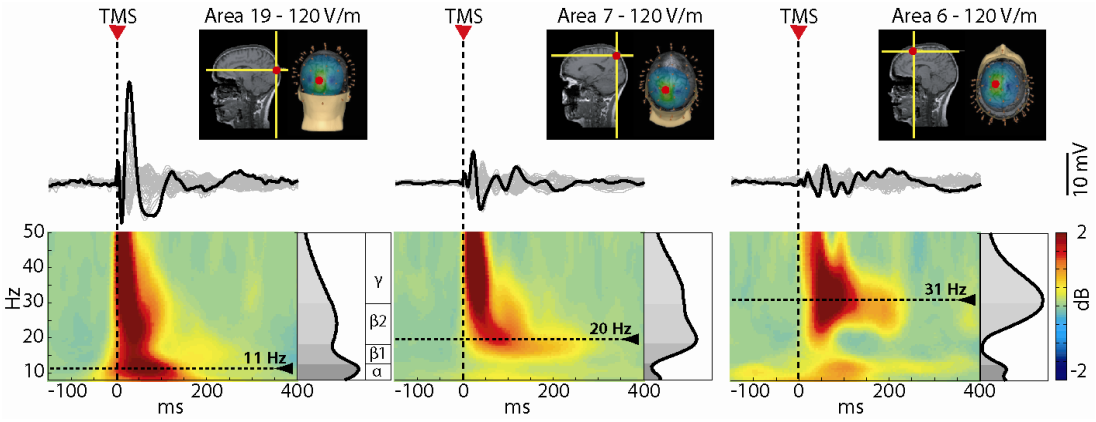

Figure 2.5.1: TMS induced global EEG oscillations that are specific for the stimulated site.
The figurine illustrates the 3 cortical sites targeted by TMS (hot spot on the individual MRI). The traces below represent butterfly plots; the black trace highlights the electrode directly underlying the stimulator. The bottom panels show the ERSP patterns calculated globally on the scalp (average of all electrodes). The rightmost graphs depict the power spectrum profile induced during the first 200ms after TMS. The dotted lines highlight the frequency with maximum power. TMS elicited early gamma components immediately followed by prominent alpha band oscillations after occipital stimulation, beta band oscillations after parietal stimulation and fast beta/gamma oscillations after perturbation of frontal cortex (adapted from Rosanova et al., 2009).

An important parameter that may potentially bias the frequency of the EEG response to TMS is the strength of the applied stimulus. We employed an MRI-guided navigation system to ensure that the strength of the electric field induced by TMS in different areas was always comparable. The maximum electric field was always kept on the convexity of the gyrus with the induced current perpendicular to its main axis. Moreover, in order to exclude an effect of

local activation thresholds in determining the observed site-specificity of the response's frequency, we probed each site at several different intensities, from sub-threshold levels to near-saturation levels. As shown in Figure 2.5.2, TMS intensities below 40 V/m did not result in any significant power modulation in any of the four EEG bands. Intensities of stimulation between 60 and 120 V/m evoked progressively larger responses in all four frequency bands. At this level the responses of the three corticothalamic modules clearly differed, displaying higher α band power after stimulation of area 19, higher β_1 band power after stimulation of area 7 and higher β_2/γ band power after stimulation of area 6. These differences further increased at stimulation intensities (140-160 V/m) that produced saturation of the TMS-evoked potentials. Thus, the specific frequency of the response did not depend on stimulation intensity, or activation threshold, but most likely depended on a number of endogenous properties of the activated circuit.

These results were reproducible in all subjects: provided that TMS intensity was above the threshold for triggering a significant EEG response, the average waveform differed according to the site of stimulation (Figure 2.5.3). Occipital stimulation triggered high-amplitude, lower-frequency components, while stimulating more rostral sites elicited smaller waves separated by shorter intervals. Panel B of Figure 2.5.3 shows the natural frequency calculated at the global sensor level in all subjects after stimulation of area 19, area 7 and area 6 at 160 V/m. In all cases, the natural frequency progressively increases from α, to β and γ when the three sites are plotted in the caudal-rostral order.

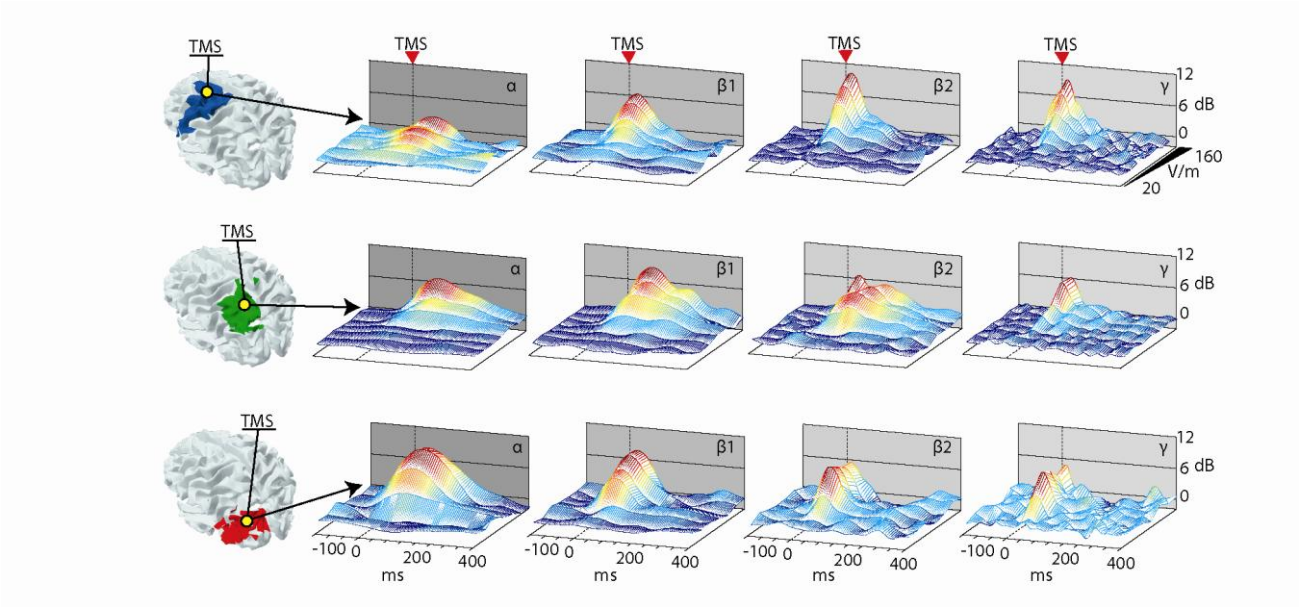

Figure 2.5.2: The specificity of natural frequencies was preserved with different stimulation intensities.
Time series (ERSP) of standard EEG frequency bands (alpha: 8-12; beta1: 13-19; beta2: 20-29; gamma: 30-50) for the three sites of stimulation (first row: area 6; second row: area 7; third row: area 19) are plotted as a function of stimulation intensity, ranging from 20 to 160 V/m (adapted from Rosanova et al., 2009).

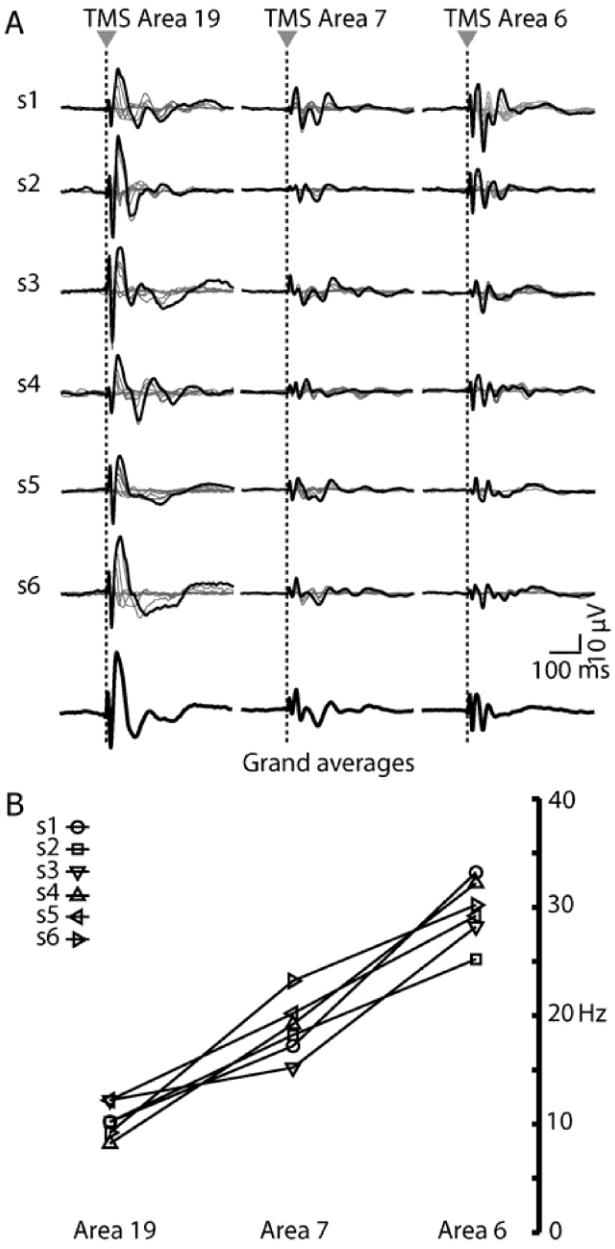

Figure 2.5.3: The specificity of the natural frequency was reproducible across subjects.
A) The traces represent TMS responses for each subject (n=6) evoked by 6-8 intensities of stimulation, recorded from one electrode underlying the stimulator. The black trace highlights the response obtained at maximal stimulation intensity (160 V/m). The thicker black traces at the bottom represent the grand averages calculated from all 6 subjects. **B)** The frequencies with maximum power, obtained by stimulating each cortical area at the maximal intensity, are plotted for each subject. A clear posterior-anterior gradient of increasing frequencies is observable (adapted from Rosanova et al., 2009).

Did these dominant frequencies, recorded globally over the scalp, reflect the frequencies of neural oscillations generated by TMS? Time series of local currents evoked by TMS activation were obtained, after source modeling and automatic classification of the individual's cortical surface, by cumulating the dipole activities recorded in each one of the 47 Brodmann's areas. At this point, the same time-frequency decomposition analysis performed at the global sensors level was carried out at the local source level. Figure 2.5.4 shows the

time series of the local current and the ERSP plots recorded from all three cortical areas of interest (area 19, area 7 and area 6) when TMS was directly applied to each of them. These sources, directly activated by TMS, generated strong currents matching the dominant frequency recorded globally at the scalp level. Moreover, even when not directly stimulated, each cortical area still tended to oscillate at a rate closer to its own natural frequency. Across all subjects, when area 19 was stimulated, area 19 responded at 10.8 Hz, area 7 at 20 Hz and area 6 at 31.3 Hz; when area 7 was stimulated, area 19 responded at 13.5 Hz, area 7 at 18.6 Hz and area 6 at 27.3 Hz; when area 6 was stimulated, area 19 responded at 10.6 Hz, area 7 at 19 Hz and area 6 at 29 Hz. Hence, each area, whether directly activated by TMS or engaged through long-range connections, expressed local oscillations at a rate closer to its own natural frequency.

The electrical rhythms triggered by TMS are more likely to reflect overall circuit properties at the level of whole cortical areas and connected thalamic/subcortical nuclei. For instance, a recent study has linked α oscillations to the presence of a subpopulation of electrically coupled neurons localized in the lateral geniculate nucleus that fire bursts of action potentials in the α range when activated by a cortical glutamatergic input (Hughes et al., 2004). This mechanism, involving a whole corticothalamic module, may explain why TMS of visual cortex readily triggers α oscillations, while TMS of frontal cortex fails to do so. Similarly a role of the thalamus can be postulated in the genesis of faster oscillations (Llinás et al., 2007). Interestingly, TMS/EEG experiments performed in patients with lesions in the ventrolateral thalamus have demonstrated a significant decrease of β band oscillations after TMS of the ipsi-lesional motor cortex (Van Der Werf et al., 2006). In this perspective, our results suggest that TMS is capable to engage the thalamocortical system of alert healthy subjects, setting in motion different connected neuronal oscillators and generating complex EEG responses composed of strong fluctuations at the natural frequency of the stimulated area and by weaker fluctuations at around the natural frequency of distant regions.

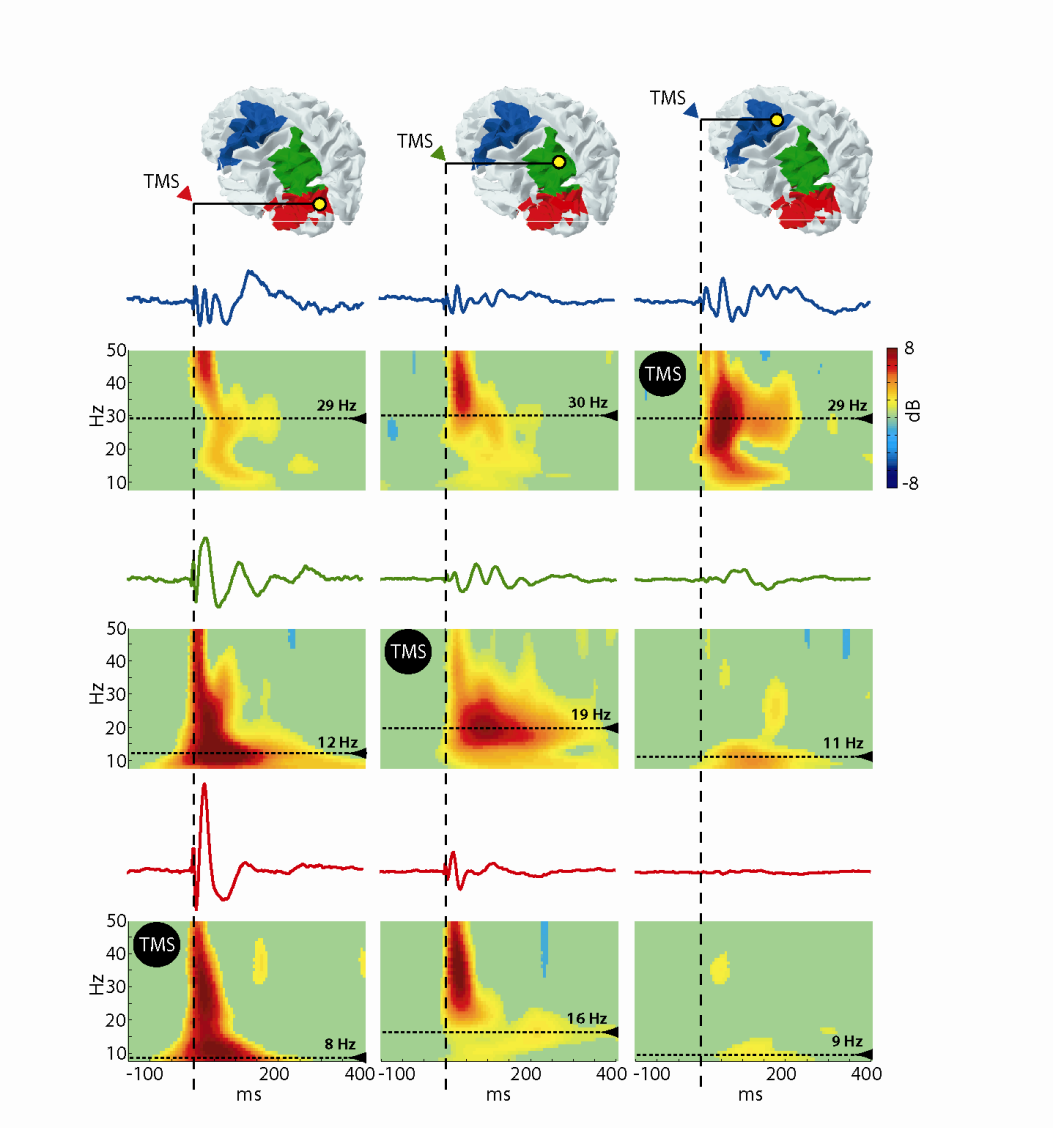

Figure 2.5.4: The natural frequency is a local property of individual thalamocortical modules.
The coloured patches on the cortical surface mark the areas from which cortical currents are recorded after source modeling. Below, time series and ERSP plots of local cortical currents are displayed for area 6 (first row, blue traces), area 7 (second row, green traces) and area 19 (third row, red traces) when area 19 was stimulated (first column), area 7 was stimulated (second column) and area 6 was stimulated (third column). The dotted lines highlight the peak frequency for each plot. Comparing the plots on the diagonal line marked by TMS icon, reveals that each cortical area responded with a clear-cut natural frequency when directly stimulated. Comparing the plots on the horizontal and on the vertical lines, reveals that the natural frequency is a local property that was partially preserved also when its cortical generator was not directly stimulated (adapted from Rosanova et al., 2009).

The Spatiotemporal Complexity of Cortical Activation Evoked by TMS during Wakefulness. As we saw in the first chapter, if the brain is to be regarded as the vehicle for the objects of consciousness, during alert wakefulness the thalamocortical system should be in a state of dynamical equilibrium, integrating activity across several neuronal modules through feedforward and feedback causal connections. Thus, if these widespread and specialized cortical areas have distinct intrinsic dynamical properties and are engaged at

different latencies, such complex reentrant system will likely be generating complex spatiotemporal patterns of causal activation. The results described in the previous section indicates that TMS/hd-EEG is capable of probing this capability of integration across neuronal modules, each one oscillating with its particular natural frequency, when TMS-evoked neural currents activated different areas of the cortex at different latencies. Figure 2.5.5 displays the significant neuronal currents evoked by TMS in a representative awake healthy subject. The black traces in the figure are the time-series for the Global Mean Field Power (GMFP) (Lehmann and Skrandies, 1980) calculated from the multichannel average signals as:

$$GMFP(t) = \sqrt{\frac{\sum_{i=1}^{k}(V_i(t) - \bar{V}(t))^2}{k}}$$

where *k* is the number of channels, V_i is the voltage measured with channel *i*, and $\overline{V}$ is the mean of the measured voltages across channels (average reference). The significant current distributions (SCD) are exhibited at latencies corresponding to high values of GMFP. TMS was targeted to BAs 6 (A), 7 (B) and 19 (C) at 100V/m. In all cases, TMS evoked a qualitatively complex spatiotemporal pattern of cortical currents: a series of low-amplitude waves of activity associated with cortical activations that propagated along long-range ipsilateral and transcallosal connections, lasting for around 300ms, and in which activity shifted through cortical areas in different times.

What does happen to these complex patterns of TMS-evoked activity when consciousness fades? Alterations in the membrane properties of subsets of cortical and subcortical (especially thalamic) neurons, as well as alterations in their patterns of connectivity may result in distinctive and detectable changes in the oscillatory properties of neuronal groups, possibly resulting in altered patterns of response to TMS. Hence, we ask in the following sections whether this complexity of neuronal response to TMS due to the integration of oscillators with different site-specific natural frequencies is preserved in states where

consciousness is lost, such as during sleep, anesthesia and in patients suffering from disorders of consciousness.

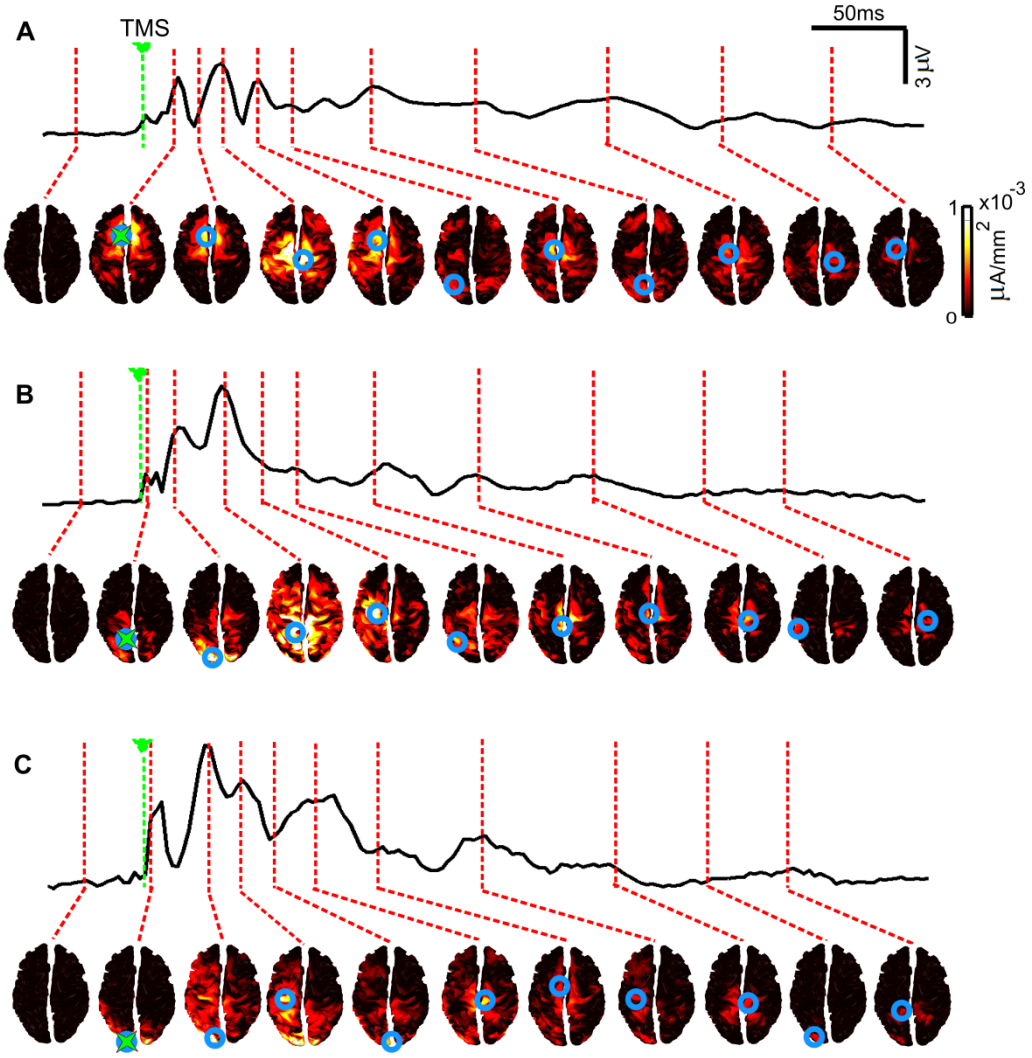

Figure 2.5.5: TMS evoked a balanced, long-range differentiated pattern of activation during wakefulness. hd-EEG GMFP (black traces) and SCD (cortical maps) are shown for a representative healthy subject during alert wakefulness with TMS (green star) target to BAs 6 (**A**), 7 (**B**) and 19 (**C**) at 100V/m. In all cases, TMS evoked a widespread activation pattern, which lasted for more than 300ms and in which the maximum significant current (blue circle) shifted through different cortical areas at different latencies.

2.5.2 – Sleep

The most common situation in which the level of consciousness changes is early NREM sleep, when subjects, if awakened, report no or little conscious experience (Hobson and Pace-Schott, 2002), despite the fact that their brain remains highly active (Steriade, 2001). In a series of studies Massimini et al. (2010, 2007, 2005) described the TMS-evoked responses during the transition from wakefulness into different stages of sleep. While during

wakefulness, TMS evoked an initial local cortical activation which invariably engaged distant cortical areas in a complex and differentiated way, the exactly same stimulation, applied 15 min later, during sleep stages 2 and 3, triggered a larger, low-frequency wave, associated with a strong initial cortical activation that did not propagate to connected brain regions, dissipating rapidly (Massimini et al., 2005). Increasing intensities of stimulation during NREM sleep may result in long-range bursts of cortical activity, but always associated to simple stereotypical and nonspecific responses (Massimini et al., 2007). Interestingly, during REM sleep, TMS triggered more complex patterns of cortical activation, resembling those observed in wakefulness (Massimini et al., 2010).

Slow-wave Sleep. Figure 2.5.6 shows our results reproducing the experiment of Massimini et al. (2005, 2007) for a subject submitted to TMS targeted to the sensory-motor cortex at 90V/m. A first TMS-EEG session (180 stimuli) was collected while the subject was awake. Subject was then allowed to fall asleep and after entering a consolidated period (>5 min) of NREM sleep stage 2, a second TMS-EEG session was collected using the same stimulation parameters. As expected, during wakefulness, averaging the TMS-locked responses revealed low-amplitude, high-frequency waves of activity associated with cortical activations that propagate along long-range ipsilateral and transcallosal connections (Figure 2.5.6A). The same stimulation however produced a slow, brief and local response during NREM sleep (Figure 2.5.6B). This finding is general and can be reproduced after the stimulation of different cortical areas, as long as the subjects are in slow-wave sleep stages.

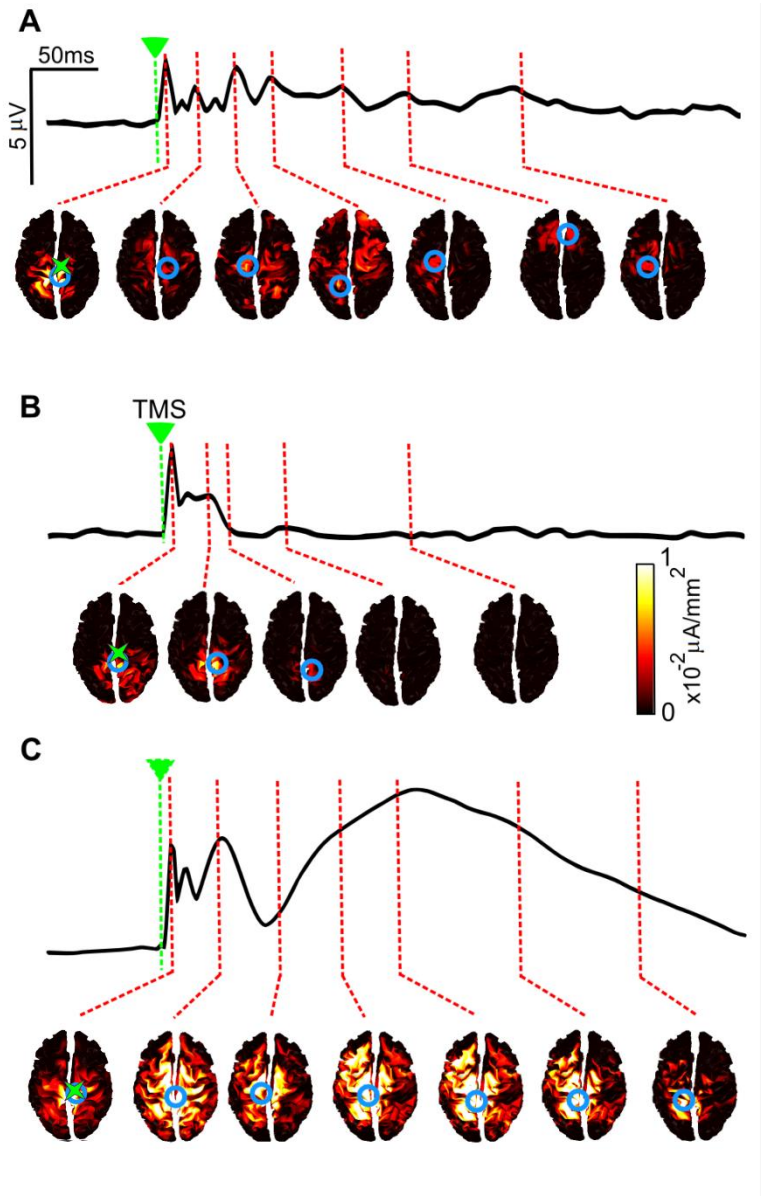

Figure 2.5.6: The balanced, long-range, differentiated pattern of activation observed in wakefulness was impaired during slow-wave sleep.
hd-EEG GMFP (black traces) and SCD (cortical maps) are shown for a representative subject in whom the sensory-motor cortex was stimulated with TMS (green star). **A)** During waking, the stimulation intensity of 90V/m evoked an activation pattern lasting for more than 300ms and spreading from near the stimulation site to other cortical locations, recruiting different cortical areas at different latencies. **B)** During slow-wave sleep, the same stimulation evoked a response that remained local, fading shortly (<100ms). **C)** Higher stimulation intensity (160V/m) during slow-wave sleep evoked strong and global but yet stereotypical responses, in which the maximum significant current (blue circles) remained fixed near the TMS target.

Thus, TMS/hd-EEG revealed a clear-cut reduction of cortico-cortical integration occurring during sleep early in the night: while the cortical area that is directly engaged by TMS reacted to the stimulation, it generally behaved as an isolated module. Moreover, TMS/hd-EEG measurements not only indicated that during slow-wave sleep the thalamocortical system tends to break down into isolated modules, but also showed that the ability of thalamocortical circuits to produce differentiated responses is impaired. We targeted TMS to premotor cortex

(BA 6) and to the visual cortex (BA 19) of a healthy subject during wakefulness and slow-wave sleep. Figure 2.5.7 displays, for each condition, the significant current evoked by TMS as cumulated over the entire post-stimulus interval and plotted on the cortical surface; on the right side of each cortical surface, the time course of the currents recorded from three selected areas are depicted. This example, as the one reported in the previous figure, confirms a clear-cut loss of integration during slow-wave sleep by showing that distant cortical areas ceased to be causally affected by the initial perturbation. On the other hand, it also reveals a clear loss of response specificity. While during wakefulness cortical areas reacted to the stimulus with a specific activation pattern, which had a characteristic shape and frequency content (see previous section), this distinction was clearly obliterated during sleep; the local response to TMS became, in both cases, a stereotypical response: a positive wave followed by a negative rebound.

The stereotypical pattern of the response to TMS during slow-wave sleep was not caused by an effect of local activation thresholds. As described by Massimini et al. (2007), increasing the intensity of TMS up to saturation levels (160V/m) during slow-wave sleep did not produce a recovering of the balanced widespread activity observed in wakefulness. Instead, the slow positive–negative component may be amplified, developing towards a full-fledged sleep slow wave (figure 2.5.6C).

Altogether, these TMS/hd-EEG measurements suggest that, during slow-wave sleep, the thalamocortical system, despite being active and reactive, either breaks down in causally independent modules or bursts into an explosive and non-specific response. In no case, during slow-wave sleep, does TMS result in a balanced, long-range, differentiated pattern of activation.

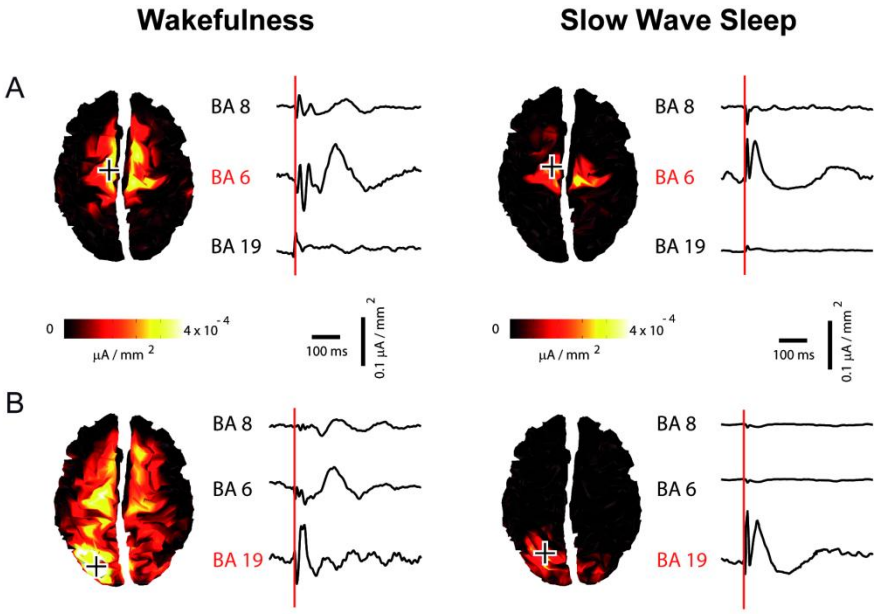

Figure 2.5.7: The ability of thalamocortical circuits to produce differentiated responses was impaired during slow-wave sleep.
TMS was applied to premotor cortex (**A**) and to visual cortex (**B**) during wakefulness (the left panels) and during slow-wave sleep (the right panels). For each condition, the significant current distribution (SCD) recorded during the entire post-stimulus interval are plotted on the cortical surface. On the right side of each cortical surface, the time series of the currents recorded from three selected areas (BAs 8, 6 and 19) are depicted (the time of stimulation is marked by a red line). With the transition from wakefulness to slow-wave sleep, distant cortical areas ceased to be causally affected by the initial perturbation and cortical responses to TMS became stereotypical (adapted from Massimini et al., 2009).

REM Sleep. Following Massimini et al. (2010), we were able to observe the gradual change of activity evoked by TMS during the transition from wakefulness through stage 1 to NREM (stages 2 and 3) and REM sleep. TMS was targeted to the rostral portion of the right premotor cortex with a maximum electrical field of 90V/m at the cortex surface while the subject, lying with eyes closed on a reclining chair, was allowed to sleep. After the experiment, trials were assorted by sleep stage, and four TMS sessions were constructed with a total of 258 trials during wakefulness, 274 at stage 1, 247 at stage 2-3 and 322 during REM sleep. Figure 2.5.8 displays how the widespread differentiated pattern observed during wakefulness (A) gradually shifted through sleep stage 1 (B) to a short-lived local and stereotypical response during stages 2 and 3 (C). Interestingly, during REM sleep (D), late in the night, when dreams become long and vivid and the level of consciousness is likely to return to levels close to wakefulness (Kahan and LaBerge, 2011), thalamocortical integration partially recovered and TMS triggered a more widespread and differentiated pattern of activation (Massimini et al., 2010).

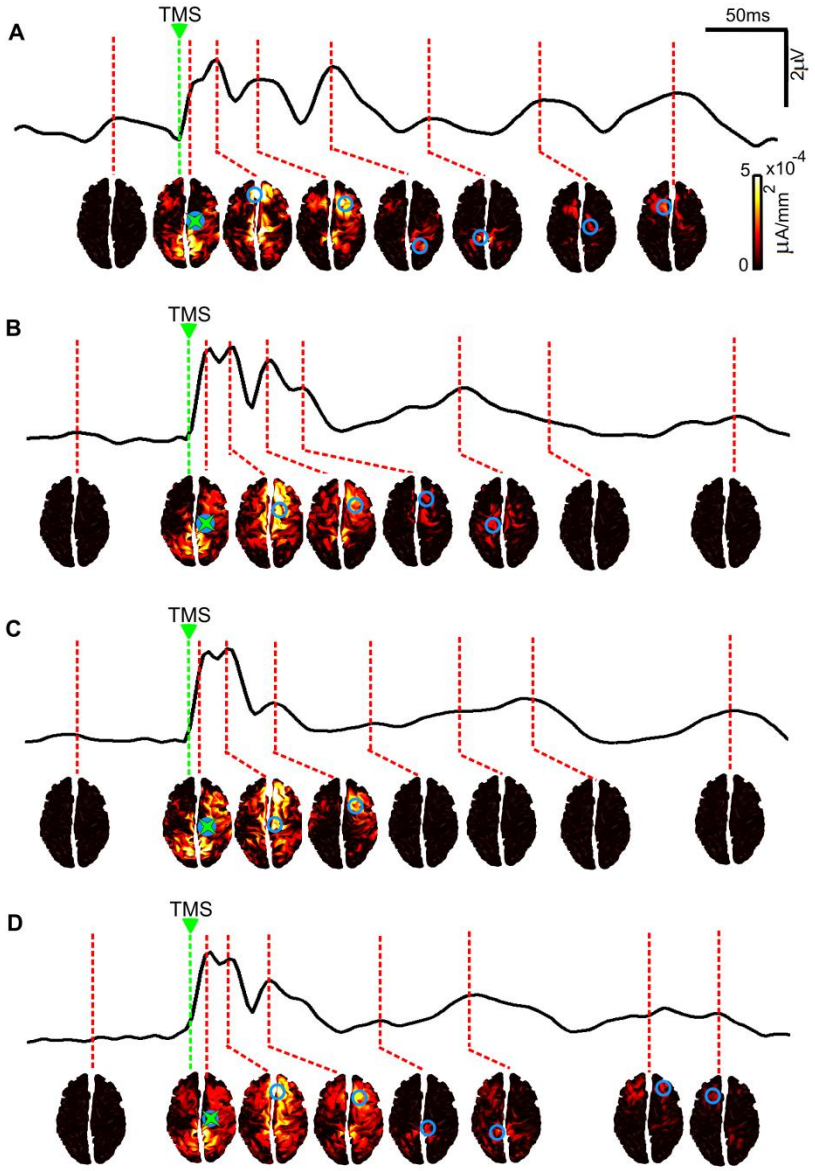

Figure 2.5.8: The widespread differentiated pattern of TMS-evoked activation observed in wakefulness was gradually impaired upon falling into NREM sleep and partially recovered during REM sleep.
hd-EEG GMFP (black traces) and SCD (cortical maps) are shown for a subject in whom the premotor cortex was stimulated (green star) while transiting from wakefulness (**A**) through sleep stage 1 (**B**), NREM sleep stages 2-3 (**C**) to REM sleep (**D**). Duration and spreading of TMS-evoked currents observed during wakefulness were lost in sleep stages 2-3 but recovered during REM sleep.

2.5.3 – Anesthesia

In addition to sleep, the most common condition in which consciousness can be lost is general anesthesia. Although several anesthetics can induce states with behavioral and electrophysiological features not unlike those of deep NREM sleep, pharmacological anesthesia and sleep are not identical and differ in terms of both neurophysiology and

neurochemistry (Van Dort et al., 2008). Moreover, general anesthesia offers several advantages for investigating the neural correlates of LOC (Franks, 2008). Specifically, in sleep studies it is not feasible to evaluate an individual's level of alertness repeatedly and reliably, because the depth of sleep varies unpredictably and subjects awakened to assess consciousness cannot rapidly return to sleep. By contrast, during general anesthesia, a subject's level of alertness may be assessed repeatedly without reversing the pharmacologically induced LOC.

In Ferrarelli et al. (2010) we described the patterns of TMS-evoked responses during loss of consciousness induced by anesthesia. In this first study of TMS/hd-EEG during anesthesia-induced LOC we chose to use the benzodiazepine midazolam, an agent that has a marked anticonvulsant effect, since TMS can, although rarely, induce seizures in epileptic patients. Also, the clinical tool used to evaluate the subjects' alertness throughout the experimental procedure, the Observer's Assessment of Alertness/Sedation (OAA/S) scale, was initially tested in subjects who received titrated doses of midazolam (Chernik et al., 1990). Finally, unlike most anesthetic agents midazolam targets $GABA_A$ receptors exclusively, leading to increased inhibitory postsynaptic currents that presumably underlie its behavioral/cognitive effects (Tanelian et al., 1993). Other general anesthetics, such as volatile and i.v. drugs, have effects that are more difficult to interpret because of multiple interactions with several proteins, such as voltage-gated and leak channels (Verbny et al., 2005). One potential drawback of midazolam is its pharmacokinetic profile, which leads to slower recovery compared with shorter-acting induction agents (Gan, 2006). Because of this slow recovery, we were able to measure TMS-evoked EEG responses after full recovery of vigilance (Level 5 OAA/S) in just one subject within the limited time frame of the TMS/hd-EEG recordings.

Experimental Protocol. Six male subjects received i.v. midazolam at doses up to 0.2mg/kg, with OAA/S reaching scores of "1" (unresponsive to verbal and mild physical stimulus) for a sufficient period that hd-EEG responses to TMS could be measured. A 20-gauge i.v. catheter was placed for anesthetic drug delivery, and participants were given supplemental oxygen at

3 L/min via nasal cannula and anantacid (Bicitra) to minimize possible complications in the event of nausea and vomiting caused by the anesthetic drug. During the TMS procedure, the participant's electrocardiogram, noninvasive blood pressure, SaO_2, exhaled CO_2, and axillary skin temperature were continuously monitored by an anesthesiologist. Additionally, the subject's level of consciousness was evaluated before and after each TMS session with the OAA/S.

TMS was targeted to the right premotor cortex and a first 8- to 10-min TMS/hd-EEG session (~250 stimuli, with a 2,000-ms period and a ±250-ms jitter) was collected in each subject before midazolam injection (level5 responsiveness of the OAA/S). Midazolam was then given at an initial dose of 0.1mg/kg, followed by additional doses of 0.02mg/kg each 2–3 min until the subject was unresponsive (level 1 of the OAA/S), up to a maximal dose of 0.2 mg/kg. During midazolam administration, 3-min TMS blocks at 0.2 Hz interleaved by alertness assessments with the OAA/S were performed and a longer TMS session mirroring the preinjection TMS session was collected.

Results. Compared with wakefulness, we found a marked change in TMS-evoked brain responses during midazolam-induced LOC (Figure 2.5.9). Before the injection of the anesthetic (level 5 alertness, OAA/S), TMS pulses to premotor cortex evoked a complex spatiotemporal pattern of low-amplitude, fast-frequency scalp waves, associated to cortical currents which lasted for at least 300ms following the stimulation and shifted among cortical areas distant from the TMS-targeted brain area (panels A and B). Conversely, following midazolam-induced LOC (level 1 OAA/S), TMS pulses gave rise to high-amplitude, low-frequency EEG voltages, produced by cortical currents which faded within 150ms and remained more localized to the stimulated site (panels A' and B').

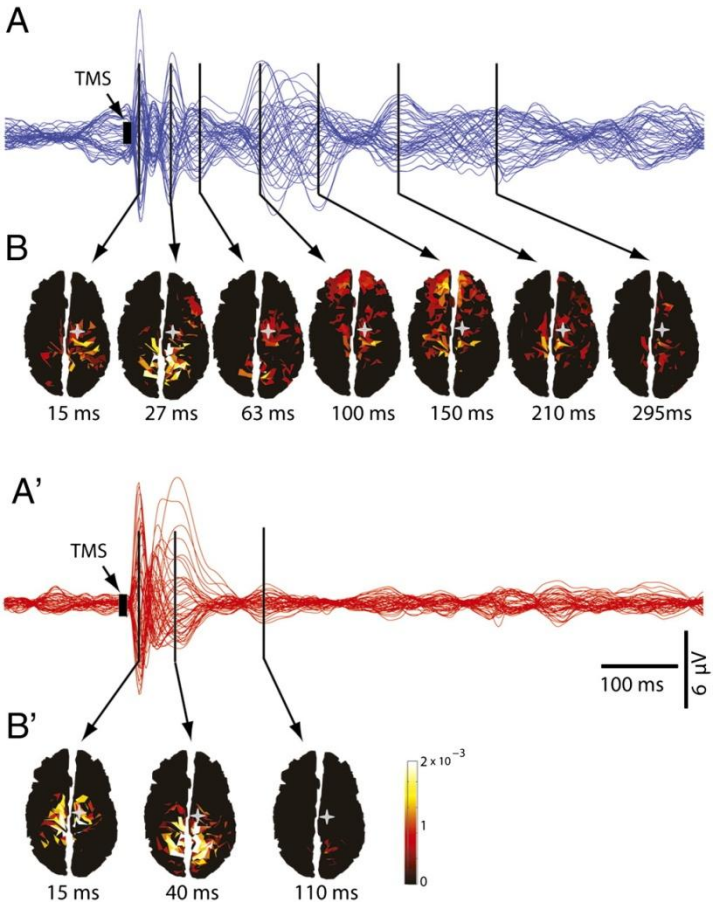

Figure 2.5.9: The balanced, long-range, differentiated pattern of activation observed in wakefulness was impaired during anesthesia-induced LOC.
A and **A'**: Averaged TMS-evoked potentials at all electrodes, superimposed in butterfly plots (the blue traces for waking, red traces for anesthesia). **B** and **B'**: Cortical currents calculated on individual cortical meshes are shown from minimal (dark red) to maximal (white) values. During wakefulness, TMS of premotor cortex determined low-amplitude, complex scalp waves corresponding to cortical currents that lasted >300 ms and shifted among distant cortical areas. Conversely, during anesthesia, TMS gave rise to high-amplitude, short-lasting scalp voltages reflecting cortical currents that remained local, and faded within 150 ms. The gray stars represent the TMS target (premotor cortex); the black arrows represent the local maxima in periods of significant TMS-evoked activation (adapted from Ferrareli et al., 2010).

Although the activity evoked by TMS at the stimulation site, the premotor cortex (BA 6), was similar across conditions, its time course was markedly different. While during wakefulness, the immediate response to TMS consisted of oscillations on the β range, during anesthesia, the oscillatory frequency of the premotor cortex was altered and TMS-evoked slower responses, consisting of a large positive wave followed by a negative deflection. This local slow response was found in all subjects during LOC. Moreover, the initial response remained largely restricted to the premotor cortices and affected only marginally the activity of other cortical areas. This breakdown of cortico-cortical effective connectivity was also evident when inspecting the time courses of the TMS-evoked cortical currents on other areas. For

instance, the time course of cortical currents in BA 8 (prefrontal cortex), which is anatomically connected to BA 6 (premotor cortex), was not affected by the strong activation evoked by TMS in the premotor cortex (Figure 2.5.10).

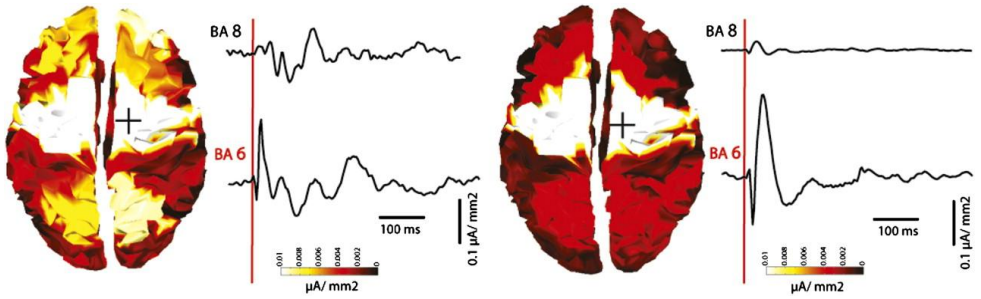

Figure 2.5.10 TMS during anesthesia evoked a large positive–negative wave in the stimulation site but little activation in distant areas.
SCD cumulated in a 0–500 ms post-TMS interval and displayed on the corresponding BA in wakefulness (Left) and anesthesia (Right). To the right of each topographic plot are time courses of currents recorded from the stimulated area, premotor cortex (BA 6), and from a more anterior cortical area (BA 8). During anesthesia, TMS-evoked SCD in BA6 was similar to the SCD recorded in wakefulness, as reflective of an initial stronger but shorter-lived response during anesthesia compared to wakefulness. Conversely, SCD from BA 8, which is anatomically connected to BA 6, were markedly reduced in anesthesia compared to wakefulness, suggesting a marked decrease in cortical effective connectivity (adapted from Ferrareli et al., 2010).

These results bear a striking resemblance with those obtained during early NREM sleep discussed in the precedent section. The depth of sleep, however, can vary unpredictably, and if awakened to assess consciousness, subjects cannot rapidly return to sleep. In this study, subjects could be repeatedly assessed for LOC. In one subject, we could also evaluate the effects of progressively reduced arousal, from level 3 (sedation) to level 1 (LOC). The results show that at sedation level, the TMS-evoked initial activity became stronger than in wakefulness (Figure 2.5.11) but was followed by smaller and shorter-lived oscillations. This initial response to TMS was even larger during LOC, with a positive–negative wave similar to the spontaneous sleep slow oscillation, while subsequent activity was obliterated, demonstrating that brain responses to TMS became progressively shorter and sleep-like while transitioning into pharmacologic LOC.

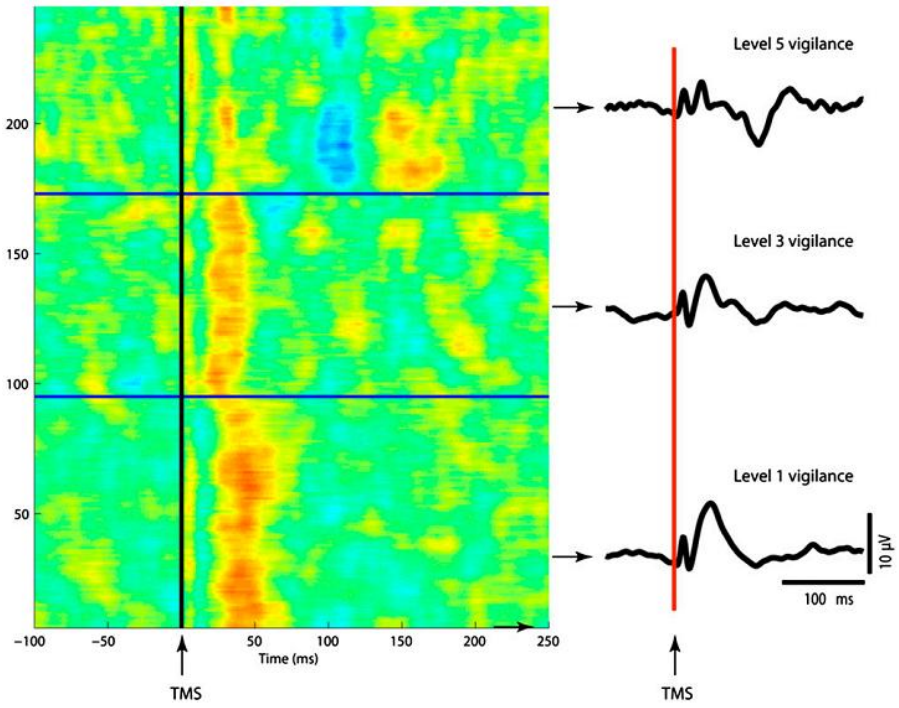

Figure 2.5.11. TMS-evoked brain responses gradually changed while transitioning from high (OAA/S = 5) to low (OAA/S = 1) levels of vigilance.
Left: single trials recorded from one channel located under the TMS coil, color-coded for voltage. Right: averaged TMS-evoked responses obtained during the three levels of vigilance. Both single and average EEG responses showed a progressive increase in the amplitude and latency of an early evoked component (positive peak), followed by the obliteration of succeeding oscillations when reaching low levels of vigilance (adapted from Ferrareli et al., 2010).

In order to further quantify changes in strength (activity) and propagation (connectivity) of TMS-evoked cortical responses during LOC, SCD and SCS were calculated for each subject in wakefulness and anesthesia. The time course of SCD revealed that, in each subject, the initial TMS-evoked cortical activity, related to the large positive–negative wave, was higher in the anesthesia condition, whereas subsequent cortical activity was stronger during wakefulness. When cumulating SCD in two post-TMS time ranges, respectively, 0–50 and 50–500 ms, we found that in the 0–50 ms interval, SCD was significantly higher during anesthesia (p = 0.016, Mann–Whitney), whereas in the 50–500 ms range, SCD was significantly higher during wakefulness (p = 0.016, Mann–Whitney). The average SCD in the entire poststimulus interval was reduced during anesthesia, indicating a diminished response to the TMS, although the two conditions differed only at trend level (p = 0.1, Mann–Whitney). By contrast, SCS discriminated effectively between the two conditions (Figure 2.5.12).

Specifically, in each subject, mean SCS was significantly higher in wakefulness compared to anesthesia (p = 0.009, Mann–Whitney). Furthermore, the time course of SCS showed that, in each subject, SCS during wakefulness was significantly increased compared to baseline for >200ms, whereas during anesthesia, SCS returned to baseline within 100 ms of TMS.

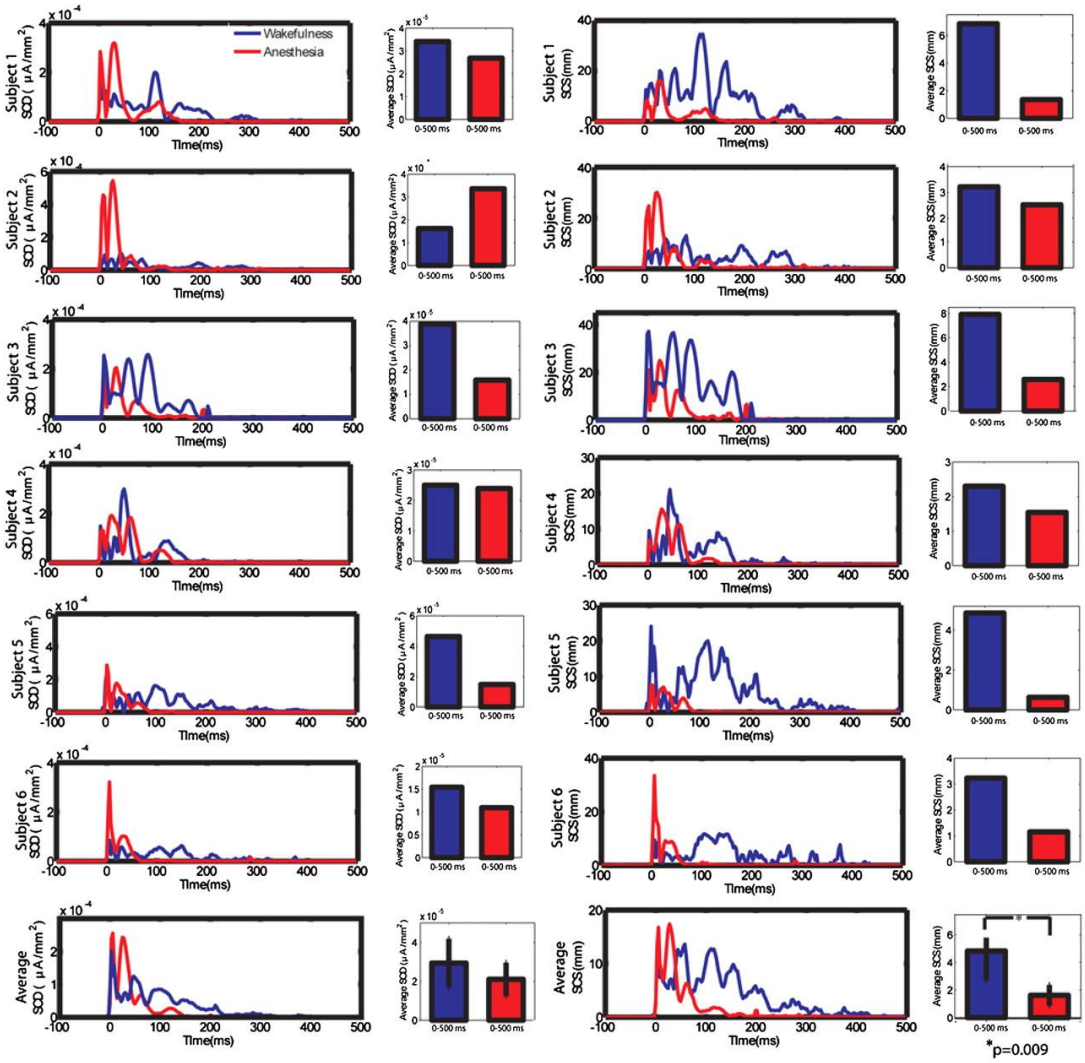

Figure 2.5.12: Cortical connectivity (SCS), but not reactivity (SCD), captured cortical changes during LOC. SCD and SCS were computed for each subject in wakefulness (blue line) and anesthesia (red line) following TMS of the premotor cortex. Left: Time course of SCD for individual and average data, and mean SCD over the entire post-TMS time interval (0–500ms). In each subject, SCD values were initially higher (first 50ms after TMS) during anesthesia but tended to dissipate shortly thereafter, consistent with a TMS-evoked larger initial response during anesthesia that was, however, short-lived. Mean SCD over the entire post-TMS period were not significantly different between wakefulness and anesthesia. Right: Time course of SCS for individual and average data, and mean SCS over the entire post-TMS interval. In each subject, during wakefulness, SCS was present for>200ms, whereas during anesthesia it faded after 100ms. Notably, mean SCS values in the 0–500ms post-TMS interval were significantly higher (p = 0.009, Mann–Whitney) in wakefulness relative to anesthesia, (adapted from Ferrareli et al., 2010).

Thus, during loss of consciousness induced by midazolam, the effective connectivity in the corticothalamic system was markedly reduced. Moreover, specific local oscillatory properties of neural circuits, as the natural frequencies of corticothalamic circuits of healthy awake subjects, were lost under LOC. Altogether these results suggest that when consciousness is absent the thalamocortical system responds to TMS with qualitatively simpler, slow and non-specific patterns of activation.

2.5.4 – Disorders of Consciousness

The results exposed in the previous sections demonstrate that in healthy awake and alert subjects TMS induced a sustained EEG response involving the sequential activation of different brain areas and affecting much of the cortex. By contrast, during NREM sleep and after loss of consciousness induced by general anesthesia, TMS pulses invariably produced a simple stereotyped response that either remained localized to the site of stimulation or bursted into an explosive and non-specific activation. Moreover, during REM sleep, when subjects are unresponsive to sensory stimuli and virtually paralyzed but report vivid dreams upon awakening, the cortical response to TMS recovered its complexity and became similar to that observed during wakefulness. If the complexity of the responses to TMS is supposed to correlate to the level of consciousness, what should we expect from the patterns of TMS-evoked cortical activity collected in patients suffering from disorders of consciousness?

TMS/hd-EEG in DOC Patients: Experimental Protocol. In Rosanova et al. (2012) we described the results of employing TMS/hd-EEG at the bedside of 17 patients who evolved from coma into different clinical states: vegetative state (VS), minimally conscious state (MCS), emergence from MCS (EMCS) and locked-in syndrome (LIS). During each TMS/hd-EEG session, patients were lying on their beds, awake and with their eyes open. If signs of drowsiness appeared, recordings were momentarily interrupted and subjects were stimulated using the CRS-R arousal facilitation protocols (Giacino, 2004). Throughout every recording session the stability of stimulation coordinates was continuously monitored. If the virtual

aiming device was signaling a displacement >4 mm, session was interrupted and the coil was repositioned. At the end of the experiment, the stimulation coordinates were recorded and the electrode positions were digitized.

Cortical targets were identified on computerized tomography (CT) scans acquired with a Siemens Senatom Sensation 16 from all patients. Stimulation was delivered with an interstimulus interval jittering randomly between 2000 and 2300 ms (0.4-0.5 Hz), at an intensity ranging from 140 V/m up to 200 V/m on the cortical surface. The CT-guided intracranial electric field estimation was a crucial step during the experimental procedure; due to shifts of intracranial volumes in brain-injured patients, it is difficult to assess whether TMS is on target and effective based on extra-cranial landmarks alone and this may result in false-negatives (absence of EEG response due to missed target, or sub-threshold stimulation).

TMS was targeted to four cortical sites: the left and right medial third of the superior parietal gyrus and the left and right medial third of the superior frontal gyrus. These cortical targets were selected for several reasons: i) they are easily accessible and far from major head or facial muscles whose unwanted activation may affect EEG recordings; ii) the posterior parietal cortex, as well as its interactions with more frontal areas, is thought to be particularly relevant for consciousness (Laureys et al., 2004); iii) our previous TMS/EEG studies have been successfully performed in these areas during wakefulness (Rosanova et al., 2009), sleep (Massimini et al., 2005, 2007) and anesthesia (Ferrarelli et al., 2010). In practice, all four cortical sites were not always accessible in all subjects due to skull breaches, external drain derivations. In all cases, we avoided stimulating over focal cortical lesions that were clearly visible in CT scans, since the EEG response of these areas may be absent or unreliable.

Data Analysis and Results. We performed a first set of TMS/hd-EEG experiments (one single session) in a group of 12 patients (**Group I**: 5 females; mean age±standard deviation: 50.3±26.21). These patients were repeatedly evaluated (4 times, every other day) for a

period of one week by means the CRS-R, in order to avoid diagnostic errors due to fluctuations in responsiveness and to obtain a stable clinical diagnosis. Five patients of **Group I** (Patients 1, 2, 3, 4 and 5), showed only reflexive behavior and were diagnosed as VS during the 4 behavioral evaluations. Five patients (Patients 6, 7, 8, 9 and 10) showed non-reflexive behaviours, such as visual tracking or responding to simple commands, satisfying the CRS-R criteria for MCS in at least 3 evaluations, including the one performed on the day of the TMS/EEG session. The two remaining patients (Patient 11 and Patient 12) could communicate reliably and were diagnosed as LIS. The VS and MCS subgroups did not differ systematically in etiology and time from injury (reported in Appendix - Table A.1). In particular, Group I included three chronic patients, one VS (Patient 5: 172 days from injury), one MCS (Patient 8: 1334 days from injury) and one LIS (Patient 12: 1399 days from injury).

Figure 2.5.13 displays examples of the cortical response evoked by TMS in VS, MCS and LIS patients. VS patients exhibited local, stereotypical evoked responses, closely resembling the cortical activations previously observed during deep sleep and anesthesia (Figures 2.5.6 and 2.5.9). In MCS, TMS invariably triggered a complex response associated with a rapidly changing pattern of cortical activation, contrasting starkly with the local, simple wave recorded in VS patients and being, instead, comparable to the one obtained in locked-in subjects. Thus, a clear-cut difference in the cortical response to TMS seems to discriminate reliably between patients who were considered VS after repeated behavioral evaluations and subjects who showed signs of consciousness.

In order to quantify this difference, we applied a statistical measure to extract latencies with significant GMFP activations and count the number of sources involved by maximal currents at these latencies. A bootstrap method (Lv et al., 2007) was applied by shuffling the time samples of GMFP pre-stimulus activity (from -300 to -50 ms) at the single-trial level and by calculating 500 surrogated pre-stimulus GMFPs. From each random realization, the maximum value across all latencies was selected to obtain a maximum distribution (control for type I error) and significance level was set at $p<0.01$. At each significant latency of the post-stimulus GMFP, the location of maximum neuronal current (10 most active sources)

was detected on the cortical surface. Plotting and counting the sources involved by maximum neuronal currents across all significant time points in the first 300 ms post-stimulus resulted in the cortical maps and in the values reported in Figure 2.5.14.

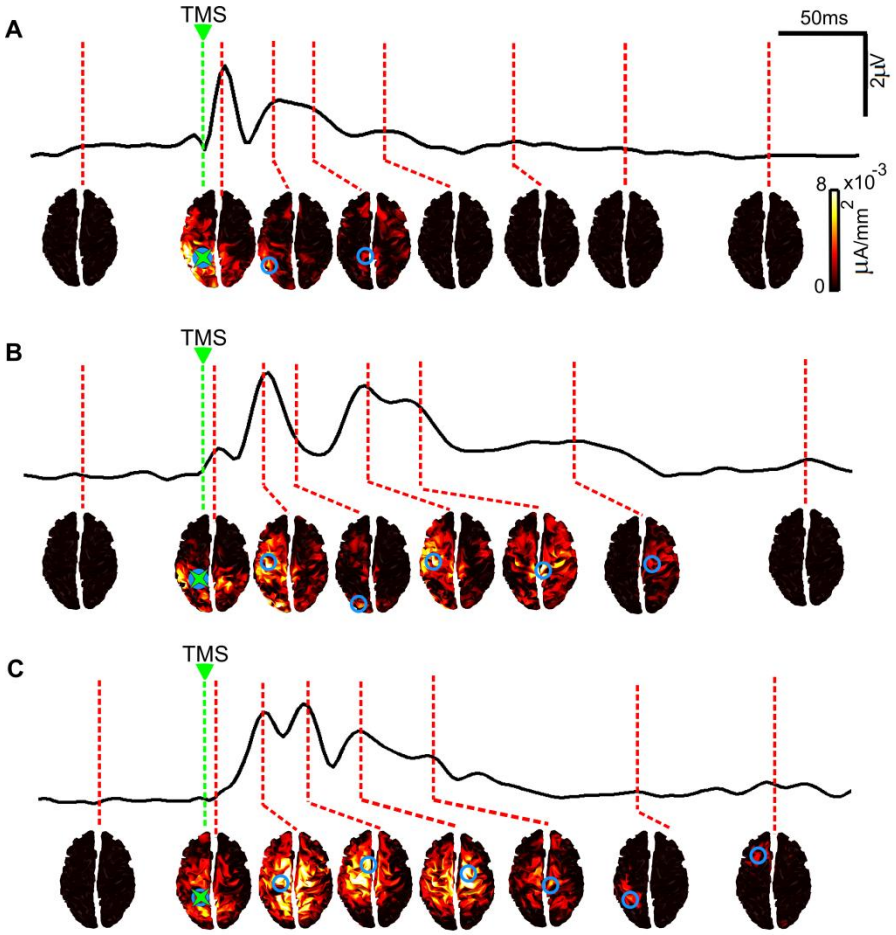

Figure 2.5.13: Examples of TMS-evoked cortical responses of patients who evolved from coma into different clinical states.
hd-EEG GMFPs (black traces) and SCD (cortical maps) are shown for TMS/EEG sessions performed in three patients in different clinical states. **A)** TMS evoked a slow, short-lived and simple response on a patient diagnosed in vegetative state (CRS-R = 4); **B)** A patient who showed fluctuating signs of non-reflexive reactions to external stimuli but were unable to communicate reliably with the examiners, diagnosed in minimally conscious state (CSR-R=14), responded to TMS with a complex, long-lasting changing pattern of cortical activation, where maximum neuronal currents (blue circle) shifted over time across different areas; **C)** A similar complex response was observed in a locked-in subject (LIS) who, though being largely paralyzed at the time of recording, could signal full awareness through vertical eye movements. The green stars mark the site of stimulation (left parietal cortex).

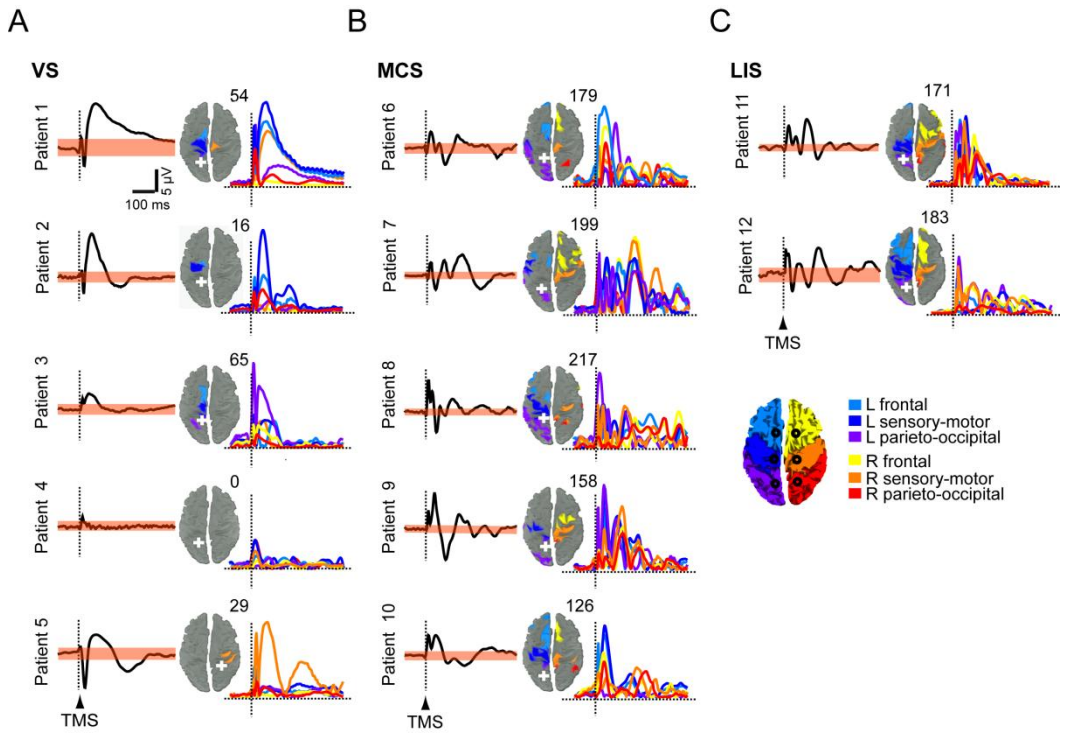

Figure 2.5.14. TMS-evoked cortical responses in Group I patients.
A group of five VS (**A**), five MCS (**B**), and two LIS patients (**C**) underwent one TMS/hd-EEG session after 7 days of repeated evaluations by means of the CRS-R. For each patient, the averaged TMS-evoked potentials recorded at one electrode under the stimulator (black trace) and the respective significance threshold (upper and lower boundaries of the pink bands; bootstrap statistics, $p<0.01$) are shown. The sources involved by maximum cortical currents (10 most active sources) during the significant post-stimulus period of the GMFP are plotted on the cortical surface and color-coded according to their location in six anatomical macro-areas as indicated in the legend at the bottom-right end of the figure; the number of detected sources is indicated at the top-right end of each map. The time-series represent TMS-evoked cortical currents recorded from an array of 6 sources (black circles on the bottom-right cortical map) located about 2 cm lateral to the midline, one for each macro-area. The white crosses mark the sites of stimulation. For all patients the responses to the left parietal cortex stimulation are shown, except for one patient (Patient 5) in whom a significant response could only be detected in the right hemisphere (adapted from Rosanova et al., 2012).

According to this procedure, the number of detected sources is small if TMS triggers stable primary neuronal currents that remain confined to the stimulated area during the entire post-stimulus period. On the contrary, the number of detected sources is large if TMS triggers primary cortical currents that involve different cortical areas at different times. In order to describe the time-course of TMS-evoked cortical activation in different areas the currents from a grid of six cortical sources (black circles plotted on the bottom-right cortical map in Figure 2.5.14) were extracted and auto-scaled to the maximum value of each session. Sources and time-series of cortical currents were color-coded according to their anatomical location in 6 arbitrary macro-areas (see colors legend in Figure 2.5.14).

In all VS patients, except for one anoxic patient (Patient 4) in whom no response could be elicited even when TMS was delivered at high intensity (200 V/m) in both hemispheres, TMS

elicited maximum cortical currents that remained localized during the entire significant post-stimulus period, involving a small number of sources around the stimulated area (Figure 2.5.14A). Conversely, in all MCS patients, maximum neuronal currents shifted over time from the stimulated site to a large number of distant sources (Figure 2.5.14B). This pattern was comparable to the one obtained in two locked-in (LIS) subjects (Figure 2.5.14C). Notably, this difference allowed for a single-subject discrimination between VS and MCS patients (see also Figure 2.5.17).

We also performed longitudinal TMS/hd-EEG measurements (session 1, session 2 and session 3) in a group of five patients (**Group II**: 3 females; mean age±standard deviation: 51.2±23.05) as they awakened from coma and progressed towards different clinical states (Figure 3.15). As assessed by the CRS-R, three of these patients (Patients 13, 14 and 15) regained functional communication evolving from VS, through MCS to EMCS, while two patients (Patients 16 and 17) remained VS. In all cases the first TMS/hd-EEG session (session 1) was performed at least 48 hours after withdrawal of sedation, when patients opened their eyes and were diagnosed VS. At this time, similar to the VS patients of Group I, TMS evoked a simple wave and a local pattern of activation or no response at all. Following session 1, two additional TMS/hd-EEG measurements were performed in the three patients who eventually recovered consciousness: session 2 was recorded as soon as they satisfied the CRS-R criteria for MCS and session 3 when they recovered functional communication and emerged from the minimally conscious state (EMCS). In these patients, TMS triggered a complex pattern of activation that sequentially involved a large set of cortical areas already during session 2; this response was substantially different from the simple, local activation of session 1 and was instead comparable to the one obtained in session 3, when subjects had recovered their ability to communicate (Figure 2.5.15A). In the two patients who did not show any clinical improvement beyond VS, a second TMS/hd-EEG measurement (session 2) was performed more than a month after session 1 and showed either a local, simple wave of activation (Patient 16) or no response (Patient 17, anoxic), although subjects were awake and open-eyed when their brains were stimulated (Figure 2.5.15B).

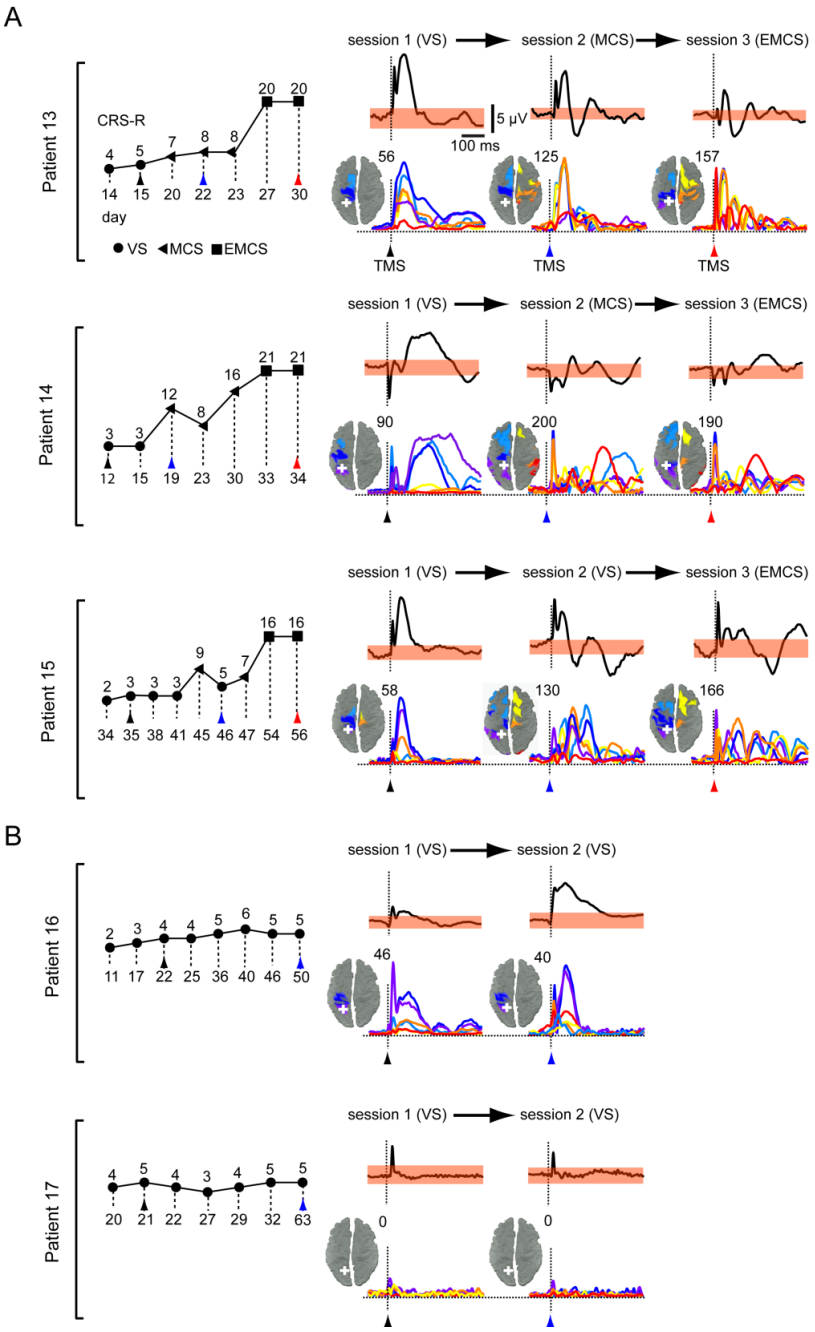

Figure 2.5.15. Clinical evaluation and TMS-evoked cortical responses in Group II patients.
CRS-R total scores are plotted for the patients who were studied longitudinally (Group II) and eventually emerged from MCS (**A**) or remained VS (**B**); the first assessment (session 1) was carried out 48 hours after withdrawal of sedation, as patients exited from coma. The symbols indicate the associated clinical diagnosis (circles=VS; triangles=MCS; squares=EMCS). Colored arrow tips mark the days when TMS/EEG recordings were performed and the time of TMS delivery (black=session 1; blue=session 2; red=session 3). For every patient and session, averaged potentials triggered by TMS (vertical dashed lines) of parietal cortex and recorded from the electrode under the stimulator are shown. The sources involved by maximum neuronal currents during the significant post-stimulus period are plotted on the cortical surface and color-coded according to their location in six anatomical macro-areas (see Figure 3.14); the number of detected sources is indicated at the top-right end of each map. The time-series represent TMS-evoked cortical currents recorded from an array of 6 sources (see their locations in Figure 3.14) located about 2 cm lateral to the midline, one for each macro-area. The white crosses mark the sites of stimulation; in each patient, the left parietal cortex was stimulated when patients entered VS from coma (session 1), soon after transition to MCS or at least 30 days of permanence in VS (session 2) and after emergence from MCS (EMCS; session 3), when subjects recovered functional communication (adapted from Rosanova et al., 2012).

These results with Group II indicate that the breakdown of the widespread balanced pattern of cortical activation observed in VS patients can be reversible and that a substantial improvement in the brain's ability to sustain internal communication occurred at an early stage during recovery of consciousness, before reliable communication could be established with the patient.

Are these changes in the activation pattern evoked by TMS associated to changes in electrophysiological arousal (EEG activation)? Spectral analysis of spontaneous EEG showed a consistent increase of high-frequency (> 7Hz) oscillations in LIS compared to MCS (Group I) and in EMCS compared to MCS (Group II). By contrast, in spite of a clear-cut change in the electrical response to TMS, no systematic changes of the background EEG could be detected between VS and MCS (Figure 2.5.16) consistent with previous reports (Kotchoubey et al., 2005). These results suggest that the transition from VS to MCS involves a substantial improvement of cortical integration that is not necessarily associated with an obvious change in the level of activation of the ongoing EEG.

Figure 2.5.17 summarizes the results obtained after applying TMS in all 17 patients, showing that it was possible to discriminate reliably between VS and MCS at the single-subject level. Crucially, this discrimination was achieved in a way that is completely independent on the patient's ability to exchange information with the surrounding environment.

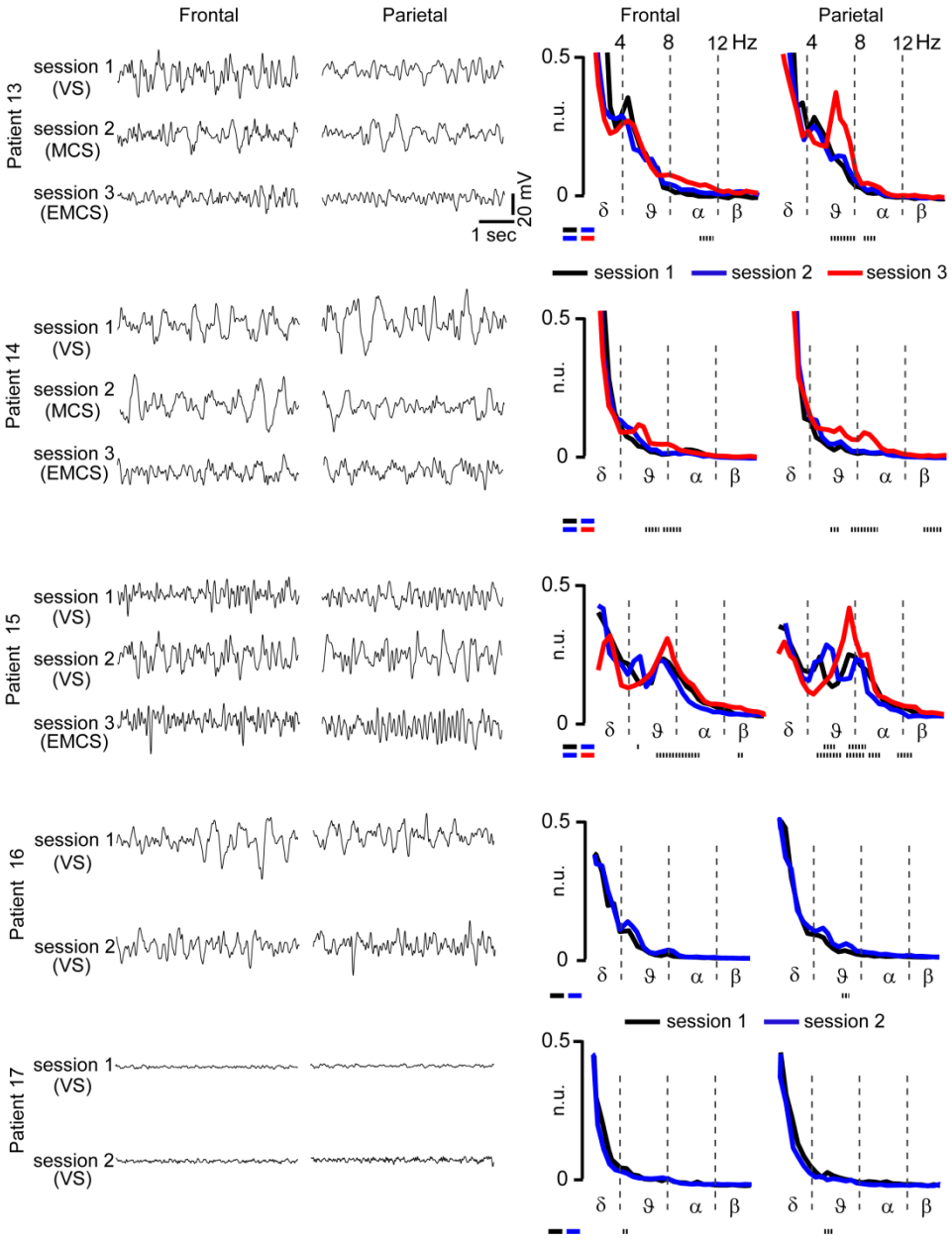

Figure 2.5.16. EEG spectra showed evident changes from MCS to EMCS but not from VS to MCS.
Spontaneous EEG traces (5 seconds) and EEG spectra (calculated on 2 minutes) are shown for the 5 subjects who underwent longitudinal recording sessions (Group II); in these patients, changes in the EEG spectrum were assessed statistically by means of a two tailed paired t-test. The dotted lines at the bottom of each plot indicate the frequency bins that show statistically significant differences of power (t-test, $p<0.01$) (adapted from Rosanova et al., 2012).

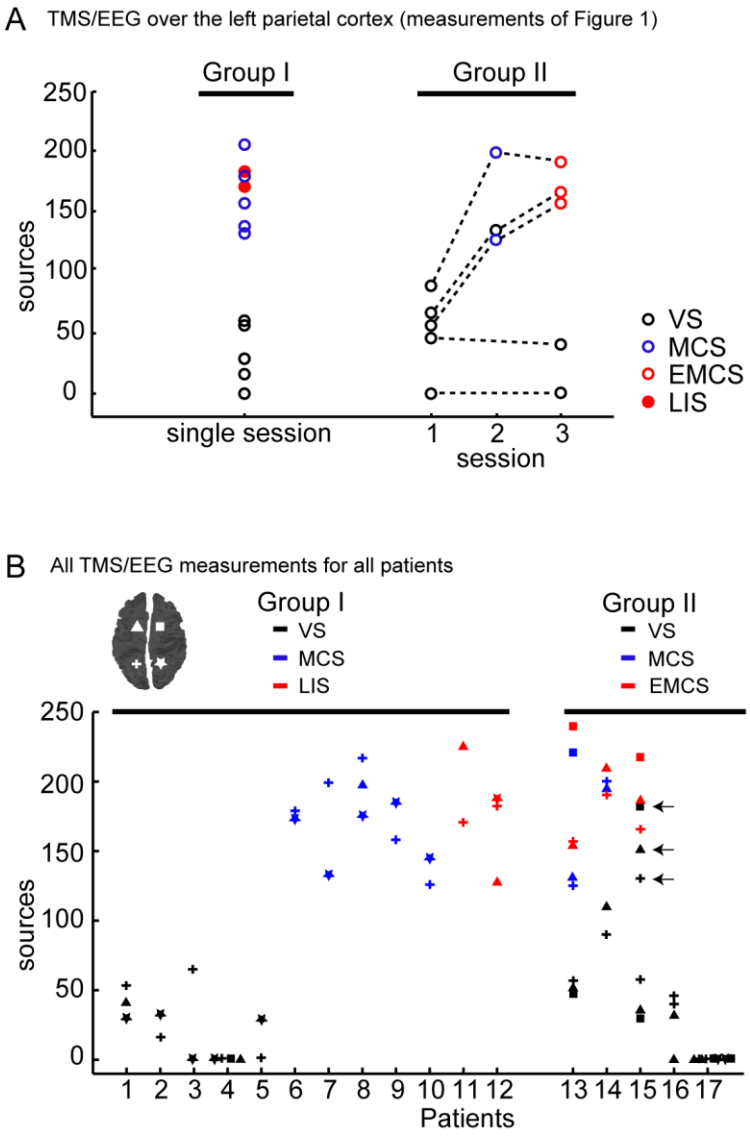

Figure 2.5.17. Effective connectivity for all patients and TMS/EEG measurements.
A) For each patient and TMS/EEG measurement (parietal stimulation, same measurements of Figures 3.14 and 3.15), the number of sources involved by TMS-evoked currents are plotted. The circles indicate the clinical diagnosis at the time of recording (open black circles for VS; open blue circles for MCS; open red circles for EMCS and filled red circles for LIS). **B)** The number of cortical sources involved by maximum cortical currents detected in all TMS/EEG measurements (n=72) is plotted for all patients (Group I on the left and Group II on the right). Each value refers to one cortical target and is marked according to both the site of stimulation (the correspondence between symbols and stimulation sites is graphically reported on the cortical map in the left upper corner of the panel) and the CRS-R diagnosis at the time of recording (black for VS; blue for MCS; red for LIS in Group I and EMCS in Group II). In all cases, effective connectivity was higher in patients who showed some level of consciousness (MCS, EMCS and LIS) compared to VS patients. An exception is represented by the 3 measurements (left parietal, left frontal, right frontal) performed in Patient 15 during session 2 (open black circles indicated by arrows). This patient was diagnosed MCS the day before the measurement, slipped back into a behavioral VS on the day of session 2 and, within days, was reassessed clinically as MCS and then EMCS (during session 3). Effective connectivity was null in the two anoxic subjects (Patients 4 from Group I and Patient 17 from Group II) (adapted from Rosanova et al., 2012).

CHAPTER 3 - BREAKDOWN OF CAUSALITY AND CORTICAL DOWNSTATE WITHIN THE SLEEPING BRAIN

3.1 – Hypothesis: cortical downstate and bistability are responsible for breakdown of causality during LOC

In addition to improving our ability to detect the presence of conscious experience, linking consciousness to brain complexity - in both theory and practice - may also shed new light on the cortical mechanisms of loss and recovery of consciousness in physiological and pathological conditions. Why complex, long-range cortical interactions collapse into a simple response whenever consciousness is lost? The striking similarity between TMS-evoked EEG responses during sleep, anesthesia and in VS/UWS patients suggests common neuronal mechanisms for LOC in these conditions. Indeed, in all cases, the complex TMS-evoked activation observed during wakefulness is replaced by a stereotypical positive-negative deflection (Figure 3.1.1) which, when TMS is delivered at high intensities, evolves into a graphoelement that matches the EEG criteria for a sleep slow wave, or a K-complex (Massimini et al., 2007).

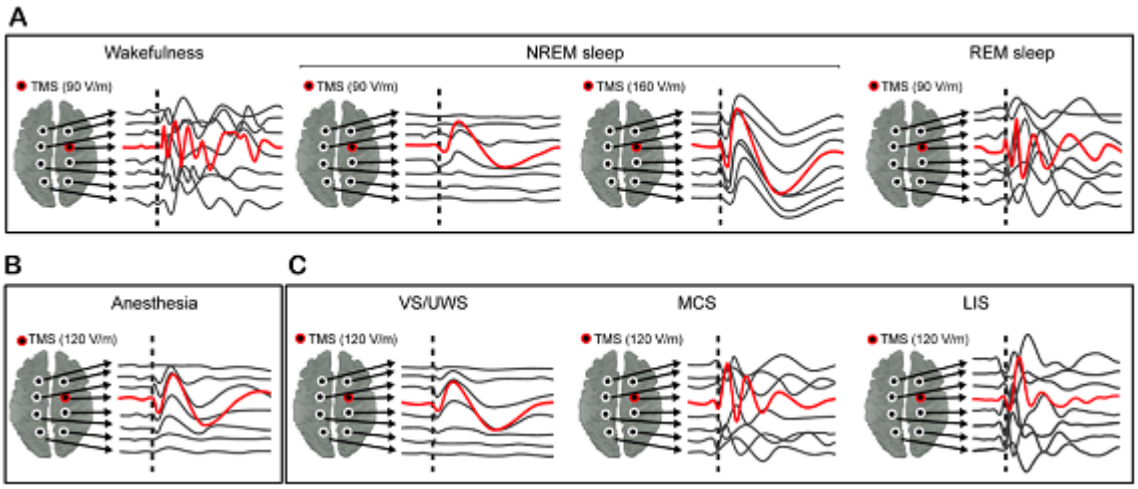

Figure 3.1.1: Loss and recovery of integration and information in thalamocortical networks.
During wakefulness (panel A, left), TMS triggers a sustained response made of recurrent waves of activity associated with spatially and temporally differentiated patterns of activation (brain complexity). During NREM sleep (panel A, middle), anesthesia (panel B) and vegetative state (panel C, left) the thalamocortical system, despite being active and reactive, loses its ability to engage in complex activity patterns and either breaks down in casually independent modules (loss of integration) or it bursts in an explosive response (loss of differentiation/information). During REM sleep (panel A, right), in MCS (panel C, middle) and LIS patients (panel C, right), the TMS response shows a recovery of recurrent waves of activity associated with spatially and temporally differentiated patterns of activation.

Animal (Amzica and Steriade, 2002, 1998) and human (Cash et al., 2009) intracranial recordings have shown that both spontaneous EEG sleep slow waves and K-complexes are underpinned by the occurrence of a silent, hyperpolarized down-state in cortical neurons, which is preceded and followed by a period of activation (up-state). This bimodal alternation between up- and down-states reflects an intrinsic bistability in thalamocortical circuits that is thought to depend on neuronal as well as network properties (Hill and Tononi, 2005; Mann et al., 2009; Sanchez-Vives and McCormick, 2000; Timofeev et al., 2000). During NREM sleep, bistability may be mainly caused by an increased activity of leak K+ channels brought about by decreased brainstem cholinergic activity (McCormick et al., 1993). Inhalational anaesthetics, including nitrous oxide and isoflurane, which strongly potentiate the activity of two pore K+ channels (Alkire et al., 2008), may act through a similar mechanism. On the other hand, increased inhibition within thalamocortical networks may play a crucial role in inducing bistability (Mann et al., 2009) in the case of other anaesthetic agents which act primarily (such as propofol or etomidate), or exclusively (such as midazolam at anaesthetic doses) on GABA receptors.

Our proposition is that, due to bistability, portions of the thalamocortical system, which are otherwise healthy, would not be able to sustain balanced patterns of activations; thus, the inescapable occurrence of a stereotypical down-state after an initial activation would prevent the emergence of complex, long-range patterns of activation in response to a direct stimulation. In order to test this hypothesis , experimentally, one should first demonstrate that the slow wave-like graphoelement triggered by TMS during NREM, anesthesia and in VS/UWS patients truly reflect a neuronal down-state (i.e., a long lasting period of membrane hyperpolarization). To this aim, ideally, one could measure modulation of high-frequencies (gamma-range), which is considered a good proxy of the hyperpolarization of cortical neurons. However, although activities in the gamma-range have been observed at the scalp level during a variety of cognitive tasks (Jerbi et al., 2009), no evidences of a phasic modulation of gamma activities during SWS in human macroscopic EEG recordings were reported so far. For example, Fell and colleagues (2002) used the scalp EEG data during

sleep and showed that sigma activity (12–16 Hz) is modulated by slow EEG oscillations. In another study, Molle and collaborators (2002) found that grouping of spindles and beta oscillations are coincident with slow waves in human SWS. However, both studies didn't find a significant phasic modulation of the gamma activities (>20 Hz) by the slow waves. It was suggested that the resistive properties of the skull, muscle artifacts and the relative distance of scalp electrodes from deeper generators may make it difficult to observe an intracortical modulation of gamma activity during sleep. These drawbacks can nevertheless be overcome with the use of intracranial recordings which furthermore allow the analysis of short-range spatially coherent activities that are not promptly available with scalp recordings (Valderrama et al., 2012).

In the following paragraphs we describe a study where we employ intracranial electrical stimulation and recordings to demonstrate that during NREM sleep (a physiological model of LOC), a perturbation of thalamo-cortical system induced a widespread suppression of high frequencies (i.e. cortical downstates) that impairs the ability of thalamocortical circuits to engage in causal interactions, a theoretical requirement for consciousness (Tononi, 2004).

3.2 – Breakdown of causality and cortical downstate within the sleeping brain

At the cortical level, the most striking difference between wakefulness and NREM sleep is represented by the occurrence of short (few hundreds of milliseconds) periods of hyperpolarization and neuronal silence (down-states) that periodically interrupt longer stretches of spontaneous neuronal activity (up-states) indistinguishable from quiet wakefulness (Llinás and Steriade, 2006). When this fluctuation between up- and down-states occurs near-synchronously over a large population of neurons it is mirrored by the appearance of high-amplitude slow waves in the EEG (Amzica and Steriade, 2000). The occurrence of the down-states reflects an intrinsic bistability of cortical circuits and is thought to be primarily due to the dynamics of activity-dependent potassium (K+) currents, which

become prominent when the neuromodulating milieu changes upon falling asleep. Due to these hyperpolarizing currents, cortical neurons tend to rapidly fall into a down-state in response to any transient activation; in fact, the stronger is the initial activation, the more K+-currents will tend to drive neurons into an hyperpolarized, silent state (Compte Sanchez-Vives, 2003).

An intriguing possibility is that intrinsic bistability, per se, may substantially change the causal structure of human thalamocortical networks in a way that is not immediately evident by observing spontaneous patterns of neuronal synchrony. Specifically, we hypothesize that (i) during NREM sleep any neuron, or group of neurons, that receive a cortico-cortical input would rapidly plunge into a down-state, (ii) that this period of silence is followed by a resumption of neuronal activity which retains no effects of the initial input and (iii) that this loss of determinism prevents the emergence of widespread causal interaction at the network level. Here, we test this hypothesis by employing intracerebral electrical stimulation (ICS) and simultaneous stereotactic EEG (SEEG) recordings during wakefulness and NREM sleep in 8 patients undergoing neurosurgical evaluation for intractable epilepsy. We analyzed cortico-cortical evoked potentials (CCEPs – see Matsumoto 2004) by means of time-frequency analysis and phase locking measures both within (phase-locking factor, PLF) and across (phase-locking value, PLV) recording sites.

3.2.1 – Materials and Methods

Patients. Eight neurosurgical patients with long-standing, drug-resistant, focal epilepsy participated in this study (table 3.2.1).

	Age	Gender	Handedness	# of electrodes	# of contacts [after contact rejection]	Outcome	Diagnosis	Focus Location	Sample Lobes
Sbj.1	31	F	R	17	189 [80]	-	-	-	Bilateral FCP

Sbj.2	21	M	R	14	147 [61]	III	Criptogenic	Right central cingulate gyrus	Bilateral FCP
Sbj.3	21	F	R	12	146 [52]	III	Cortical dysplasia	Left posterior medial frontal gyrus	Left FCP
Sbj.4	36	M	R	14	170 [51]	Ia*	-	Right temporal neocortex	Right FCTI
Sbj.5	31	M	R	15	179 [69]	(3 months)	Cortical dysplasia	Right orbital gyrus	Right FTI
Sbj.6	18	M	R	14	165 [110]	Ia (6 months)	Cortical dysplasia	Right genus cinguli	Bilateral F
Sbj.7	20	M	R	14	186 [79]	II	Criptogenic	Right posterior mesial frontal gyrus	Bilateral FCP
Sbj.8	25	M	R	12	143 [53]	-	-	Right posterior mesial frontal gyrus	Right FCI

Table 3.2.1: Patients. Table shows personal and clinical data for each subject.

All patients were candidates for surgical removal of the epileptic focus. During pre-surgical evaluation all patients underwent individual investigation with stereotactically implanted intracerebral multilead electrodes for the precise localization of the epileptogenic zone (Cossu et al.). Before intracerebral electrode implantation patients gave written informed consent as approved by the local Ethical Committee. Confirmation of the hypothesized seizure focus and localization of epileptogenic tissue in relation to essential cortex was achieved by simultaneous scalp and intracerebral electrode recording, as well as

intracerebral stimulations during wakefulness and NREM to further investigate connectivity of epileptogenic and healthy tissue (Valentin, Brain, Valentin, Lancet). The decision on the investigated hemisphere, the duration of implantation and stimulation site(s) was made according to clinical assessment needs.

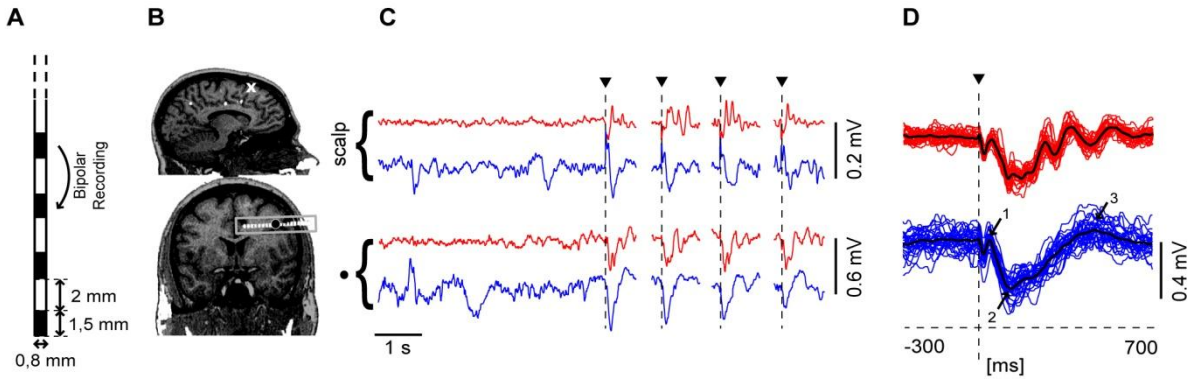

Figure 3.2.1: Experimental setup and methods for intracerabral stimulation and recordings.
Panel A. Outline of multilead intracerebral electrode. **Panel B**. Sagittal and coronal sections of Sbj.1 MRI showing an example of a multilead intracerebral electrode (grey rectangle). Contacts are depicted in white (see methods) while a white X indicates stimulation site. **Panel C.** Representative raw intracerebral EEG recordings and the concurrent scalp EEG for W (red) and NREM (blue). The first 5 s of each trace display spontaneous EEG activity followed by evoked responses to the intracerebral stimulation (dotted lines and black triangles). **Panel D**. Evoked EEG activity at an intracerebral site. All stimulations occurred at the same bipolar derivation indicated by the white X in panel A (top left). Colored traces represent single trials collected in W and NREM (red and blue rispectively) at a given recording site (black circle onto the MRI axial section of panel A). Average responses are overlaid in black. Dotted lines and triangles represent stimulus onset.

Data recording. SEEG activity was recorded from platinum–iridium semiflexible multilead intracerebral electrodes, with a diameter of 0.8 mm, a contact length of 2 mm, an intercontact distance of 1.5 mm and a maximal contact number of 18 (Dixi Medical, Besancon France - Figure 1B – Cossu, 2005). The individual placement of electrodes was ascertained by post-implantation tomographic imaging (CT) scans. Scalp EEG activity was recorded from two platinum needle electrodes placed during surgery at “10–20” positions Fz and Cz on the scalp. Electroocular activity was recorded at the outer canthi of both eyes, and submental electromyographic activity was also recorded. EEG and SEEG signals were recorded using a 192-channel recording system (NIHON-KOHDEN NEUROFAX-110) with a sampling rate of 1000Hz. Data was recorded and exported in EEG Nihon-Kohden format (Nobili et al., 2012). Recordings were referenced to a contact located entirely in the white matter.

ICS was performed three days after electrode implantation. A 5mA current was applied through one pair of adjacent contacts, while SEEG activity was simultaneously recorded from all other bipolar contacts. A single stimulation session consisted of a 30 pulse stimulation train at a frequency included in the range of 0.2-1Hz. All patients were stimulated during stage N3 of NREM-sleep. Sleep staging was performed by two of the authors (L.N. and P.P.) using standard AASM criteria (Silber et al., 2007). Stimulations which elicited muscle twitches, sensations or cognitive symptoms, were excluded from this study, in order to prevent possible awareness of stimulation or alteration of sleep depth. The stability of stage N3 was assessed by comparing the power spectra of scalp EEG (Fz-Cz) spontaneous activity before and after stimulation train.

Data preprocessing. Data recorded during both wakefulness and NREM were imported from EEG Nihon Kodhen format into Matlab and converted using a customized Matlab-based script. For all recording contacts, bipolar montages were calculated by subtracting the signals from adjacent contacts of the same depth-electrode to minimize common electrical noise and to maximize spatial resolution (Cash et al., 2009; Gaillard et al., 2009) (Figure 3.2.1A). In order to extract LFPs from the recordings, data were subjected to linear detrend and bandpass filtering (0.5 - 300Hz), using a High-/and a Lowpass third order Butterworth filter. An addition a 50Hz notch filter was used to minimize electrical artifact contamination. Stimulation peaks were detected from the channel closest to the stimulation site and used as triggers to split the recordings into single trials using an automated customized Matlab script. Stimulation artifact was then removed by applying a median filtering between -5 and 5 ms (Chang et al., 2012).

Contacts located in white matter, as assessed by means of MRI, were excluded (by two of the authors: L.N. and C.S.) from further analysis. Furthermore, we rejected all contacts that (1) were located in the epileptogenic zone, (2) were located over regions of documented structural brain damage as measured by the radiographic assessment, or (3) exhibited spontaneous or evoked epileptiform SEEG activity (Valentín et al., 2005, 2002; van ’t

Klooster et al., 2011). For all the selected bipolar contacts, single trials were inspected manually using a semi-automatic, customized Matlab script to reject all trials exhibiting pathological or abnormal interictal activity and electrical artifacts.

Data processing and statistical analysis.

Event related spectral perturbation (ERSP). We calculated the event related spectral perturbation (ERSP) of every CCEP using EEG-Lab (Delorme and Makeig, 2004) routines as shown in Figure 3.2.2A. In particular, time-frequency spectra were calculated on a single trial basis using Wavelet Transform (Morlet, 3 cycles). The color at each image pixel then indicates power (in dB) at a given frequency and latency relative to the time locked event. Significance of deviations from baseline power (calculated from -250 ms to -50 ms) is assessed using a bootstrap method (α=0.05, number of permutation=500). Non-significant activity is set to zero (green).

Power >20Hz. For every channel high frequency power was calculated as the mean value of the ERSP over 20 Hz (Cash et al., 2009).

Power >20Hz. For every channel low frequency power was calculated as the squared absolute value of the CCEP after 4Hz low-pass third order Butterworth filtering, normalized for the baseline (from -250 ms to -50 ms).

Phase locking factor (PLF). For every contact, on single trial data filtered with a 8Hz high-pass third order Butterworth filter, instantaneous PLF was calculated as in Sinkkonen et al. (1995) , Palva et al. (2005) and Casali et al. (2009). Specifically, given a set of complex numbers on the unit circle, phase-locking factor (PLF) can be defined as the absolute value of their average. Complex analytic signals can be computed from single-trial time series of each channel $v(ch_v,t,k)$ by means of the Hilbert transform (H(•)) as $z(ch_v,t,k)=v(ch_v,t,k)+iH(v(ch_v,t,k))$, and then normalized to obtain unitary absolute values $z_n(ch_v,t,k)$. Therefore, instantaneous PLF of a single CCEP can be obtained as (Casali et al., 2010; Palva et al., 2005; Sinkkonen et al., 1995):

$$PLF(ch_v, t) = |\bar{z}_n(ch_v, t)| = \left|\frac{\sum_k z_n(ch_v, t, k)}{N_k}\right|.$$

PLF is dimensionless and ranges from 0 (random phases) to 1 (perfect phase locking). Under the null hypothesis that the complex numbers $\{z_n(ch_v,t,k)\}$ at each time sample *t* are randomly uncorrelated and uniformly distributed, PLF values follow a Rayleigh distribution

$$P\big(PLF(ch_v, t)\big) = \frac{\pi \cdot PLF(ch_v, t)}{2m^2} e^{-\frac{\pi PLF^2(ch_v,t)}{4m^2}},$$

with *m* being the mean distribution value, that can be estimated from baseline by

$$m(ch_v) = \frac{\sum_{t=-T}^{-1} PLF(ch_v, t)}{T}.$$

The null hypothesis of random phase distribution of CCEP can be rejected with a level of significance *α* when $P(PLF(ch_v,t)) > 1 - \alpha$.

Summing up, this adimensional (range 0-1) index is defined as the absolute value of the average of the Hilbert Transform of all single trials and, in the case of CCEPs, it reflects the ability of an external electrical stimulus (ICS) to affect the phase of ongoing oscillations across trials (Casali,2009). For statistical analysis we used a Rayleigh distribution with $\alpha<0.05$.

Phase locking value (PLV). Finally, we measure PLV for every couple of contacts. PLV is defined as the phase difference across trials between X and Y -each one being the complex representation (obtained by Hilbert transform) of the filtered LFP x and y respectively- within a given frequency range (Lachaux, 1999). Specifically, defining $x'(t) = x(t) + iH(x(t))$ as the complex representation of the bipolar signals where (H(•)) denotes the Hilbert transform, PLV is computed as:

$$PLV = \frac{1}{K}\left|\sum_{r=1}^{N}\sum_{t=1}^{T}\frac{x_r'(t)}{|x_r'(t)|}\frac{y_r'^{*}(t)}{|y_r'(t)|}\right|$$

where *r=1…N* indicates the trials, each lasting *T* samples, *K = NxT* and * indicates the complex conjugate. This method extracts *de facto* the phase differences between every couple of channels.

In the case of CCEPs, PLV allows detecting phase difference between two recording sites. In particular, this method uses responses to a repeated stimulus and looks for latencies at which the phase difference between the signals varies across trials within a given frequency range (Lachaux, 1999). PLV is adimensional and bounded between 0 and 1 meaning respectively uncorrelated and full phase correlation.

Statistical analysis was performed by means of bootstrap-based method ($\alpha<0.05$) on single trial data (Lachaux et al., 1999) filtered with a 8Hz high-pass third order Butterworth filter.

For every subject, PLV was firstly calculated for every couple of channels over time obtaining a three dimensional matrix (channels x channels x time) and non-significant samples are set to zero. Then, for ease of display, we average PLV matrices over time using 100 ms time steps (see Figure 3.2.5A).

3.2.2 – Results

ICS evokes different responses in NREM sleep and wakefulness*.* In all subjects (table 3.2.1) ICS was delivered both during wakefulness and NREM through one pair of adjacent (2 mm apart) contacts pertaining to the same depth-electrode, while SEEG recordings were obtained from all other bipolar contacts (Figure 3.2.1A-B; see materials and methods for a detailed description of the number and location of the stimulating and recording contacts in each subject). Depending on clinical needs, in each subject a selected number of cortical sites were stimulated with 30 pulses at frequencies between 0.2 and 1 Hz (see materials and methods for details about the stimulation parameters) during wakefulness preceding lights off and during sleep stage N3 (AASM). Sleep stages were identified by scoring the EEG

recorded from one electrode at the scalp (Sarasso et al., 2014), while stability of stage N3 was assessed by comparing the power spectra of scalp EEG spontaneous activity before and after the stimulation train.

As illustrated in Figure.3.2.1C, CCEP were characterized by a high signal-to-noise ratio, could be detected in the scalp EEG and were clearly visible in intracranial recordings. At this level, the waveform of CCEPs was reproducible from trial to trial but differed markedly between wakefulness and NREM sleep (Figure.3.2.1D). Generally, during wakefulness ICS evoked a composite response made of recurrent waves of activity that persisted until 300 - 600 ms. Conversely, during NREM sleep the CCEPs consisted in a simpler and slower wave, composed of three consecutive electrical events, which we will call henceforth component 1, 2 and 3 (as illustrated in the example of Figure 3.2.1D). The polarity of these components could be inverted depending on the location of the recording contacts. In all cases, component 1 was a sharp peak (between 20 and 50 ms), component 2 was a prominent rebound of opposite polarity (peaking between 100 and 400 ms) and component 3 was the ensuing, smoother positive deflection.

ICS induces suppression of high-frequency power in NREM sleep but not in wakefulness. As first step, we wanted to verify whether the slow-wave-like response triggered by ICS during NREM sleep was associated, like spontaneously occurring sleep slow waves (REF), with a cortical downstate. According to animal and human intracranial recordings, the silent hyperpolarized period that characterizes the downstate of cortical neurons is reflected in the local field potential (LFP) by a clear-cut suppression of high-frequency (above 20Hz) oscillations. Hence, we characterized the differences in cortico-cortical responsiveness during wakefulness and sleep by performing time-frequency decomposition of CCEPs (see material and methods). Figure 3.2.2A shows the responses obtained in one subject at three representative cortical targets and the associated power modulation in different frequency bands (from 2Hz - 100Hz) as assessed by ERSP (Delorme and Makeig, 2004 - 3 cycles, $\alpha<0.05$).

This analysis shows that while the composite CCEPs recorded during wakefulness corresponded to a steady increase in spectral power, the slow wave-like response elicited in NREM sleep was subtended by an alternation of positive and negative significant power modulations (compared to baseline, bootstrap, $\alpha<0.05$). Specifically, component 1 of the NREM sleep response coincided with a transient broad-band increase of spectral power, component 2 was associated with a significant strong suppression of high-frequency oscillations (>20 Hz), whereas component 3 corresponded to a regain of spectral power, that was observable in a wide range of frequencies above 8 Hz. The suppression of high frequency (>20 Hz) that followed ICS during NREM was comparable to the suppression in the LFP occurring during the negative going phase of scalp recorded spontaneous sleep slow waves. Notably, this suppression was always associated with component 2 irrespectively of its polarity.

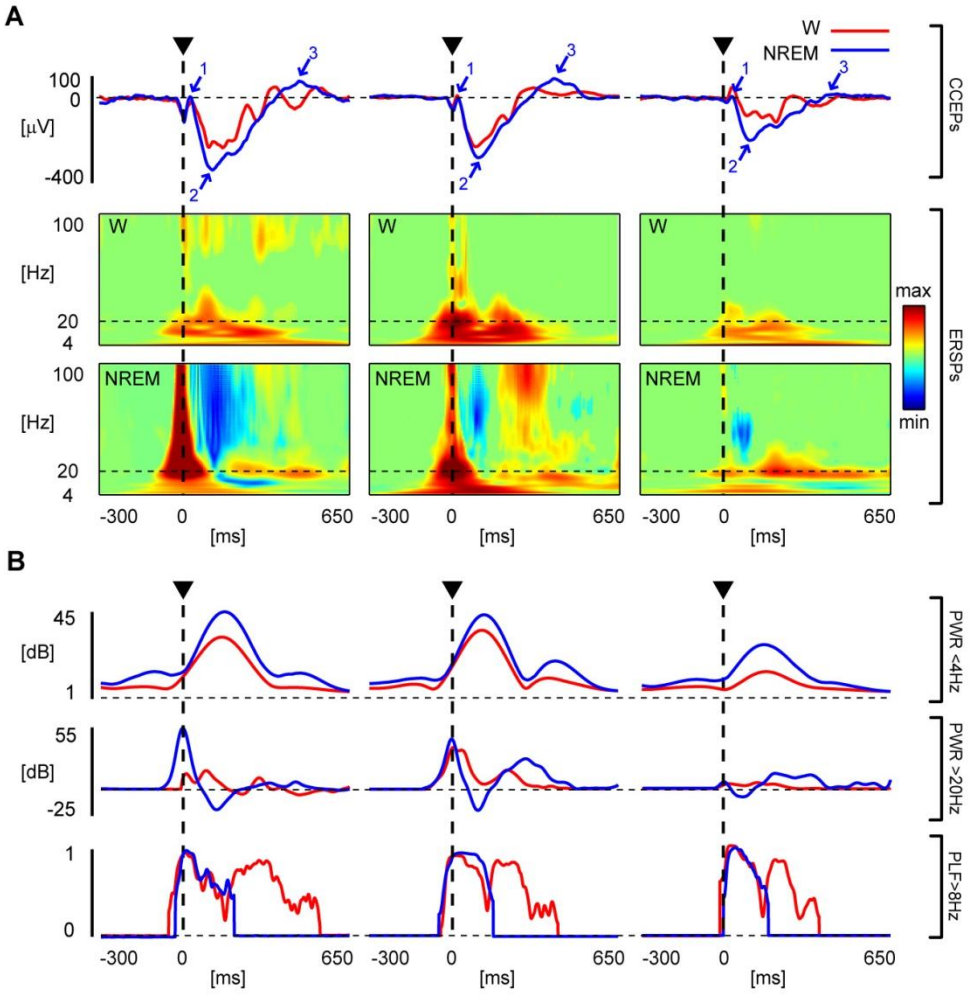

Figure 3.2.2. Processing and analysis of ICEPs. ICS triggers a cortical downstate in NREM that underlies loss of PLF.

This figure is all referred to Sbj.1. Dotted lines and triangles represent stimulus onset. **Panel A**. top panel shows representative ICEPs recorded in W (red) and NREM (blue) from three recordings bipolar derivations. From top to bottom following analysis are all referred to these three examples. Bottom panel shows time-frequency power spectra of ICEPs recorded in W and NREM. Time-frequency decomposition is applied at a single trial level using Wavelet Transform (Morlet, 3 cycles) and significance is set with p<0.05 (bootstrap). Non significant activity is set to zero (green). Blue color indicates a significant reduction compared to the baseline, while red indicates significant increase. **Panel B.** For the same three contacts of Panel A, Panel B shows from top to bottom: Power<4Hz, suppression of high frequency an PLF in wakefulness (red)and NREM sleep (blue). Power of low frequencies (<4Hz) is shown in autoscaled plots. High frequency suppression are obtained by averaging statistically significant spectral activity over frequencies higher than 20Hz. Plots are autoscaled. PLF is calculated on a single trial level after high-pass filtering (>4Hz). Non significant activity is set to zero. Significance of deviations from baseline is assessed using Rayleigh distribution. In particular plots are set to the same threshold to show significant ($p < 0.05$) changes of PLF compared with a period of 250 to 50 ms before the stimulus (Reyleight distribution, see methods).

Phase-locking to ICS is short-lasting during NREM sleep but sustained during wakefulness . Next, we tested the main hypothesis that, while during wakefulness a local perturbation with ICS triggers in its cortical targets an unabridged sequence of deterministic neuronal events, during NREM sleep this causal chain is interrupted by the occurrence of a silent neuronal down-state. We quantified the downstate evoked by ICS according to the accepted definition - a slow (<4 Hz) wave associated with a suppression of high-frequency

(20-100 Hz) power (REF) - and we employed phase-synchrony measures to quantify the causal effects of ICS. In this latter case, we computed the time course of the PLF in the signal filtered between 8 and 100 Hz, the frequency range that characterized both wakefulness activity and the resumption of the wakefulness-like neuronal oscillation associated with the component 3 of the NREM sleep response.

Figure 3.3.2B shows, for three representative contacts, the time courses of low frequency (<4 Hz) power, the significant (α=0.05) power changes cumulated between 20 and 100 Hz, together with the profile of the significant (Rayleigh, α=0.05) PLF (8-100 Hz), calculated during wakefulness and NREM sleep. Cortical responses to ICS during NREM sleep were characterized by a low frequency (0-4 Hz) fluctuation, by a significant suppression of high-frequency (20-100Hz) activity (corresponding to component 2), and by a concurrent drop of PLF, which remained below significance level throughout component 3. By contrast, during wakefulness, the low frequency component was reduced, the suppression of high frequency was absent and the time course of PLF persisted above chance levels until 400-600 ms. These differences in low frequency modulation, high-frequency suppression and phase-locking duration between wakefulness and NREM sleep were reproducible across cortical targets, as shown in Figure 3.2.3A. Moreover, by averaging low frequency power and high frequency power in the time interval included between -50 and 50ms around slow wave peak and considering the last significant point of PLF, the differences between wakefulness and sleep were consistent in all eight subjects (ttest $p<0.05$) (Figure 3.2.3B) and across subjects (Figure 3.2.3C – Wilcoxon ranksum test, $p<0.05$). An exception to the rule was represented by the contacts immediately adjacent to the stimulation site, which showed a larger increase in slow wave power during wakefulness and a concurrent significant suppression of high-frequency power (top contacts in Figure 3.2.3A). Notably, this suppression during wakefulness was never followed by a decay of PLF.

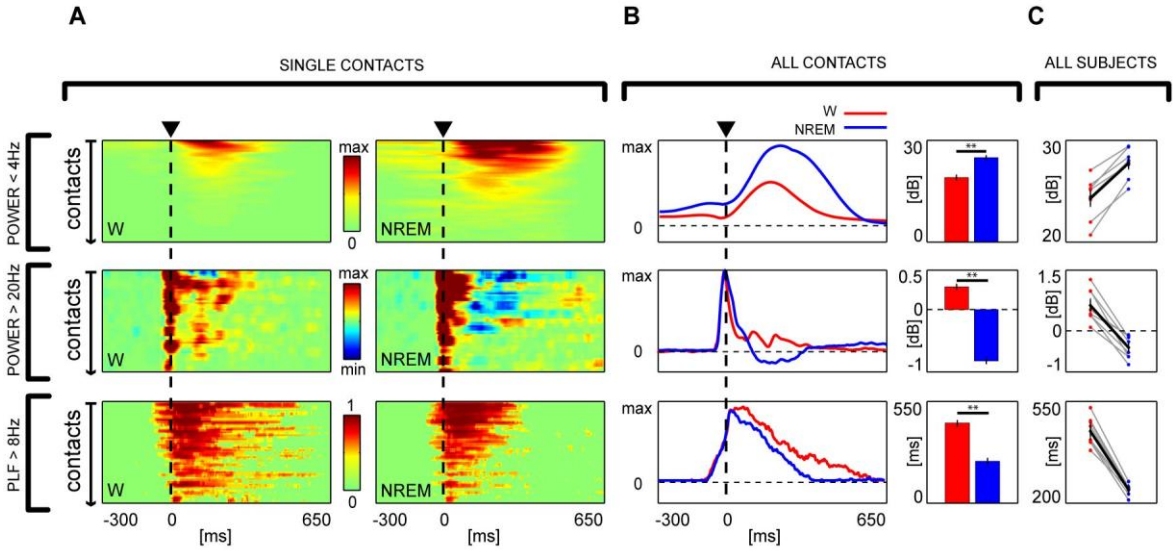

Figure 3.2.3. Statistical analysis across contacts and subjects.
Panel A. Color coded plots for low frequencies power (0.5-4Hz), for gamma frequencies power (20-100Hz) and for PLF (>4Hz), all calculated as a function of time and across channels both for W and NREM. For both conditions (W and NREM) and each plot, every row represents a single channel and y-axis is ranked based on low frequency power during NREM. **Panel B.** For each measure Panel B show the time series for W (in red) and NREM (in blue) obtained averaging across channels the activity of the color coded plots (low frequencies on the top panel, high frequencies in the central panel, PLF on the bottom panel). As in Figure 3.2.2, for high frequency suppression, significance is set with $p<0.05$ with non-significant activity set to zero (green). Blue color indicates a significant reduction compared to the baseline, while red indicates significant increase. For PLF analysis, plots are set to the same threshold to show significant ($p < 0.05$) changes of PLF compared with a period of 250 to 50 ms before the stimulus (Reyleight distribution, see methods). The histograms in Panel B show (both for W and NREM) the mean value of low frequency power and high frequency power in a time interval including time samples around the peak of the mean low frequency power (-50:50ms) and the last significative point of PLF. Black vertical lines indicates one standard error. ** indicate significant differences (paired ttest, $p<0.05$) between W and NREM. **Panel C.** Mean value across channels of low frequency power, high frequency power and last significant time point of PLF for all subjects. Statistical analisys across subject reveled significant differences in all cases (Wilcoxon Ranksum test, $p<0.05$).

Power and phase-locking modulations of cortical responses are related during NREM sleep. We then asked whether the three distinctive features of the NREM sleep response found at the level of each contact (i.e. larger slow wave, high frequency suppression and shorter PLF duration) were related. For each subject, we selected the contacts that showed the highest low frequency power (top 20%) during NREM sleep. Across these contacts we then computed (i) the correlation between the maximum power of the evoked slow wave (max SWp) activity and the maximum level of suppression of high-frequency power with respect to baseline (max SHFp) as well as (ii) the correlation between the timing of the maximum value of high frequency suppression (max SHFt) and the latency at which PLF dropped below the level of significance (max PLFt). This analysis showed significant correlations in all subjects suggesting (i) that larger evoked slow waves corresponded to

more pronounced suppressions of high frequencies and (ii) that earlier suppressions corresponded to an earlier decay of PLF (Figure 3.2.4).

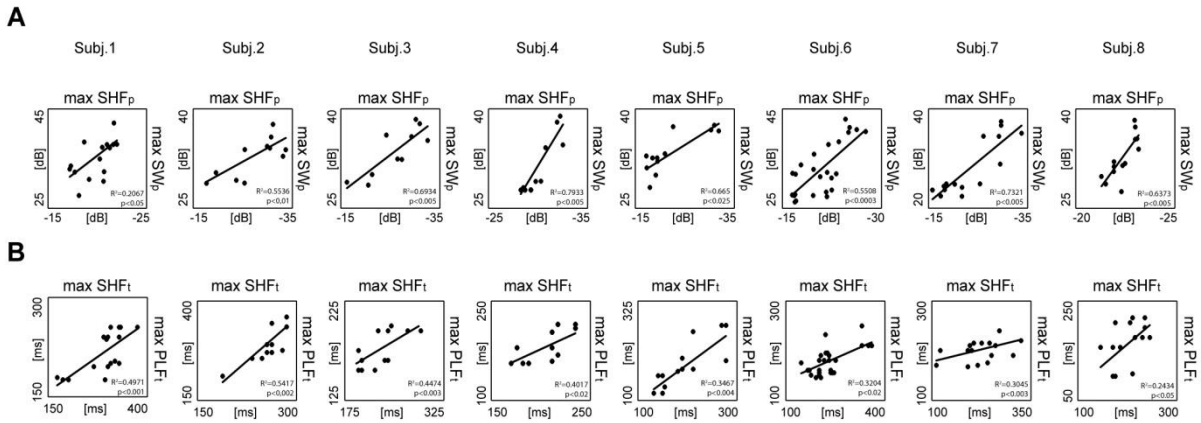

Figure 3.2.4. In NREM, suppression of high frequencies is proportional to low frequency power and time-related with PLF.

Panel A. For every subject, focusing on the higher low power ICEPs (top 20%) during NREM, correlation between minimum of suppression of high frequency power (x-axis) and maximal amplitude of low frequency power (y-axis) is shown. Pearson product-moment correlation coefficient ρ and coefficient of determination R2 indicate a linear negative correlation for all subjects (ρsbj1=-0.85563, R2sbj1=0.7321, ρsbj2=-0.74406, R2sbj2=0.5536, ρsbj3=-0.83269, R2sbj3=0.6934, ρsbj4=-0.8907, R2sbj4=0.7933, ρsbj5=-0.81549, R2sbj5=0.665, ρsbj6=-0.74219, R2sbj6=0.5508, ρsbj7=-0.45413, R2sbj7=0.2067, ρsbj8=-0.79783, R2sbj8=0.6373). Statistical significance of correlations is assessed using a paired t-test (psbj1<0.00005, psbj2<0,01, psbj3<0.005, psbj4<0.005, psbj5<0.025, psbj6<0.00003, psbj7<0.09, psbj8<0.005).**Panel B.** For every subject, focusing on the higher low power ICEPs (top 20%) during NREM, correlation between timing of minimum of suppression of high frequency power (x-axis) and last significant time point of PLF (y-axis) is shown. Pearson product-moment correlation coefficient ρ and coefficient of determination R2 indicate a linear positive correlation for all subjects (ρsbj1=0.551843, R2sbj1=0.3045, ρsbj2=0.736013, R2sbj2=0.5417, ρsbj3=0.66887, R2sbj3=0.4474, ρsbj4=0.633759, R2sbj4=0.4017, ρsbj5=0.58885, R2sbj5=0.3467, ρsbj6=0.566041, R2sbj6=0.3204, ρsbj7=0.70504, R2sbj7=0.4971, ρsbj8=0.493347, R2sbj8=0.2434). Statistical significance of correlations is assessed using a paired t-test (psbj1<0.003, psbj2<0,002, psbj3<0.003, psbj4<0.02, psbj5<0.004, psbj6<0.02, psbj7<0.001, psbj8<0.03).

Phase-locking among contacts is short-lasting during NREM sleep but sustained during wakefulness. Finally, we asked whether the lack of PLF to ICS at each cortical target depends on local properties of single cortical areas or depends on network properties. In order to shed a light on this issue and to investigate the effects induced by NREM on network phase synchrony, we compared PLV calculated during sleep and wakefulness (see materials and methods and supplementary materials for a detailed description of PLV calculation). Figure 3.2.5A shows the HFS of a representative subject (upper panel – blue line) and the PLV matrices (lower panel) averaged in 100 ms time windows (see methods). Overall, after the stimulation PLV had a widespread increase both in wakefulness and in NREM. After the 100-200 ms time window, in correspondence to the HFS minimum, PLV breaks down in sleep while it persist until 400-500 ms in wakefulness. These results are consistent across individuals as confirmed (Figure 3.2.5B) by computing a two way repeated

measure analysis of variance (ANOVA) between condition (wakefulness, NREM) and time windows (BL, 0-100 ms, 100-200 ms, 200-300 ms, 300-400 ms, 400-500 ms, 500-600 ms). The temporal overlap between the occurrence of HFS and the drop in PLV is suggestive of a relationship between neuronal silencing and the loss of phase synchrony across distributed cortical sites.

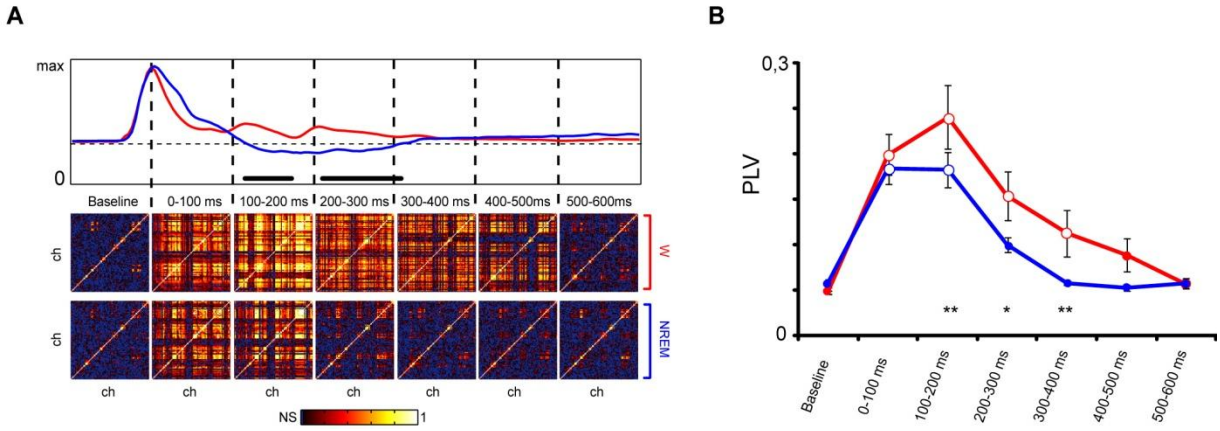

Figure 3.2.5. Breakdown of PLV following suppression of high frequencies.
Panel A. For one representative subject top panel show suppression of high frequencies occurring during NREM and not during wakefulness. Bottom panel shows PLV matrices calculated averaging PLV of every couple of contacts over 100ms range. Every point of the depicted matrices correspond to a couple of contacts. Non significant (phase locking statistics, $p<0.05$) were set to zero (dark blue). **Panel B.** Results obtained by computing a two way repeated measure analysis of variance (ANOVA) between condition (wakefulness in red, NREM in blue) and time windows (BL, 0-100 ms, 100-200 ms, 200-300 ms, 300-400 ms, 400-500 ms, 500-600 ms) across all subjects. ** and * indicate time interval where conditions (W and NREM) are statistically different across subjects ($p<0.01$ and $p<0.05$ respectively). White bullets, per each condition, indicate time interval in which PLV is statistically different from baseline.

3.2.3 - Discussion

In the work presented in this chapter we performed and compared CCEPs recorded during wakefulness and NREM sleep by means of time-frequency analysis and phase-locking measures in 8 epileptic patients with implanted SEEG electrodes for pre-surgical evaluation. Our results showed that low frequency power evoked by ICS was significantly higher during deep sleep than during wakefulness (Figure 3.2.2-3.2.3) and was associated with an intense and widespread suppression of high frequency power across channels. Moreover, during NREM, suppression of high frequency correlates in time with a breakdown of phase synchrony both at a single channel level (PLF – Figure 3.2.2 and Figure 3.2.3) and at a network level (PLV - Figure 3.2.5).

Intracerebral recording and generator mechanisms of CCEPs

Intracerebral recordings, both spontaneous or in combination with single or repetitive electrical stimulation, are often the only viable solution for the precise localization of the epileptic zone in drug-resistant focal epilepsy patients (Duffau et al., 2005; Ojemann et al., 2008; Valentín et al., 2005, 2002; van 't Klooster et al., 2011; Wilson and Engel, 1993; Wilson et al., 1998). Intracerebral recording associated with intracerebral stimulation was also employed to map functional connectivity of different networks of human brain: language system (Matsumoto et al., 2004), cortical motor system (Matsumoto et al., 2007) and parieto-frontal network (Matsumoto et al., 2012). In these studies from Matsumoto and colleagues the possible generator mechanisms of CCEPs have already been largely discussed. In brief, after an electrical pulse performed into the grey matter, orthodromic excitation of cortico-cortical projection neurons occurs close to the stimulation site through (i) direct depolarization of the initial segment of the axons and (ii) synaptic excitation in the local circuit (Matsumoto, 2004, 2011). Then, with polisynaptic excitation of connected neurons, the impulse travels through direct cortico-cortical pathways or through indirect cortico-subcortical-cortical pathways generating CCEPs in adjacent or remote areas (Matsumoto, Brain, 2004). Thus, the differences between the CCEPs evoked during wakefulness and NREM (see results, Figure 3.2.1D and Figure 3.2.2) may be reasonably related to functional changes in cortico-cortical networks and/or cortico-subcortico-cortical networks.

During NREM, a cortical downstate is associated with a breakdown of causality in thalamo-cortical system

Computer simulations (Bazhenov et al., 2002; Compte et al., 2003; Hill and Tononi, 2005) and in vitro recordings (Sanchez-Vives and McCormick, 2000) showed that the occurrence of slow waves during NREM sleep reflects an intrinsic bistability of thalamocortical networks between periods of depolarization and intense firing (upstates), interrupted by short, deeply hyperpolarized periods of neural silence (downstates). The latter, in particular, are reflected in slow deflections of EEG signal associated with corresponding strong and consistent

decreases in gamma EEG power (>20Hz) and multiunit activity, as shown by both animal (Contreras et al., 1996; Sanchez-Vives and McCormick, 2000; Steriade, 2001) and human (Cash et al., 2009; Csercsa et al., 2010) intracranial recordings.

Along the same line, unlike during wakefulness in which ICS lead to complex, long-range patterns of activation, differentiated among various cortical areas, during sleep ICS triggers a short leave slow EEG response - highly resembling the spontaneous slow wave- that was found associated with high frequency suppression thus possibly reflecting a cortical downstate. This result is in line with previous non-invasive empirical studies that combined EEG recordings with Transcranial Magnetic Stimulation (TMS/EEG) during NREM sleep (Massimini, 2005) showing that a TMS pulse evokes a stereotypical slow wave only in the case of LOC and not in aware conditions, possibly revealing an intrinsic bistability of thalamocortical networks during LOC (Massimini, 2007). Similarly, other TMS/EEG studies showed that this slow wave characterizes also pharmacologically induced LOC (Ferrarelli et al., 2010) and pathological conditions such as vegetative state (Rosanova et al., 2012), thus suggesting that bistability, and in particular the occurrence of a downstates, could be a common mechanism of LOC.

This hypothesis is in line with the information integration theory (Tononi, 2008), which states that the level of consciousness is given by a system's capacity to generate integrated information. According to the theory, the brain substrate of consciousness is a complex of neural elements within the thalamocortical system that has a large repertoire of available states (information), yet cannot be decomposed in a collection of causally independent subsystem (integration). In this view, integrated information would be high during wakefulness because thalamocortical networks have a large repertoire of global firing patterns that are continuously available on a background of tonic depolarization. During LOC, instead, bistability would reduce this global repertoire possibly through two mechanisms. First, a local activation would cause a local downstate preventing effective interactions with other brain areas breaking down thalamocortical complex in causally independent, segregated modules (loss of integration). Second, to the extent that global activation patterns

can still occur, they too would be rapidly followed by a global stereotypical downstate, thereby greatly reducing the repertoire of available states (loss of information).

Our observations strengthen the binding between these theoretical predictions and previous TMS/EEG studies and, furthermore, confirm that the downstate has a key role in the mechanisms of LOC during deep sleep. Specifically, phase-locking measures (of CCEPs) point to a disrupting effect of the neural silence (i.e. the downstate) on information flow in thalamocortical system breaking down causality among different cortical areas. Indeed, first the PLF of long latency (over 300 ms) high frequency (>8Hz) components breaks down after the downstate (correlations in Figure 3.2.4) suggesting a loss of information, if compared to PLF of wake. Second, PLV measures showed a long-latency cross-channels synchronization just in wake and not in NREM, suggesting that the breakdown of PLF after the downstate is not merely due to intrinsic properties of single thalamo-cortical modules, but depends on the loss of interactions (integration) among and within them.

As a note, a slow wave with corresponding HFS was observed in the CCEPs evoked during wakefulness only in the channels close to stimulation site as shown for instance in Figure 3.2.3 (top contacts). This is in line with Bochers et al. (2012) where the authors proposed a possible paraphysiological mechanism describing the response to a direct electrical stimulation as an inhibition induced in those cortical areas that receive direct (monosynaptic) input from the fibers of the stimulated neurons. Interestingly, in these cases of suppression of high frequency evoked by ICS during wake, PLF of long latency activity doesn't breakdown as during NREM (Figure 3.2.3). Thus, it is likely that in the former case information flow is guaranteed by feedbacks from integrated distant cortical areas, while in the latter case the segregation of different cortical areas breaks down information flow.

Upstate: "fragment of wakefulness" or just stochastical regain on firing?

Fast oscillatory activity (>20Hz) and spindles activity (12-15 Hz) in cats have been found to be distinctly grouped by slow (<1 Hz) oscillations (Amzica and Steriade, 1998; Contreras and Steriade, 1997, 1995; Contreras et al., 1996; Steriade, 1999). A grouping of spindle activity

by slow waves has been shown also in the human EEG (Achermann and Borbély, 1997; Mölle et al., 2002) and were suggested to be driven during the depolarizing phase of slow waves (upstate), during which the firing of neurons is increased. Moreover, slow oscillation upstate and the fully activated brain state (wakefulness) were found to be dynamically quite similar by both electrophysiological and modeling studies (Destexhe et al., 2007). Thus, individual corticothalamic upstates have been interpreted as micro-wake-like contexts, named “fragments of wakefulness” (Destexhe et al., 2007). However, the reason why their occurrence do not rise to conscious experience is yet to be explained. One possibility stems from recent intracerebral human studies showing that most sleep slow waves, and the underlying active and inactive neuronal states, occur locally and out-of-phase in different brain regions (Hangya et al., 2011; Nir et al., 2011; Nobili et al., 2012). Thus, whereas some regions could be silenced by the occurrence of a downstate impairing long-range interactions (see previous paragraph), other regions are active but segregated. This idea is supported by our results. Indeed, above and byond local coherent interactions revealed by the simple observation of the upstates (Destexhe et al., 1999), the perturbational approach we performed in the present study suggest that they just reflect a stochastic regain on firing of single segregated thalamo-cortical modules and not their interactions. This is particularly evident comparing CCEPs evoked during NREM with CCEPs evoked during wakefulness since a deterministic long-latency relationships among thalamo-cortical modules occurs just in the latter case. Specifically, even if long latency (over 200-300 ms) components are present in both behavioral conditions, in wake they are phase locked with ICS (high PLF) and synchronized over a significant number of channels (high PLV), whereas in NREM, PLF and PLV brake down after the downstate. Thus, during NREM, the upstate following the downstate is not phase locked with ICS across trials and is not even synchronized among channels, suggesting loss of networks deterministic components, likely due to loss of networks feedbacks, and an essential nature of stochastic regain of firing of the upstates. Nevertheless, our results do not exclude that cortical upstates might provide brief epochs of network dynamics that aid memory consolidation. Indeed, they are compatible with the

hypothesis that the differences existing between the dynamics of continuous waking and slow-oscillation upstate might function to alter the direction of information flow between cortical areas (Destexhe et al., 2007). Thus, LOC during sleep could be a mechanism employed by thalamo-cortical system to isolate specific networks from external inputs facilitating internal interaction aimed at memory consolidation. Future intracerebral studies on hippocampal-cortical networks could further investigate this issue.

CHAPTER 4 - IN VITRO CHARACTERIZATION OF THE NEURONAL AND NETWORK RESPONSES TO ELECTRICAL STIMULATION

As discussed in the previous chapter, at the cortical level, the most striking difference between wakefulness and NREM sleep is represented by the occurrence of short (few hundreds of milliseconds) periods of hyperpolarization and neuronal silence (down-states) that periodically interrupt longer stretches of spontaneous neuronal activity (up-states) indistinguishable from quiet wakefulness (Steriade et al., 2006). This alternation reflects an intrinsic bistability of cortical circuits and is thought to be primarily due to the dynamics of activity-dependent potassium (K+) currents, which become prominent when the neuromodulating milieu changes upon falling asleep.

Our hypothesis is that intrinsic bistability, per se, may substantially change the causal structure of thalamocortical networks in a way that is not immediately evident by observing spontaneous patterns of neuronal synchrony. Specifically, we hypothesize that (i) during NREM sleep any neuron, or group of neurons, that receive a cortico-cortical input would rapidly plunge into a down-state, (ii) that this period of silence is followed by a resumption of neuronal activity which retains no effects of the initial input and (iii) that this loss of determinism prevents the emergence of widespread causal interaction at the network level.

We have already tested these hypothesis as reported in the previous chapter. However, the physiological mechanism underling the loss of determinism occurring during NREM sleep has still to be explained. In order to deepen this phenomenon, we record from visual cortical slices (ferret) both spontaneous activity and activity evoked by electrical stimulation. This experimental model allows to simulate “sleep-like” and “wake-like” condition and to study the effect of different cellular mechanism (blocked or promoted by different drugs) on a small, controlled neuronal network. Moreover, comparing spontaneous and evoked electrical activity should allow measuring the causal effect of single pulse electrical stimulation on

cortical slices treated with different kinds of drug affecting, in turn, different kinds of cellular mechanisms.

4.1 – Experimental design

The array displayed in Figure 4.1 was used to electrically stimulate and record LFPs from ferret visual cortex. Recording was performed by the electrodes indicated by red numbers in Figure 4.1. The vertical dimension of the array allows recording from layer II, III (supragranual) and V (infragranular). Specifically, cortical slices were cut with the dimensions of the array and displaced on the array so that supragranular layers were recorded by electrodes from 1 to 8, while infragranual layers were recorded from electrodes from 9 to 16.

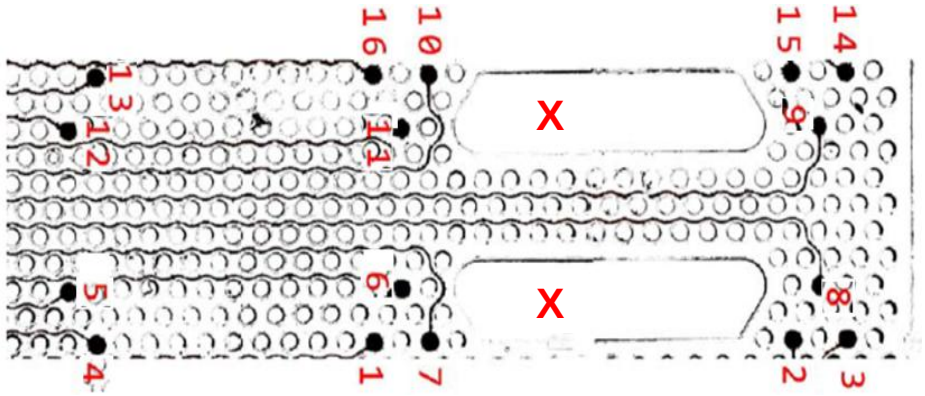

Figure 4.1: Array for stimulation and recording in cortical slices.
Horizontal distance between triodes was 692.8 µm, vertical distances between triodes was 1500 µm. Between electrodes distances was 200 µm while the diameters was 50 µm. Impedences was set between approximately 10 and 100kOhm at 1 kHz.

For each cortical slice we recorded both spontaneous and evoked activity. The latter was obtained by electrical stimulations performed alternatively in supragranular layers or infragranular layers by means of a bipolar electrode placed in the empty spaces of the array (red X in Figure 4.1). Stimulations were delivered on cortical slices using trains of 30 electrical stimuli with a duration of 0.3 ms, each 8s with a jitter of +/- 2s. Different stimulation intensities (30µA, 80µA and 150µA) were tested during the first experimental session in order to obtain a good SNR. Finally we set stimulation intensity to 150µA.

Both spontaneous and evoked electrical activity were performed in different conditions including control condition (no drugs), and conditions in which cortical slices were treated with different drugs (once at time or simultaneously, depending on the sessions). Specifically we employed:

- **Kainate**: a natural marine acid present in some seaweed. It is a specific agonist for the kainate receptor used as an ionotropic glutamate receptor which mimics the effect of glutamate.
- **Norepinephrine**: a catecholamine with multiple roles including as a hormone and a neurotransmitter. It is the hormone and neurotransmitter most responsible for vigilant concentration in contrast to its most chemically similar hormone, dopamine, most responsible for cognitive alertness.
- **Carbachol**: a cholinomimetic drug that binds and activates the acetylcholine receptor. Thus it is classified as a cholinergic agonist.

4.2 – Guided user interface

During the last year of PhD, I worked to develop a guided user interface (GUI) for data analysis of spontaneous and evoked electrical activity of cortical slices (Figure 4.2). This interface was used to explore preliminary data and to define, during the first experiments, an experimental protocol.

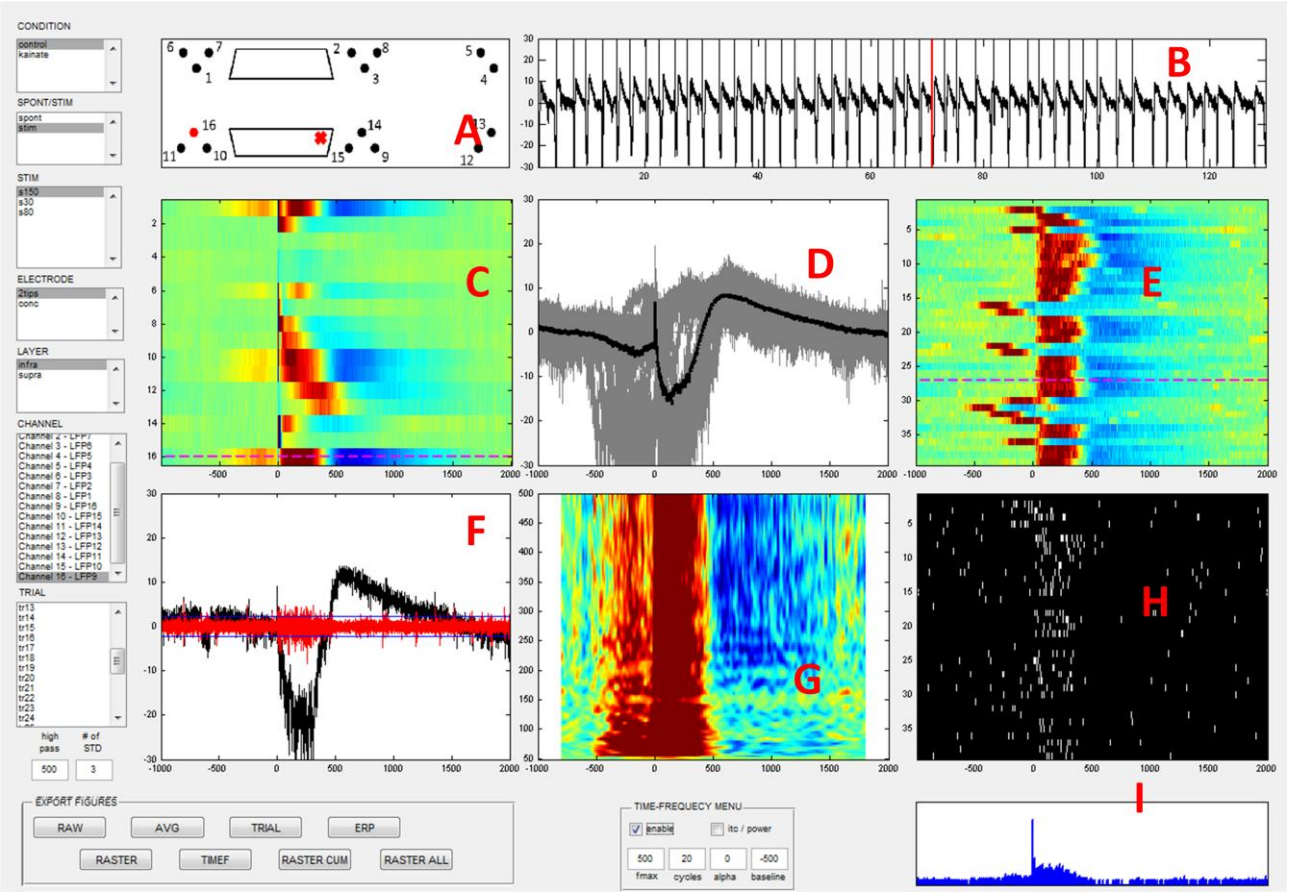

Figure 4.2: guided user interface for analysis of data recorded from cortical slices.
A- setup. Red cross indicates stimulation site, red dot indicates recording channels (the same shown in panels D, E, G and H; see below) **B**- raw data; red vertical line indicates the selected trial (the same shown in panel F); **C**- LFP for all channels is shown. The matrix is time x channel; in color-coding, red colors indicate negative amplitudes, blue colors indicate positive amplitudes. Dashed pink line indicates the selected channel shown in panel A by red dot. **D**- single trial and average for the selected channel (the one indicated by red dot in panel A). Single trials in gray, average in black. **E**- ERP image of the selected channel (the one indicated by red dot in panel A). Every line is a single trial. Red colors indicate negative amplitudes, blue colors indicate positive amplitudes. Dashed pink line indicates the selected trial shown in panel F. **F**- only one single trial (the same indicated in panel B by the vertical red line). Black sweep indicates the raw single trial, red sweep indicated the same trial high-pass (1000Hz) filtered. Blue horizontal lines are mean +/- 3 std of the baseline. **G**- time-frequency spectrum of the selected channel (the same of panel D). Compared to baseline, positive power in red, negative power in blue **H**- Raster-plot of the selected channel. Every line is a trial. For every trial white dots indicates the value of the filtered (1000) single trials that overcome 3 std of the baseline. **I**- Sum over trial of the raster-plot.

4.3 – Preliminary results

During the last year we performed four preliminary experiment to adjust experimental protocol and stimulation parameters.

Experiment 1. We explored the feasibility of electrical stimulation in cortical slices testing different stimulation intensities (30µA, 80µA and 150µA) delivered both in infragranular layers and supragranular layers using not only bipolar electrodes, but also concentric electrodes. All this parameters were tested in control condition and kainite.

Experiment 2. We tested the same parameters of Experiment 1 by comparing the same cortical slices in control condition and treated with norepinephrine. Based on the results of experiment 1 and 2 we selected for the further experiments bipolar electrode for stimulation, 150μA of stimulation intensity and infragranular layers as location for stimulation.

Experiment 3. We compared spontaneous and evoked activity obtained from the same cortical slices in control condition, treated with Kainate alone and treated with Kainate + Norepinephrine + Carbachol.

Experiment 4. We compared spontaneous and evoked activity obtained from the same cortical slices in control condition, treated with Norepinephrine + Carbachol and treated with Kainate + Norepinephrine + Carbachol.

4.3.1 – Setting parameters for experimental protocol

Starting from control condition we first evaluated the effects of electrical stimulation delivered at different intensities and using two different electrodes (bipolar or concentric).

Comparing stimulation intensities. Figures 4.3 was obtained by experiment 1 and displays three representative examples of response to electrical stimulation at three different intensities, from top to bottom 30 μA, 80 μA and 150 μA. From left to right panel shows the same measure of Figure 4.2 C,D and E, respectively the average of all trials for each channel (color coded), the average and single trials for channel 16 and color-coded single trials for channel 16. The comparison shown in Figure 4.3 allowed us to select 150 μA as standard intensity to achieve effective stimulations in later experiments.

Comparing stimulating electrodes. Figure 4.4 was obtained by experiment 1 and displays two representative examples of response to electrical stimulation achieved by delivering stimulation using bipolar or, alternatively, concentric electrode for stimulation (at 150 μA). From left to right panel shows the same measure of Figure 4.2 C,D and E, respectively the average of all trials for each channel (color coded), the average and single trials for channel 16 and color-coded single trials for channel 16. The comparison shown in Figure 4.4 allowed

us to select bipolar electrode as standard stimulator to achieve effective stimulations in later experiments.

Comparing stimulation site (infragranular VS supragranular). Figure 4.5 was obtained by experiment 1 and displays two representative examples of response to electrical stimulation delivered at 150 µA, using bipolar electrode in two different location: infragranular and supragranular. From left to right panel shows the same measure of Figure 4.2 C,D and E, respectively the average of all trials for each channel (color coded), the average and single trials for channel 16 and color-coded single trials for channel 16. The comparison shown in Figure 4.5 allowed us to select supragranular layers as standard site to achieve effective stimulations in later experiments.

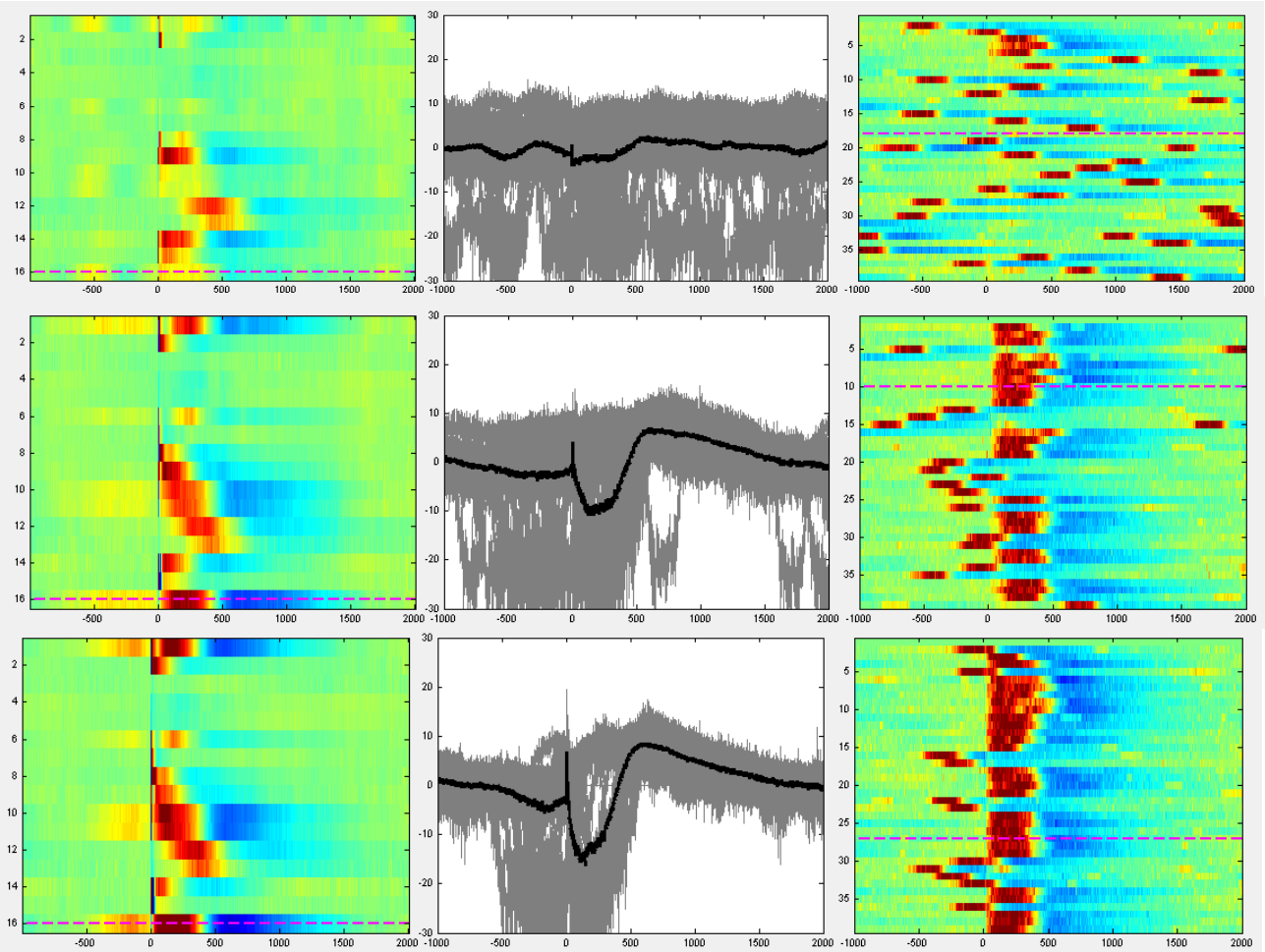

Figure 4.3: comparison between different intensities.

From left to right - LFP for all channels is shown. The matrix is time x channel; in color-coding, red colors indicate negative amplitudes, blue colors indicate positive amplitudes. Dashed pink line indicates the selected channel shown in panel A by red dot. - Single trial and average for the selected channel (the one indicated by red dot in panel A). Single trials in gray, average in black. - ERP image of the selected channel (the one indicated by red dot in panel A). Every line is a single trial. Red colors indicate negative amplitudes, blue colors indicate positive amplitudes. **From top to bottom.** The time courses obtained at three different intensieties: 30 µA, 80 µA and 150 µA. All figures are set to the same scale across condition.

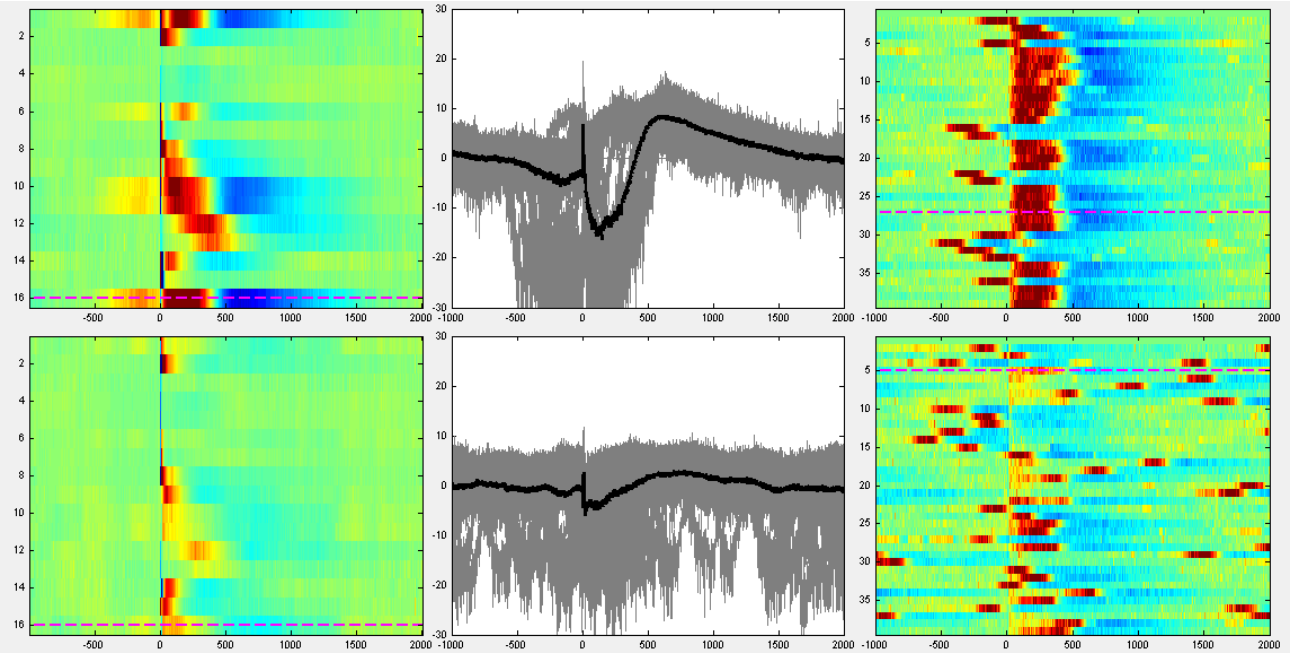

Figure 4.4: comparison between different stimulator.
From left to right - LFP for all channels is shown. The matrix is time x channel; in color-coding, red colors indicate negative amplitudes, blue colors indicate positive amplitudes. Dashed pink line indicates the selected channel shown in panel A by red dot. - Single trial and average for the selected channel (the one indicated by red dot in panel A). Single trials in gray, average in black. - ERP image of the selected channel (the one indicated by red dot in panel A). Every line is a single trial. Red colors indicate negative amplitudes, blue colors indicate positive amplitudes. **From top to bottom.** The time courses obtained by stimulating with two different electrodes: bipolar and concentric. All figures are set to the same scale across condition.

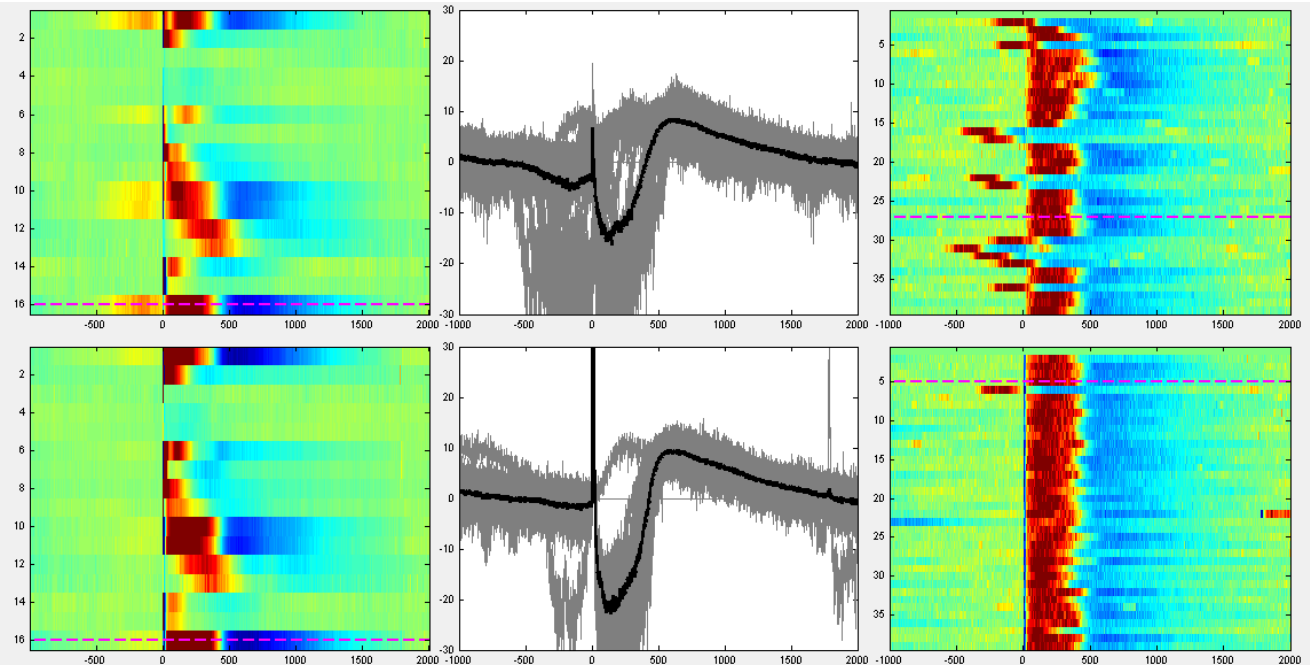

Figure 4.5: comparison between different stimulation site.
From left to right - LFP for all channels is shown. The matrix is time x channel; in color-coding, red colors indicate negative amplitudes, blue colors indicate positive amplitudes. Dashed pink line indicates the selected channel shown in panel A by red dot. - Single trial and average for the selected channel (the one indicated by red dot in panel A). Single trials in gray, average in black. - ERP image of the selected channel (the one indicated by red dot in panel A). Every line is a single trial. Red colors indicate negative amplitudes, blue colors indicate positive amplitudes. **From top to bottom.** The time courses obtained by stimulating in two different stimulation sites: infragranular layers and supragranular layers. All figures are set to the same scale across condition.

4.3.2 – Comparing the effects of Kainate, Norepinephrine and Carbachol.

Once stimulation parameters were set, we started to test the effects of different drugs on the activity evoked in cortical slices. Figure 4.6 shows some representative examples of LFP evoked in cortical slices treated with different drugs. Specifically, Figure 4.6 shows the same time courses displayed in Figure 4.2 C,D and E, with stimulation intensity set to 150 µA, stimulating with bipolar electrode the same cortical slice (from top to bottom) in control condition, treated with kainite alone, with norepinephrine alone, with norepinephrine + charbacol, with norepinephrine + charbacol + kainite. As shown in the figure, kainite alone induce in the LFP an increase of non-phase locked high frequency activity. Norepinephrine alone induce an increase of phase locking of frequencies between 1 and 2 Hz, while adding charbacol the increase of phase locked moves to the range 2-3 Hz. Finally, adding kainite to the "cocktail" the increase of phase locked activity range move beyond 3 Hz. In all cases, the downstate evoked in control condition is not present. These results are just preliminary and descriptive. Further experiments and a specific statistical analysis are needed to deepen the effects of different drugs and their effect at the network level.

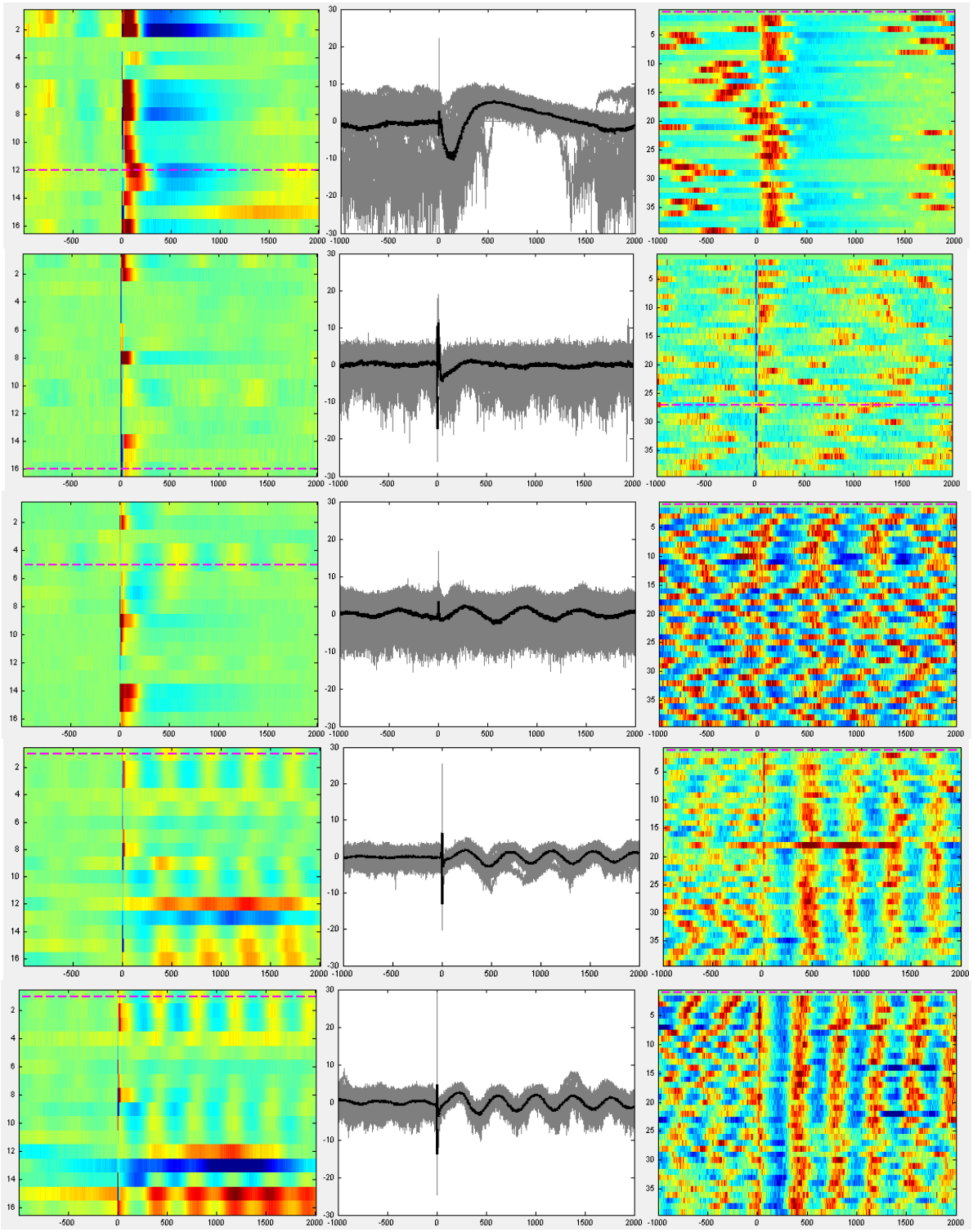

Figure 4.6: comparison between different drugs.

From left to right - LFP for all channels is shown. The matrix is time x channel; in color-coding, red colors indicate negative amplitudes, blue colors indicate positive amplitudes. Dashed pink line indicates the selected channel shown in panel A by red dot. - Single trial and average for the selected channel (the one indicated by red dot in panel A). Single trials in gray, average in black. - ERP image of the selected channel (the one indicated by red dot in panel A). Every line is a single trial. Red colors indicate negative amplitudes, blue colors indicate positive amplitudes. **From top to bottom.** The time courses obtained by stimulating the same slice in different condition: control, kainite alone, norepinephrine alone, norepinephrine + charbacol, norepinephrine + charbacol + kainite.

4.5 – Conclusions

Preliminary results showed that, as compared to a control condition, a solution containing kainite, norepinephrine and carbachol allows to evoke in cortical slices a more phase-locked response, indicating a possible increase of causal effect due to electrical stimulation. These results are encouraging and demonstrate the feasibility of the study. Moreover, they suggest that it is possible to use the tested drugs (kainite, norepinephrine and carbachol) to change the condition of cortical slices, moving them from a “sleep-like” condition to a “wakefulness-like” condition. Further experiments are already planned in order to confirm these results.

CHAPTER 5- BREAKDOWN OF INFORMATION INTEGRATION DURING SLEEP: AN INTRACEREBRAL STUDY IN HUMANS

As described in the first chapter of this work, a recently proposed theory suggests that the coexistence of integration and information is a key feature in the functional architecture of the thalamocortical system (Friston, 2008). This feature allows carrying out distributed computations among specialized nodes of a network. Most important, the balance between information and integration in thalamocortical networks has been considered as a fundamental requirement for the generation of conscious experience (Tononi, 2004). Neurophysiologically, this depends on the ability of neural elements to engage in complex activity patterns that are, at once, distributed within a system of interacting cortical areas (integrated) and differentiated in space and time (information-rich). Practically, a straightforward way to gauge the conjoint presence of integration and information in real brains involves directly probing the cerebral cortex (in order to avoid possible subcortical filtering and gating) by employing a perturbational approach (thus testing causal interactions rather than temporal correlations) and examining to what extent cortical regions can interact as a whole (integration) to produce differentiated responses (information).

In this chapter we report the results of a recent empirical study where we approximate information integration (by now just a theoretical measure) in real human brain. Specifically, using ICS and intracerebral recordings we demonstrate in a methodological paper the feasibility of calculation of Φ (integrated information) and its variations across sleep-wake cycle.

5.1 – Multivariate autoregressive models with exogenous inputs for intracerebral responses to direct electrical stimulation of the human brain

In Chang et al. (2012) we demonstrate the feasibility of calculation of information integration. The methodological procedure proposed in this paper is beyond the scope of this thesis, here we just summarize results and conclusions. In brief, multivariate autoregressive (MVAR) model with exogenous inputs (MVARX) was developed for describing the cortical interactions excited by direct electrical current stimulation of the cortex. Current stimulation is challenging to model because it excites neurons in multiple locations both near and distant to the stimulation site. Our approach models these effects using an exogenous input that is passed through a bank of filters, one for each channel. The filtered input and a random input excite a MVAR system describing the interactions between cortical activity at the recording sites. The exogenous input filter coefficients, the autoregressive coefficients, and random input characteristics were estimated from the measured activity due to current stimulation. The effectiveness of the approach was demonstrated using intracranial recordings from three surgical epilepsy patients. Specifically, we evaluate models for wakefulness and NREM sleep in these patients with two stimulation levels in one patient and two stimulation sites in another resulting in a total of 10 datasets. Excellent agreement between measured and model-predicted evoked responses were obtained across all data sets. Furthermore, one-step prediction was used to show that the model also describes dynamics in pre-stimulus and evoked recordings.

Finally, as a proof of concept application, we used the MVARX model to assess changes in the level of information-integration between wakefulness and deep sleep in human subjects. Using a simple, bipartition approximation we found that, as predicted by theoretical considerations (Tononi,2004;Sethetal.,2008), integrated information is higher in wakefulness than sleep for each subject/condition (as shown in Figure 4.7, modified by Chang et al.), supporting the notion that integrated information reflects the capacity for consciousness.

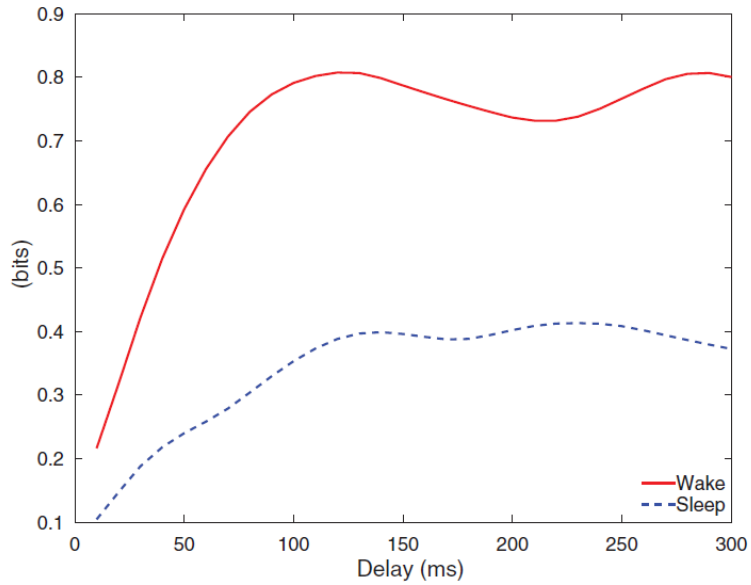

Figure 5.2.1: Time course of integrated information.
Time course of integrated information calculated for wakefulness (red) and sleep (blue).

Our findings indicate that the human cerebral cortex is better suited at information-integration (being both functionally specialized and functionally integrated) when awake and conscious. In contrast, when consciousness fades in deep sleep, the parameters of the system change in such a way that information integration is diminished in all subjects (Figure 4.8, modified from Chang et al.), in line with theoretical predictions (Tononi,2004) and consistent with qualitative evidence obtained from experiments employing TMS/EEG (Massiminietal.,2005).

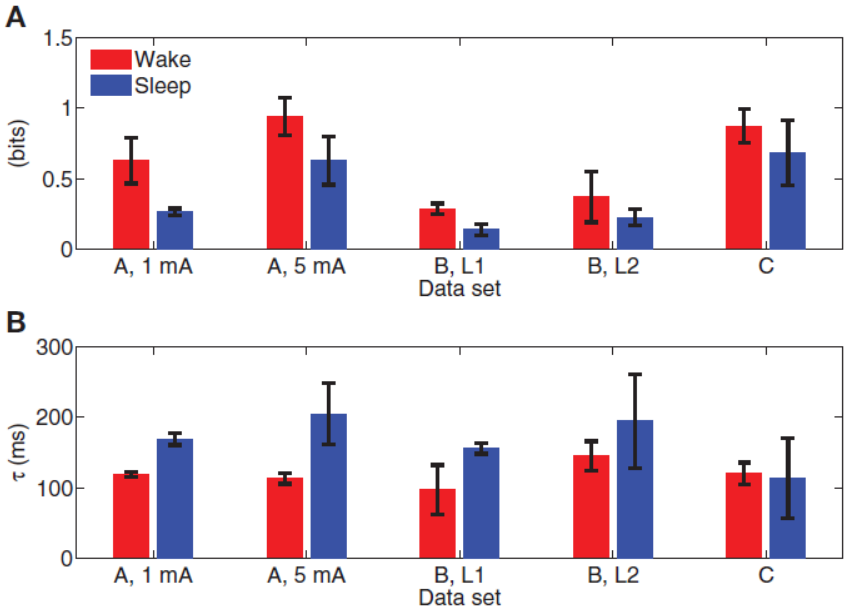

Figure 5.2.2: Integrated information for all subjects.
Panel A. Average of maximum value of integrated information for each subject, black errorbars indicate one standard error. Average lag at which maximum integrated information is achieved, black errorbars indicate one standard error.

We also found that the lag at which the maximum level of information-integration is attained is consistently longer in sleep than wakefulness. Maximum information integration in wakefulness occurred at lags of 30–110ms, while those in sleep were from 70 to 140ms longer, consistent with the increased low frequency activity of sleep.

REFERENCES

Achermann, P., Borbély, A.A., 1997. Low-frequency (< 1 Hz) oscillations in the human sleep electroencephalogram. Neuroscience 81, 213–222.

Alkire, M.T., Hudetz, A.G., Tononi, G., 2008. Consciousness and anesthesia. Science 322, 876–880.

Amzica, F., Steriade, M., 1998. Electrophysiological correlates of sleep delta waves. Electroencephalogr. Clin. Neurophysiol. 107, 69–83.

Amzica, F., Steriade, M., 2000. Integration of low-frequency sleep oscillations in corticothalamic networks. Acta Neurobiol. Exp. (Warsz.) 60, 229–245.

Amzica, F., Steriade, M., 2002. The functional significance of K-complexes. Sleep Med. Rev. 6, 139–149.

Arthuis, M., Valton, L., Régis, J., Chauvel, P., Wendling, F., Naccache, L., Bernard, C., Bartolomei, F., 2009. Impaired consciousness during temporal lobe seizures is related to increased long-distance cortical-subcortical synchronization. Brain J. Neurol. 132, 2091–2101.

Balduzzi, D., Tononi, G., 2008. Integrated information in discrete dynamical systems: motivation and theoretical framework. PLoS Comput. Biol. 4, e1000091.

Bartels, A., Zeki, S., 2005. Brain dynamics during natural viewing conditions--a new guide for mapping connectivity in vivo. NeuroImage 24, 339–349.

Bazhenov, M., Timofeev, I., Steriade, M., Sejnowski, T.J., 2002. Model of thalamocortical slow-wave sleep oscillations and transitions to activated States. J. Neurosci. Off. J. Soc. Neurosci. 22, 8691–8704.

Berthomier, C., Drouot, X., Herman-Stoïca, M., Berthomier, P., Prado, J., Bokar-Thire, D., Benoit, O., Mattout, J., d' Ortho, M.-P., 2007. Automatic analysis of single-channel sleep EEG: validation in healthy individuals. Sleep 30, 1587–1595.

Blumenfeld, H., Taylor, J., 2003. Why do seizures cause loss of consciousness? Neurosci. Rev. J. Bringing Neurobiol. Neurol. Psychiatry 9, 301–310.

Bonato, C., Miniussi, C., Rossini, P.M., 2006. Transcranial magnetic stimulation and cortical evoked potentials: a TMS/EEG co-registration study. Clin. Neurophysiol. Off. J. Int. Fed. Clin. Neurophysiol. 117, 1699–1707.

Borchers, S., Himmelbach, M., Logothetis, N., Karnath, H.-O., 2012. Direct electrical stimulation of human cortex - the gold standard for mapping brain functions? Nat. Rev. Neurosci. 13, 63–70.

Casali, A.G., Casarotto, S., Rosanova, M., Mariotti, M., Massimini, M., 2010. General indices to characterize the electrical response of the cerebral cortex to TMS. NeuroImage 49, 1459–1468.

Cash, S.S., Halgren, E., Dehghani, N., Rossetti, A.O., Thesen, T., Wang, C., Devinsky, O., Kuzniecky, R., Doyle, W., Madsen, J.R., Bromfield, E., Eross, L., Halász, P., Karmos, G., Csercsa, R., Wittner, L., Ulbert, I., 2009. The human K-complex represents an isolated cortical down-state. Science 324, 1084–1087.

Chang, J.-Y., Pigorini, A., Massimini, M., Tononi, G., Nobili, L., Van Veen, B.D., 2012. Multivariate autoregressive models with exogenous inputs for intracerebral responses to direct electrical stimulation of the human brain. Front. Hum. Neurosci. 6, 317.

Chernik, D.A., Gillings, D., Laine, H., Hendler, J., Silver, J.M., Davidson, A.B., Schwam, E.M., Siegel, J.L., 1990. Validity and reliability of the Observer's Assessment of Alertness/Sedation Scale: study with intravenous midazolam. J. Clin. Psychopharmacol. 10, 244–251.

Compte, A., Sanchez-Vives, M.V., McCormick, D.A., Wang, X.-J., 2003. Cellular and network mechanisms of slow oscillatory activity (<1 Hz) and wave propagations in a cortical network model. J. Neurophysiol. 89, 2707–2725.

Contreras, D., Destexhe, A., Sejnowski, T.J., Steriade, M., 1996. Control of spatiotemporal coherence of a thalamic oscillation by corticothalamic feedback. Science 274, 771–774.

Contreras, D., Steriade, M., 1995. Cellular basis of EEG slow rhythms: a study of dynamic corticothalamic relationships. J. Neurosci. Off. J. Soc. Neurosci. 15, 604–622.

Contreras, D., Steriade, M., 1997. Synchronization of low-frequency rhythms in corticothalamic networks. Neuroscience 76, 11–24.

Cruse, D., Chennu, S., Chatelle, C., Bekinschtein, T.A., Fernández-Espejo, D., Pickard, J.D., Laureys, S., Owen, A.M., 2011. Bedside detection of awareness in the vegetative state: a cohort study. Lancet 378, 2088–2094.

Csercsa, R., Dombovári, B., Fabó, D., Wittner, L., Eross, L., Entz, L., Sólyom, A., Rásonyi, G., Szucs, A., Kelemen, A., Jakus, R., Juhos, V., Grand, L., Magony, A., Halász, P., Freund, T.F., Maglóczky, Z., Cash, S.S., Papp, L., Karmos, G., Halgren, E., Ulbert, I., 2010. Laminar analysis of slow wave activity in humans. Brain J. Neurol. 133, 2814–2829.

Delorme, A., Makeig, S., 2004. EEGLAB: an open source toolbox for analysis of single-trial EEG dynamics including independent component analysis. J. Neurosci. Methods 134, 9–21.

Destexhe, A., Contreras, D., Steriade, M., 1999. Spatiotemporal analysis of local field potentials and unit discharges in cat cerebral cortex during natural wake and sleep states. J. Neurosci. Off. J. Soc. Neurosci. 19, 4595–4608.

Destexhe, A., Hughes, S.W., Rudolph, M., Crunelli, V., 2007. Are corticothalamic “up” states fragments of wakefulness? Trends Neurosci. 30, 334–342.

Duffau, H., Lopes, M., Arthuis, F., Bitar, A., Sichez, J.-P., Van Effenterre, R., Capelle, L., 2005. Contribution of intraoperative electrical stimulations in surgery of low grade gliomas: a comparative study between two series without (1985-96) and with (1996-2003) functional mapping in the same institution. J. Neurol. Neurosurg. Psychiatry 76, 845–851.

Engel, A.K., Fries, P., Singer, W., 2001. Dynamic predictions: oscillations and synchrony in top-down processing. Nat. Rev. Neurosci. 2, 704–716.

Esser, S.K., Huber, R., Massimini, M., Peterson, M.J., Ferrarelli, F., Tononi, G., 2006. A direct demonstration of cortical LTP in humans: a combined TMS/EEG study. Brain Res. Bull. 69, 86–94.

Fell, J., Elfadil, H., Röschke, J., Burr, W., Klaver, P., Elger, C.E., Fernández, G., 2002. Human scalp recorded sigma activity is modulated by slow EEG oscillations during deep sleep. Int. J. Neurosci. 112, 893–900.

Ferrarelli, F., Massimini, M., Peterson, M.J., Riedner, B.A., Lazar, M., Murphy, M.J., Huber, R., Rosanova, M., Alexander, A.L., Kalin, N., Tononi, G., 2008. Reduced evoked gamma oscillations in the frontal cortex in schizophrenia patients: a TMS/EEG study. Am. J. Psychiatry 165, 996–1005.

Ferrarelli, F., Massimini, M., Sarasso, S., Casali, A., Riedner, B.A., Angelini, G., Tononi, G., Pearce, R.A., 2010. Breakdown in cortical effective connectivity during midazolam-induced loss of consciousness. Proc. Natl. Acad. Sci. U. S. A. 107, 2681–2686.

Franks, N.P., 2008. General anaesthesia: from molecular targets to neuronal pathways of sleep and arousal. Nat. Rev. Neurosci. 9, 370–386.

Friston, K., 2008. Hierarchical models in the brain. PLoS Comput. Biol. 4, e1000211.

Gaillard, R., Dehaene, S., Adam, C., Clémenceau, S., Hasboun, D., Baulac, M., Cohen, L., Naccache, L., 2009. Converging intracranial markers of conscious access. PLoS Biol. 7, e61.

Gan, T.J., 2006. Pharmacokinetic and pharmacodynamic characteristics of medications used for moderate sedation. Clin. Pharmacokinet. 45, 855–869.

Giacino, J.T., 2004. The vegetative and minimally conscious states: consensus-based criteria for establishing diagnosis and prognosis. NeuroRehabilitation 19, 293–298.

Hangya, B., Tihanyi, B.T., Entz, L., Fabó, D., Erőss, L., Wittner, L., Jakus, R., Varga, V., Freund, T.F., Ulbert, I., 2011. Complex propagation patterns characterize human

cortical activity during slow-wave sleep. J. Neurosci. Off. J. Soc. Neurosci. 31, 8770–8779.
Hill, S., Tononi, G., 2005. Modeling sleep and wakefulness in the thalamocortical system. J. Neurophysiol. 93, 1671–1698.
Hobson, J.A., Pace-Schott, E.F., 2002. The cognitive neuroscience of sleep: neuronal systems, consciousness and learning. Nat. Rev. Neurosci. 3, 679–693.
Huang, N.E., Shen, Z., Long, S.R., Wu, M.C., Shih, H.H., Zheng, Q., Yen, N.-C., Tung, C.C., Liu, H.H., 1998. The empirical mode decomposition and the Hilbert spectrum for nonlinear and non-stationary time series analysis. Proc. R. Soc. Lond. Ser. Math. Phys. Eng. Sci. 454, 903–995.
Huang, N.E., Wu, M.-L.C., Long, S.R., Shen, S.S.P., Qu, W., Gloersen, P., Fan, K.L., 2003. A confidence limit for the empirical mode decomposition and Hilbert spectral analysis. Proc. R. Soc. Lond. Ser. Math. Phys. Eng. Sci. 459, 2317–2345.
Hughes, S.W., Lörincz, M., Cope, D.W., Blethyn, K.L., Kékesi, K.A., Parri, H.R., Juhász, G., Crunelli, V., 2004. Synchronized oscillations at alpha and theta frequencies in the lateral geniculate nucleus. Neuron 42, 253–268.
Ilmoniemi, R.J., Virtanen, J., Ruohonen, J., Karhu, J., Aronen, H.J., Näätänen, R., Katila, T., 1997. Neuronal responses to magnetic stimulation reveal cortical reactivity and connectivity. Neuroreport 8, 3537–3540.
Jerbi, K., Ossandón, T., Hamamé, C.M., Senova, S., Dalal, S.S., Jung, J., Minotti, L., Bertrand, O., Berthoz, A., Kahane, P., Lachaux, J.-P., 2009. Task-related gamma-band dynamics from an intracerebral perspective: review and implications for surface EEG and MEG. Hum. Brain Mapp. 30, 1758–1771.
Kahan, T.L., LaBerge, S.P., 2011. Dreaming and waking: similarities and differences revisited. Conscious. Cogn. 20, 494–514.
Kähkönen, S., 2005. MEG and TMS combined with EEG for mapping alcohol effects. Alcohol Fayettev. N 37, 129–133.
Kähkönen, S., Komssi, S., Wilenius, J., Ilmoniemi, R.J., 2005. Prefrontal TMS produces smaller EEG responses than motor-cortex TMS: implications for rTMS treatment in depression. Psychopharmacology (Berl.) 181, 16–20.
Kähkönen, S., Komssi, S., Wilenius, J., Ilmoniemi, R.J., 2005. Prefrontal transcranial magnetic stimulation produces intensity-dependent EEG responses in humans. NeuroImage 24, 955–960.
Komssi, S., Aronen, H.J., Huttunen, J., Kesäniemi, M., Soinne, L., Nikouline, V.V., Ollikainen, M., Roine, R.O., Karhu, J., Savolainen, S., Ilmoniemi, R.J., 2002. Ipsi- and contralateral EEG reactions to transcranial magnetic stimulation. Clin. Neurophysiol. Off. J. Int. Fed. Clin. Neurophysiol. 113, 175–184.
Komssi, S., Kähkönen, S., 2006. The novelty value of the combined use of electroencephalography and transcranial magnetic stimulation for neuroscience research. Brain Res. Rev. 52, 183–192.
Komssi, S., Kähkönen, S., Ilmoniemi, R.J., 2004. The effect of stimulus intensity on brain responses evoked by transcranial magnetic stimulation. Hum. Brain Mapp. 21, 154–164.
Kotchoubey, B., Lang, S., Mezger, G., Schmalohr, D., Schneck, M., Semmler, A., Bostanov, V., Birbaumer, N., 2005. Information processing in severe disorders of consciousness: vegetative state and minimally conscious state. Clin. Neurophysiol. Off. J. Int. Fed. Clin. Neurophysiol. 116, 2441–2453.
Laarne, P., Hyttinen, J., Dodel, S., Malmivuo, J., Eskola, H., 2000. Accuracy of two dipolar inverse algorithms applying reciprocity for forward calculation. Comput. Biomed. Res. Int. J. 33, 172–185.
Lachaux, J.P., Rodriguez, E., Martinerie, J., Varela, F.J., 1999. Measuring phase synchrony in brain signals. Hum. Brain Mapp. 8, 194–208.
Laureys, S., Owen, A.M., Schiff, N.D., 2004. Brain function in coma, vegetative state, and related disorders. Lancet Neurol. 3, 537–546.

Lehmann, D., Skrandies, W., 1980. Reference-free identification of components of checkerboard-evoked multichannel potential fields. Electroencephalogr. Clin. Neurophysiol. 48, 609–621.
Lioumis, P., Kicić, D., Savolainen, P., Mäkelä, J.P., Kähkönen, S., 2009. Reproducibility of TMS-Evoked EEG responses. Hum. Brain Mapp. 30, 1387–1396.
Llinás, R.R., Choi, S., Urbano, F.J., Shin, H.-S., 2007. Gamma-band deficiency and abnormal thalamocortical activity in P/Q-type channel mutant mice. Proc. Natl. Acad. Sci. U. S. A. 104, 17819–17824.
Llinás, R.R., Steriade, M., 2006. Bursting of thalamic neurons and states of vigilance. J. Neurophysiol. 95, 3297–3308.
Lv, J., Simpson, D.M., Bell, S.L., 2007. Objective detection of evoked potentials using a bootstrap technique. Med. Eng. Phys. 29, 191–198.
Mann, E.O., Kohl, M.M., Paulsen, O., 2009. Distinct roles of GABA(A) and GABA(B) receptors in balancing and terminating persistent cortical activity. J. Neurosci. Off. J. Soc. Neurosci. 29, 7513–7518.
Massimini, M., Boly, M., Casali, A., Rosanova, M., Tononi, G., 2009. A perturbational approach for evaluating the brain's capacity for consciousness. Prog. Brain Res. 177, 201–214.
Massimini, M., Ferrarelli, F., Esser, S.K., Riedner, B.A., Huber, R., Murphy, M., Peterson, M.J., Tononi, G., 2007. Triggering sleep slow waves by transcranial magnetic stimulation. Proc. Natl. Acad. Sci. U. S. A. 104, 8496–8501.
Massimini, M., Ferrarelli, F., Huber, R., Esser, S.K., Singh, H., Tononi, G., 2005. Breakdown of cortical effective connectivity during sleep. Science 309, 2228–2232.
Massimini, M., Ferrarelli, F., Murphy, M., Huber, R., Riedner, B., Casarotto, S., Tononi, G., 2010. Cortical reactivity and effective connectivity during REM sleep in humans. Cogn. Neurosci. 1, 176–183.
Matsumoto, R., Nair, D.R., Ikeda, A., Fumuro, T., Lapresto, E., Mikuni, N., Bingaman, W., Miyamoto, S., Fukuyama, H., Takahashi, R., Najm, I., Shibasaki, H., Lüders, H.O., 2012. Parieto-frontal network in humans studied by cortico-cortical evoked potential. Hum. Brain Mapp. 33, 2856–2872.
Matsumoto, R., Nair, D.R., LaPresto, E., Bingaman, W., Shibasaki, H., Lüders, H.O., 2007. Functional connectivity in human cortical motor system: a cortico-cortical evoked potential study. Brain J. Neurol. 130, 181–197.
Matsumoto, R., Nair, D.R., LaPresto, E., Najm, I., Bingaman, W., Shibasaki, H., Lüders, H.O., 2004. Functional connectivity in the human language system: a cortico-cortical evoked potential study. Brain J. Neurol. 127, 2316–2330.
McCormick, D.A., Wang, Z., Huguenard, J., 1993. Neurotransmitter control of neocortical neuronal activity and excitability. Cereb. Cortex N. Y. N 1991 3, 387–398.
Mölle, M., Marshall, L., Gais, S., Born, J., 2002. Grouping of spindle activity during slow oscillations in human non-rapid eye movement sleep. J. Neurosci. Off. J. Soc. Neurosci. 22, 10941–10947.
Myles, P.S., Leslie, K., McNeil, J., Forbes, A., Chan, M.T.V., 2004. Bispectral index monitoring to prevent awareness during anaesthesia: the B-Aware randomised controlled trial. Lancet 363, 1757–1763.
Nir, Y., Staba, R.J., Andrillon, T., Vyazovskiy, V.V., Cirelli, C., Fried, I., Tononi, G., 2011. Regional slow waves and spindles in human sleep. Neuron 70, 153–169.
Nobili, L., De Gennaro, L., Proserpio, P., Moroni, F., Sarasso, S., Pigorini, A., De Carli, F., Ferrara, M., 2012. Local aspects of sleep: observations from intracerebral recordings in humans. Prog. Brain Res. 199, 219–232.
Ojemann, G., Ojemann, J., Lettich, E., Berger, M., 2008. Cortical language localization in left, dominant hemisphere. An electrical stimulation mapping investigation in 117 patients. 1989. J. Neurosurg. 108, 411–421.
Owen, A.M., Coleman, M.R., Boly, M., Davis, M.H., Laureys, S., Pickard, J.D., 2006. Detecting awareness in the vegetative state. Science 313, 1402.

Palva, J.M., Palva, S., Kaila, K., 2005. Phase synchrony among neuronal oscillations in the human cortex. J. Neurosci. Off. J. Soc. Neurosci. 25, 3962–3972.
Paus, T., 2005. Inferring causality in brain images: a perturbation approach. Philos. Trans. R. Soc. Lond. B. Biol. Sci. 360, 1109–1114.
Paus, T., Sipila, P.K., Strafella, A.P., 2001. Synchronization of neuronal activity in the human primary motor cortex by transcranial magnetic stimulation: an EEG study. J. Neurophysiol. 86, 1983–1990.
Pfurtscheller, G., Aranibar, A., 1979. Evaluation of event-related desynchronization (ERD) preceding and following voluntary self-paced movement. Electroencephalogr. Clin. Neurophysiol. 46, 138–146.
Rosanova, M., Casali, A., Bellina, V., Resta, F., Mariotti, M., Massimini, M., 2009. Natural frequencies of human corticothalamic circuits. J. Neurosci. Off. J. Soc. Neurosci. 29, 7679–7685.
Rosanova, M., Gosseries, O., Casarotto, S., Boly, M., Casali, A.G., Bruno, M.-A., Mariotti, M., Boveroux, P., Tononi, G., Laureys, S., Massimini, M., 2012. Recovery of cortical effective connectivity and recovery of consciousness in vegetative patients. Brain J. Neurol. 135, 1308–1320.
Sanchez-Vives, M.V., McCormick, D.A., 2000. Cellular and network mechanisms of rhythmic recurrent activity in neocortex. Nat. Neurosci. 3, 1027–1034.
Sarasso, S., Proserpio, P., Pigorini, A., Moroni, F., Ferrara, M., De Gennaro, L., De Carli, F., Lo Russo, G., Massimini, M., Nobili, L., 2014. Hippocampal sleep spindles preceding neocortical sleep onset in humans. NeuroImage 86, 425–432.
Seth, A.K., 2005. Causal connectivity of evolved neural networks during behavior. Netw. Bristol Engl. 16, 35–54.
Seth, A.K., Dienes, Z., Cleeremans, A., Overgaard, M., Pessoa, L., 2008. Measuring consciousness: relating behavioural and neurophysiological approaches. Trends Cogn. Sci. 12, 314–321.
Silber, M.H., Ancoli-Israel, S., Bonnet, M.H., Chokroverty, S., Grigg-Damberger, M.M., Hirshkowitz, M., Kapen, S., Keenan, S.A., Kryger, M.H., Penzel, T., Pressman, M.R., Iber, C., 2007. The visual scoring of sleep in adults. J. Clin. Sleep Med. JCSM Off. Publ. Am. Acad. Sleep Med. 3, 121–131.
Sinkkonen, J., Tiitinen, H., Näätänen, R., 1995. Gabor filters: an informative way for analysing event-related brain activity. J. Neurosci. Methods 56, 99–104.
Steriade, M., 1999. Coherent oscillations and short-term plasticity in corticothalamic networks. Trends Neurosci. 22, 337–345.
Steriade, M., 2001. Impact of network activities on neuronal properties in corticothalamic systems. J. Neurophysiol. 86, 1–39.
Tanelian, D.L., Kosek, P., Mody, I., MacIver, M.B., 1993. The role of the GABAA receptor/chloride channel complex in anesthesia. Anesthesiology 78, 757–776.
Timofeev, I., Grenier, F., Steriade, M., 2000. Impact of intrinsic properties and synaptic factors on the activity of neocortical networks in vivo. J. Physiol. Paris 94, 343–355.
Tononi, G., 2004. An information integration theory of consciousness. BMC Neurosci. 5, 42.
Tononi, G., 2005. Consciousness, information integration, and the brain. Prog. Brain Res. 150, 109–126.
Tononi, G., 2008. Consciousness as integrated information: a provisional manifesto. Biol. Bull. 215, 216–242.
Tononi, G., Sporns, O., 2003. Measuring information integration. BMC Neurosci. 4, 31.
Tononi, G., Sporns, O., Edelman, G.M., 1994. A measure for brain complexity: relating functional segregation and integration in the nervous system. Proc. Natl. Acad. Sci. U. S. A. 91, 5033–5037.
Valderrama, M., Crépon, B., Botella-Soler, V., Martinerie, J., Hasboun, D., Alvarado-Rojas, C., Baulac, M., Adam, C., Navarro, V., Le Van Quyen, M., 2012. Human Gamma Oscillations during Slow Wave Sleep. PLoS ONE 7, e33477.

Valentín, A., Alarcón, G., García-Seoane, J.J., Lacruz, M.E., Nayak, S.D., Honavar, M., Selway, R.P., Binnie, C.D., Polkey, C.E., 2005. Single-pulse electrical stimulation identifies epileptogenic frontal cortex in the human brain. Neurology 65, 426–435.

Valentín, A., Anderson, M., Alarcón, G., Seoane, J.J.G., Selway, R., Binnie, C.D., Polkey, C.E., 2002. Responses to single pulse electrical stimulation identify epileptogenesis in the human brain in vivo. Brain J. Neurol. 125, 1709–1718.

Van de Velde, M., van Erp, G., Cluitmans, P.J., 1998. Detection of muscle artefact in the normal human awake EEG. Electroencephalogr. Clin. Neurophysiol. 107, 149–158.

Van Der Werf, Y.D., Paus, T., 2006. The neural response to transcranial magnetic stimulation of the human motor cortex. I. Intracortical and cortico-cortical contributions. Exp. Brain Res. 175, 231–245.

Van Der Werf, Y.D., Sadikot, A.F., Strafella, A.P., Paus, T., 2006. The neural response to transcranial magnetic stimulation of the human motor cortex. II. Thalamocortical contributions. Exp. Brain Res. 175, 246–255.

Van Dort, C.J., Baghdoyan, H.A., Lydic, R., 2008. Neurochemical modulators of sleep and anesthetic states. Int. Anesthesiol. Clin. 46, 75–104.

Van 't Klooster, M.A., Zijlmans, M., Leijten, F.S.S., Ferrier, C.H., van Putten, M.J.A.M., Huiskamp, G.J.M., 2011. Time-frequency analysis of single pulse electrical stimulation to assist delineation of epileptogenic cortex. Brain J. Neurol. 134, 2855–2866.

Verbny, Y.I., Merriam, E.B., Banks, M.I., 2005. Modulation of gamma-aminobutyric acid type A receptor-mediated spontaneous inhibitory postsynaptic currents in auditory cortex by midazolam and isoflurane. Anesthesiology 102, 962–969.

Virtanen, J., Ruohonen, J., Näätänen, R., Ilmoniemi, R.J., 1999. Instrumentation for the measurement of electric brain responses to transcranial magnetic stimulation. Med. Biol. Eng. Comput. 37, 322–326.

Von Stein, A., Chiang, C., König, P., 2000. Top-down processing mediated by interareal synchronization. Proc. Natl. Acad. Sci. U. S. A. 97, 14748–14753.

Wilson, C.L., Engel, J., Jr, 1993. Electrical stimulation of the human epileptic limbic cortex. Adv. Neurol. 63, 103–113.

Wilson, C.L., Khan, S.U., Engel, J., Jr, Isokawa, M., Babb, T.L., Behnke, E.J., 1998. Paired pulse suppression and facilitation in human epileptogenic hippocampal formation. Epilepsy Res. 31, 211–230.

Youden, W.J., 1950. Index for rating diagnostic tests. Cancer 3, 32–35.